


FACULTY OF SCIENCE
Department of Analytical Chemistry

Tetrasulphonated phthalocyanine thin films deposited on gold electrodes: a study using voltammetry and synchrotron micro X-ray fluorescence

Karl Peeters

Thesis submitted in fulfillment of the requirements
for the degree of Doctor in Science, Chemistry

Academic year 2006-2007

Promotor

Prof. Dr. A. Adriaens

Copromotors

Prof. Dr. L. Vincze

Dr. K. De Wael

Graag zou ik iedereen willen danken die op welke wijze dan ook heeft bijgedragen tot het verwezenlijken van dit werk.

I would like to thank everybody who contributed to the realization of this work.

Table of contents

Articles

Introduction

Since their discovery in the beginning of the previous century, phthalocyanines and their derivatives have been widely used as dyestuffs and colors. More recently, they have also attracted a wide research interest including that of electrochemists. Nowadays they are used in high-tech applications such as photovoltaic, electronic and sensing devices. Their major characteristics are their intensive color, their redox activity, their high thermal stability and non-toxicity. Most of the applications rely critically on the redox properties of the phthalocyanine species. The aromatic ring can indeed undergo oxidation, reduction or both. Moreover, more than 70 different metal ions can form a complex by coordinating with a phthalocyanine ring. If the central metal ion is a transition element, it can be oxidized and reduced at potentials comparable to those of the ring processes. These properties make them useful as electrocatalysts. It has also been shown that the phthalocyanines are able to form thin films on different types of supporting materials, including electrodes. The immobilization of these phthalocyanines on an electrode can lead to modified electrodes with important electrocatalytic properties.

It is from this point of view that the goal of this research is the study of the modification process of gold electrodes with water soluble phthalocyanines in a pH 12 buffer solution. The modified gold electrodes are characterized with electrochemical and spectroscopic techniques and in a final stage the modified electrodes are used for the oxidation of environmental pollutants. The emphasis has been put on the electrochemical deposition with cyclic voltammetry (referred to as electrodeposition in this work) of cobalt(II) tetrasulphophthalocyanine (CoTSPc) and copper(II) tetrasulphophthalocyanine (CuTSPc) on a gold electrode in a pH 12 buffer solution. Electrodeposition has been used for the modification of the gold electrodes since it enables one to control and to characterize the formed thin film by following the potential and current during the process. This electrodeposition procedure, however, has also been compared to other modification techniques as there are; immersion and drop drying.

The heterogeneity and morphology of the CoTSPc and CuTSPc thin films on the gold electrodes has been studied by spectroscopic techniques. Therefore

synchrotron micro X-ray fluorescence (SR-XRF) has been used. Also X-ray photoelectron spectroscopy (XPS) has been used for the quantification of the CoTSPc and CuTSPc on the gold surface. UV-Vis spectroscopy has been used to characterize the phthalocyanine in solution. Finally, the oxidation of 4-chlorophenol (4-Cp) on a bare gold electrode has been compared with the oxidation of the 4-Cp on the gold electrodes modified with CoTSPc or CuTSPc.

In the first part of this work (chapters 1-4) an overview is given of the properties of the used chemicals. The theoretical background on the electrochemical and spectroscopic techniques used during this work is shown, together with the experimental setup of these techniques as applied for this study. A summary of the already published results concerning the modification procedure and thin film build-up is given.

Chapter 1 deals with the properties of phthalocyanines and the electrocatalytic detection of different target molecules at electrodes modified with phthalocyanines. Also the basics of electrocatalysis and different modification techniques are introduced. At the end of this chapter, the properties of the chlorophenols, together with their electrochemical behavior are shown. Chapter 2 describes cyclic voltammetry together with the electrochemical cell and the modification procedures used in this work. In chapter 3, the important issues concerning SR-XRF spectroscopy are shown which include the exposition of synchrotron induced X-rays, the interaction of X-rays with matter, the principle of XRF, the resonant Raman effect, the experimental setup used during the SR-XRF study and the quantification procedure used. Furthermore, in this chapter the basic principles of XPS and UV-Vis spectroscopy are shown. In the final introductory chapter, chapter 4, the earlier published results concerning the properties of the bare gold electrode and the electrodes modified with CoTSPc or CuTSPc are discussed.

The second part (chapters 5-10) includes the scientific articles published or prepared during this work. Chaper 5 discusses the immobilization characteristics of CoTSPc purchased from three different suppliers on gold electrodes using three different techniques (electrodeposition, immersion and drop-drying). A detailed comparison is made between these techniques with respect to the resulting Co thin film properties on the electrode surface, based on electrochemical and SR-XRF

measurements. Moreover, the degree of aggregation of the CoTSPc species purchased from three different suppliers was studied by performing UV-Vis spectroscopy. The characterization of CoTSPc thin films electrochemically deposited on gold electrodes as a function of scan numbers by means of SR-XRF and cyclic voltammetry has been described in chapter 6. Chapter 7 focuses on the characteristics of CuTSPc on gold electrodes. The electrochemical behavior of CuTSPc with the sulphonated groups randomly placed over the phthalocyanine ring and with the sulphonated groups at the 3,4',4'',4''' places have been compared. The three different modification techniques will be discussed and a comparison will be made with the modification of gold with CoTSPc. Also the degree of aggregation, studied with UV-Vis spectroscopy, will be discussed. In chapter 8, the characterization of CoTSPc and CuTSPc thin films, electrochemically deposited on gold electrodes as a function of the phthalocyanine concentration in solution during modification, by means of SR-XRF has been investigated. Also the data reduction method applied for the quantification and the determination of the heterogeneity of CoTSPc or CuTSPc has been discussed. Chapter 9 encompasses the study of X-ray Resonant Raman Scattering (XRRS) in the context of its analytical influence on the outcome of scanning XRF measurements on CuTSPc thin film detection on gold substrates using SR-XRF. Therefore, the detection limits and peak-to-background ratios of the Cu species on the gold surface are derived as a function of the excitation energy. In the final chapter, the modified electrodes are used for the oxidation of an environmental pollutant, 4-chlorophenol. The oxidation of this molecule on a modified electrode is compared with its oxidation on a bare gold electrode and the thin film buildup of the phthalocyanine is linked with its electrochemical properties towards the oxidation.

Introductory chapters

Chapter 1:
The basic properties of phthalocyanines and their electrocatalytic behavior

Since their discovery in the early twentieth century, probably as byproduct in the synthesis of o-cyanobenzamide in 1907 [BRAU-07], phthalocyanines have established themselves as blue and green dyestuffs par excellence. More recently they are also used in high-tech applications, such as photovoltaic, electronic and sensing devices. Their major characteristics are their thermal and chemical stability, coupled with their extensive redox chemistry. These properties make them useful for electrocatalysis [KATO-85, LEVE-87, KUDE-88, TEMO-89, LEZN-93]. Important for this work, is that most phthalocyanines are not toxic. In this chapter, the structural and redox properties of phthalocyanines will be discussed together with their electronic structure. The basic principles of electrocatalysis and electrode modification will be explained and a short overview of the electrocatalytic detection of some target molecules at modified electrodes described in literature will be discussed. Furthermore, a brief introduction on the detection of chlorophenols, the target molecule in this work, will be given.

1.1 Properties of phthalocyanines [LEZN-93]

The phthalocyanine ring (H_2Pc) (Fig. 1.1b) consists of four isoindole groups (Fig. 1.1a) which are connected via four aza-nitrogens. The weak azide bonds are broken when a central metal ion is complexated in the central cavity of the phthalocyanine. By substitution of the functional groups (e.g. ethylhexyloxy, sulphonyl, methoxy or tetraneopentoxy phthalocyanine) [ZAGA-99] and insertion of a central metal ion (e.g. Ni, Fe, Co, Cu, Mn), a large variety of phthalocyanine derivates can be formed.

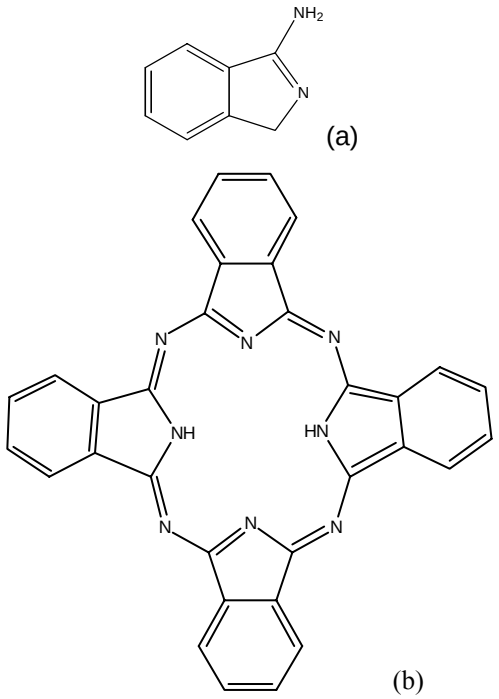

Fig. 1.1: Structure of isoindole (a) and phthalocyanine (b).

Many applications of metal ion phthalocyanines rely critically upon the redox properties of the metal phthalocyanine (MPc) species. The phthalocyanine unit is an 18 π electron system that, in its common oxidation state, carries two negative charges. In what follows this will be indicated as Pc^{2-}. This unit is capable of oxidation or reduction [ROLL-68, CLAC-76]. Emission of one or two electrons yields Pc^{1-} and Pc^{0} (oxidation of the ring), while admission of one to four electrons forms Pc^{3-}, Pc^{4-}, Pc^{5-} and Pc^{6-} (reduction of the ring). Whenn the central metal ion is a main group element, it is incapable of a redox process; when it is a transition element, it can undergo oxidation or reduction at potentials comparable to the phthalocyanine ring processes [LEZN-93].

Another important issue is the symmetry of the phthalocyanine structure. Insertion of a metal ion positioned in the plane of the phthalocyanine ring causes an increase in symmetry from D_{2h} for H_2Pc to D_{4h} for MPc. However, when the metal ion is tilted out of the plane of the phthalocyanine ring (‘domed’ structure), the symmetry decreases to C_{4v}. When the phthalocyanine is substituted with four sulphonate groups the symmetry becomes C_{4h}, in the presence of an out-of-plane metal ion it becomes C_4. [SIMI-83, AROC-86, LEZN-89]

Fig. 1.2 shows the conventional scheme of the energy levels in MPcs and the various transitions. The highest occupied molecular orbital (HOMO) is $1a_{1u}(\pi)$, the next low lying filled orbital is $1a_{2u}(\pi)$. The lowest unoccupied molecular orbital (LUMO) is $1e_g(\pi^*)$ and the one above is $1b_{1u}(\pi^*)$. Transitions from the two upper filled π orbitals to $1e_g(\pi^*)$ yield the so called Q (near 600-700 nm) and Soret (or B) (near 300-450 nm) bands. Both of these involve an excited state, but they are not significantly mixed because the $1a_{1u}$ and $1a_{2u}$ orbitals are fairly well separated in energy. In main group phthalocyanines the redox activity is directly associated, in oxidation, by the successive removal of the electrons from the HOMO, $1a_{1u}$, while up to four electrons are readily added to $1e_g$ (LUMO) (reduction), terminating in the Pc^{6-} species. The Pc^{3-}, Pc^{4-}, Pc^{5-} and Pc^{6-} ring reduced species have the ground state electron configurations $(a_{1u})^2e_g$, S = ½; $(a_{1u})^2(eg)^2$, S = 0; $(a_{1u})^2(eg)^3$, S = ½; and $(a_{1u})^2(eg)^4$, S = 0, respectively.

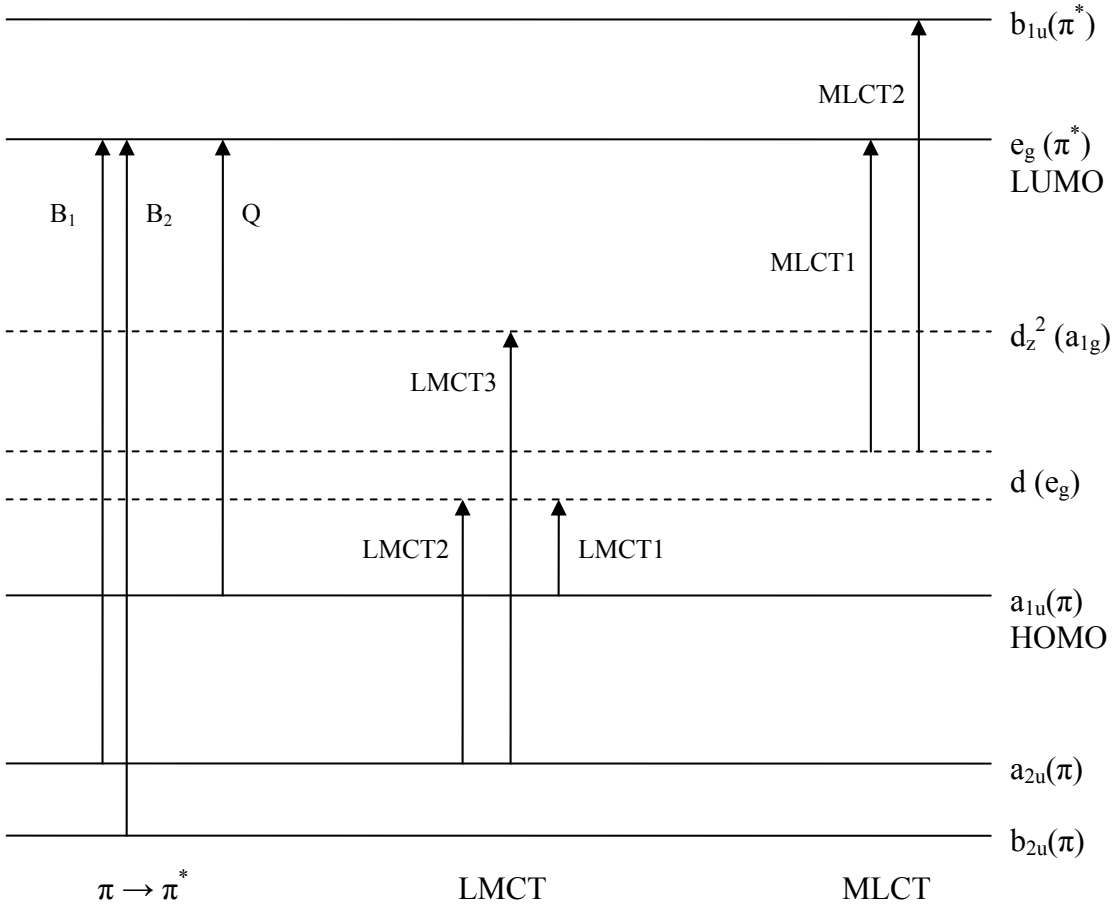

Fig. 1.2: The conventional scheme of the energy levels in MPc and the various transitions (Q, Soret, LMCT, MLCT bands). After [LEZN-93].

The redox properties of the transition MPcs differ from those of main group MPcs due to the fact that metal d levels may be positioned between the HOMO (π) and the LUMO (π^*) orbitals of the phthalocyanine ligand. This has the spectroscopic consequence that one or more metal to ligand (MLCT), or ligand to metal (LMCT) charge transfers, may be observed in the visual or the near-infrared region. The redox consequence is that oxidation or reduction of the metal ion may occur at potentials similar to those of ring oxidation or reduction. It is important also to recognize that such internal metal ion redox processes greatly influence the potentials for ring reactions.

Many MPc systems bind one or two axial ligands. Such coordination can have a major effect upon the observed redox activity [WAGN-74]. These species are normally designated to as LMPc or L_2MPc, where the placing of L ahead of M implies L binding axially to the central metal ion M. Most unsubstituted MPc species have only very limited solubility in virtually all solvents. However, ring substitution has proved to be a very effective procedure for rendering these substituted MPc species very soluble in a range of solvents. Even with such species, additional solubility is conferred by axially coordinating central ions. This has led to systems that are extremely soluble in many solvents (e.g. tetraneopentoxyphthalocyanine in organic solvents or the for this work important tetrasulphophthalocyanines in water). Moreover, many transition MPcs are more soluble in donor solvents through an axial interaction between the metal ion center and the donor solvents. This last statement applies especially to those central metal ions that strongly prefer six-coordination rather than four-coordination. Thus, for example cobalt(II) phthalocyanines are soluble in a wide range of donor solvents, while copper(II) phthalocyanine is very much less soluble because its preference for a four-coordination [LEZN-93].

Many phthalocyanines show the tendency to aggregate to a greater or lesser extent, both in water and organic phase. Such aggregation is influenced by pH, ionic strength, temperature, the amount of electrolyte in solution, etc. Six-coordinate MPc species generally do not aggregate because they are kept apart by the axially bound ligands, four-coordinate MPc species on the other hand aggregate very easy.

The structure of the sodium salts of cobalt(II) tetrasulphophthalocyanine (CoTSPc) and copper(II) tetrasulphophthalocyanine (CuTSPc), the two

phthalocyanines used during this research, are shown in Fig. 1.3. The synthesis of these water soluble phthalocyanines has been described by Webber et al. [WEBB-65].

In Wagnerova et al. [WAGN-74], it has been shown that CoTSPc forms a stable adduct with molecular oxygen. Similarly as with natural oxygen carriers, two types of oxygen adducts are known to form cobaltous complexes (stoichiometry $Co:O_2 = 1:1$ or 2:1). The adducts being produced in an aqueous solution are binuclear with the oxygen bridge between both central atoms (2:1). The molecular oxygen may be released again from the adduct by bubbling inert gas through the solution and the oxygenation-deoxygenation cycle can be repeated many times. For CuTSPc, on the other hand there is no adduct formation expected because of its four coordination.

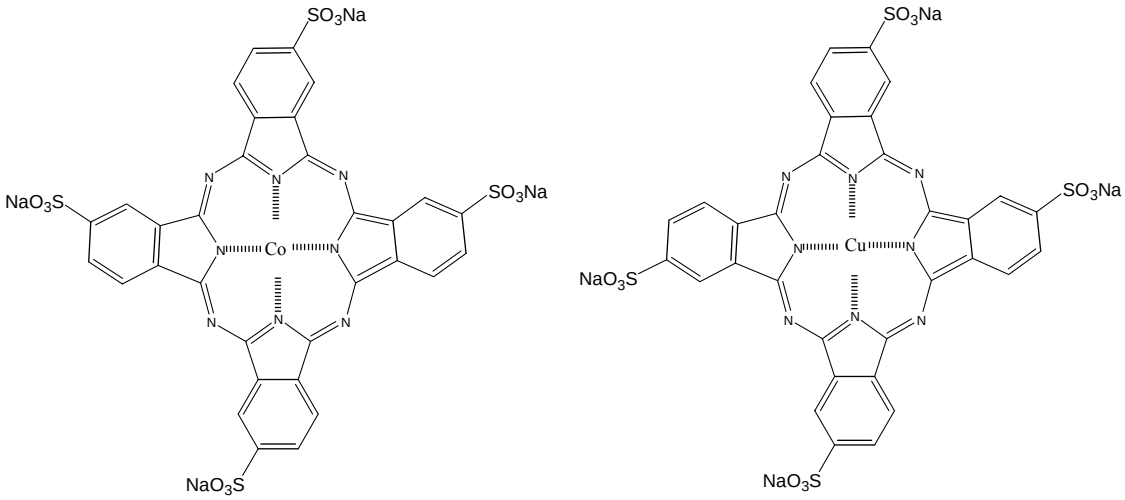

Fig. 1.3: Structure of CoTSPc and CuTSPc.

1.2. Electrocatalysis and modification of electrodes

Many chemical reactions, although thermodynamically very favorable, do not occur at a significant rate. For such reactions to be useful, it is necessary to find a homogeneous or heterogeneous catalyst which will increase the reaction rate. Likewise, in the absence of a catalyst, many electrode reactions occur, if at all, only at very high overpotentials because of poor kinetics, i.e. such electrode reactions have a low exchange current density. The objective of electrocatalysis is therefore to provide an alternative pathway with lower activation energy and hence to permit such electrode reaction to occur at high current densities close to the equilibrium potential. [SOUT-01]

In view of this, the development of chemically modified electrodes (CMEs) has attracted wide research interest in the last decades. The theoretical details of the CMEs have been described in several reviews [MURR-87, WANG-91, ARRI-94]. In (electro) chemical sensing, the emphasis of this relatively modern approach has been on improving the selectivity, efficiency and sensitivity of electroanalytical measurements. The basic feature of a CME is that generally a quite thin film of a selected chemical is bound to or coated on the electrode to provide the electrode with the desired (electro) chemical, optical, electrical, transport or other properties and they are generally used as amperometric sensors. A response reflects two separate components: a usual electrochemical one controlled by the potential and a chemical one given by the reactivity of a confined chemical modifier. Hence, a chemically altered bare electrode exhibits new qualities concerning selectivity, efficiency and sensitivity as well as against fouling and interferences. The electrocatalysis itself involves electron transfer mediation between the target analyte (A) and the surface of the immobilized catalyst (M) [LABU-00] (see Fig. 1.4).

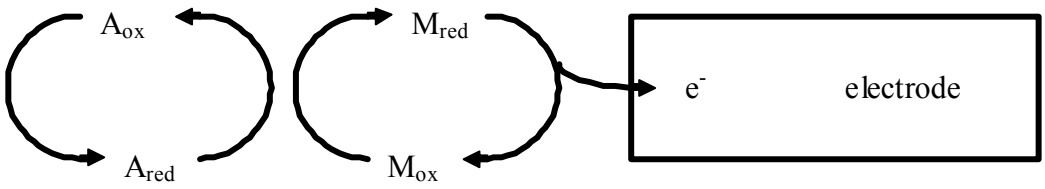

Fig. 1.4: Electrocatalysis at modified electrodes; electron transfer mediated reaction between the target analyte (A) and surface bound catalyst (M). After [BARD-01].

Because of the enormous variation on electron transfer mediators, modification procedures and experimental conditions (pH, solvent, temperature,…), this research domain can be considered to be inexhaustible. Only a small part of it has been investigated until now. In this work, emphasis is on the modification of gold electrodes with phthalocyanine since, as already discussed in one previous section, MPcs are suitable electron transfer mediators for electrocatalysis. MPcs can be immobilized onto electrode materials with different adsorption techniques, such as drop-drying, spin-coating, spontaneous adsorption (in this work referred to as immersion method), inclusion, electrodeposition,… [DURS-97, KUTN-98]. The simplest technique is drop-drying were a drop of the phthalocyanine solution is brought on the electrode and dried in air or nitrogen atmosphere. Spin coating is based

on the same principle, the only difference is that the electrode is rotating and that excess of solution is flung away. With spontaneous adsorption, a self assembled monolayer (SAM) is formed on the electrode when the electrode is immersed in the phthalocyanine solution [FINK-00]. Another modification technique is the inclusion of reagentia in the electrode material as for example in carbon paste [ONI-02]. Electrodeposition* is the adsorption of a phthalocyanine from the solution on the electrode surface by means of a linear and continuous variation of the potential. The gradual buildup of the thin film is very often promoted by cyclic potential variation. By measuring the current during the potential variation, the modification process can be followed in situ.

1.3 Electrocatalytic detection at phthalocyanine modified electrodes

In this section an overview will be given of the electrocatalytic oxidation and reduction processes of target molecules with MPc modified electrodes described in literature. Because of the numerous different phthalocyanines, the classification will be based on the target molecules instead of on the nature of the phthalocyanine. The target molecules can be subdivided in four subgroups: inorganic molecules (I), organic molecules (II), neurotransmitters (III) and biological and pharmaceutical molecules (IV). Table 1.1 shows some of the target molecules discussed in literature, together with the used phthalocyanine and the electrode material. In this study CoTSPc and CuTSPc have been used as electrocatalyst and chlorophenol has been selected as target molecule because of its toxicity, its solubility in aqueous solution and its structural relationship with dioxins and PCB's. In the next section, an overview will be given on its presence, toxicity and electrochemical properties.

* The term electrodeposition is in this work not used in its original meaning but as a potential dependent adsorption phenomenon.

Table 1.1:Overview of a few electrocatalytic phthalocyanine systems studied in the past.

Target molecule	**MPc**	**Electrode material**	**reference**
I. Anorganic Molecule			
NO_3^- en NO_2^-	Mn, Fe, Co, Ni, Cu en ZnPc	C	[CHEB-97]
NO	Co en FePc	C	[NYOK-03]-[VILA-01]
O_2	CoTSPc CoPc	C C	[ZAGA-77] [ELZI-86]
SO_2	FeTSPc	C	[THAM-02]
CO_2	CoPc CuTAPc	C C	[SAVI-92] [MAGD-02]
H_2N-NH_2	CoPc	C	[SIAN-05]
II. Organic molecules			
2-mercaptoethanol	FePc CoTAPc	C C	[AGUI-02] [GRIV-03]
phenol	Fe, Co en CuPc CoPc	zeolite C	[QI-95] [MAFA-97]
Cresol, chlorophenol	CoPc	C	[MAFA-97]
amitrole	FePc	C	[SISW-06]
III. Neurotransmitters			
serotonin, dopamine	FeTSPc	C-paste	[ONI-01] [ONI-03]
IV. Biological and pharmaceutical molecules			
ascorbic acid	FePc	C-paste	[AMIN-01]
vitamin B1	MnPc	C-paste	[ONI-02]
L-cysteine	CoTAPc Co-octabutylthioPc CoPc	C Au C	[GRIV-03] [OZOE-01] [MARE-00]
glucose	CoPc	C	[OZOE-06]

1.4 Application: detection of chlorophenols

Chlorophenols (Fig. 1.5) are organic chemicals formed from phenol by substitution in the phenol ring with one or more atoms of chlorine. Nineteen configurations are possible, ranging from monochlorophenols to the fully chlorinated pentachlorophenol [WHO-89]. In this section an overview will be given on the presence and toxicity of chlorophenols and on the current detection procedures. Emphasis will be put on the electrochemical detection of chlorophenol.

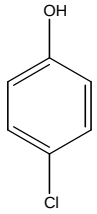

Fig.1.5: Structure of 4-chlorophenol.

1.4.1 Presence and toxicity

Chlorophenols are known to be widespread as components in industrial wastes (e.g. pulp and paper mills, petrochemical refineries and coke plants [WHO-89, KINA-81]) and have been used in many industrial processes such as the manufacture of plastics, dyes and pesticides [GALC-95, VENI-94]. Moreover, chlorophenols are used as wood preservatives in agricultural and domestic applications, and in additives to inhibit microbial growth in a wide array of products such as adhesives, oils, textiles, and pharmaceutical products [WHO-89]. Another source of chlorophenol contamination results from the fact that phenols react with chlorine during water treatment to produce chlorophenols [TERA-02]. They became commercially important in the 1930s [CROS-81], but were only recognized as environmental pollutants in the 1960s [HITC-95].

Their presence in the environment is of particular concern because of the toxicity to humans and most aquatic organisms and their tendency to bio accumulate in the food chain [VUOR-85, SARK-85] which explains for example their relatively high concentration in human urine [ANGE-92]. Some of these compounds are

suspected to be embryotoxic and teratogenic [WHO-89]. The mechanism of the toxic effects seems to be connected with their gradual dechlorination in the tissues, yielding the corresponding peroxides, which in turn cause inactivation of enzymes, liver dystrophy and enhanced humoral immune responsiveness [EXON-84]. This makes that the toxicity depends on the total number of chlorine atoms present in the molecule with pentachlorophenol being the most toxic [MUNA-05]. They also have an adverse effect on the taste and odor of drinking water at low concentration [REAL-81] and chlorophenols in flue gases from waste incinerators are considered to be the precursors of the more toxic polychlorinated dibenzo-*p*-dioxins and dibenzofurans (PCDD/F) [GHOR-96, ALTW-96, WEBE-99, HELL-00].

This makes that phenol and its chlorinated derivatives are classified as priority pollutants by the EPA (US Environmental Protection Agency) [TERA-02], that the European Community legislation requires maximum admissible concentration of phenols in water for human consumption and in bathing water [DIRE-76, DWD-80] and that they were inserted in VLAREM II, "het Vlaams regelement milieuvergunning" [VLAR-04].

The standard detection method of these components, described in VLAREM II, includes the extraction in an organic solvent, separation with HPLC or GC and detection with an electron capture detector [VLAR-04]. This method, however, can be quite time consuming. Moreover the fact that samples need to be taken from the site into the laboratory potentially implies the possibilities for sample contamination, alteration or fraud. This makes that there is a need for sensitive, reproducible, stable, easy-to-use, and low-cost analytical methods for monitoring chlorophenols in water. In recent years the detection of chlorophenols has been investigated intensively together with the degradation and adsorption of these components [STAF-97, AZZA-00, WALD-03, TONO-03, PERA-04, ZILO-06].

1.4.2 Detection

The early procedures used to analyze chlorophenols were colorimetric techniques, the most popular being the 4-aminoantipyrine method [BEVE-67]. None of these methods was either very specific or sensitive and they are, consequently, no longer used. Instead, more sophisticated techniques [WHO-89] are being used and investigated during recent years, including thin layer chromatography (TLC) [LEPR-

82], gas chromatography (GC) [VENI-94,CAMP-05], High performance liquid chromatography (HPLC) [BUTL-92, SULI-06, DERU-88] ion exchange chromatography, infrared (IR), ultraviolet (UV) and mass spectroscopy (MS) [TONO-03], mass fragmentation and electrochemical oxidation [URET-03, CODO-03, SATE-01]. Very often, an extraction procedure is followed and a combination of above mentioned techniques is used to make detection limits in the ng L^{-1} concentration range and even lower [REAL-81, KWAK-91, RUAN-93, GALC-95].

1.4.3 Electrochemical oxidation

In the second decade of last century, Fichter and co-workers [FICH-13, FICH-14, FICH-16, FICH-19], oxidized some aromatic compounds anodically. They reported that during anodic oxidation of these aromatic compounds, surface films were formed and that a consequential instability and lack of precision was observed in subsequent electroanalytical measurements. This accumulation of reaction products is commonly referred to as “blocking”, “poisoning”, or “fouling” [KOIL-79]. In the almost 100 years that have passed after this report, a tremendous number of electrode materials has been tested for the anodic oxidation of numerous aromatic compounds. In this section the oxidation mechanism of chlorophenol and the poisoning of the electrode with phenol and chlorophenol will be discussed.

It has been postulated that the oxidation of chlorophenol, for example on a gold electrode, begins with the interaction of the chlorophenol molecule with an adsorbed OH which has been formed by electro oxidation of an Au-H_2O site. In this way a phenoxy radical is formed which on its turn can start a polymerization reaction. Stabilization of the radical occurs by the delocalization of the radical center over the aromatic ring (Fig. 1.6) [URET-01, URET-02].

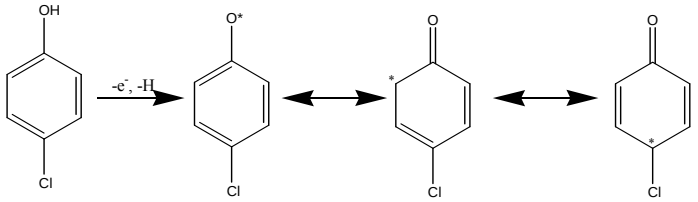

Fig. 1.6: Electro oxidation of 4-cholophenol and delocalization of the radical center over the aromatic ring. After [URET-02].

The (chloro)phenol oxidation and subsequent polymerization pathways have been described postulating a passivation model in which layers of immobile unreactive material are formed at the electrode surface inhibiting further reaction (Fig. 1.7). Initially, there is the formation of high molecular weight material which remains in the vicinity of the electrode surface (A, Fig. 1.7). This leads to locally rapid molecular weight growth resulting in differentiation of the polymeric film structure in an accelerating manner. Once this immobilized material is oxidized to less reactive forms (B, Fig. 1.7), the electrode surface becomes effectively shielded for further reaction. Further reactions than occur by tunneling through this inhibiting layer. [GATT-92, GATT-93, GATT-93b]

Another pathway that can be followed yields quinone like structures which are water soluble (C, Fig. 1.7). It is shown that the way in which the phenoxy radical reacts depends on its formation rate [URET-02]. Higher chlorophenol concentrations and/or low scan rates favor the polymerization and the resulting film behaves as an insulator, passivating the film. On the contrary, lower chlorophenol concentrations and/or high potential scan rates favor the oxidation to quinonic species and the polymer film can be porous enough for charge transfer to continue [URET-02]. Overall it can be concluded that at low potential scan rates, high chlorophenol concentrations and high pH, the formation of films with low porosity is favored [URET-01].

The polymerization rate is also a function of the chlorophenol structure, increasing in the order of pentachlorophenol < 2,4,6-trichlorophenol < 2,4-dichlorophenol < 4-chlorophenol < 2,6-dichlorophenol < 2-chlorophenol. This can be explained by the fact that the additions take place at the *ortho* and *para* positions, irrespective of the nature of the substituent. In case of chlorophenols, steric hindrance by the phenolic OH group directs the radical attack to the *para* position. On the other hand, electronic delocalization in the phenoxy radical leads to bond formation in the polymers through the ortho and mainly para carbon atoms. These effects explain the poor reactivity of all chlorophenols that have the *para* position blocked by a Cl atom. The diminished reactivity of the disubstituted 2,6-dichlorophenol, as compared with the monosubstituted 2-chlorophenol, is probably a consequence of the greater stability, and consequently lower reactivity, of the phenoxy radical at 2,6-dichlorophenol. The increase in the number of *ortho* substituents helps electronic delocalization, which increases the stability [URET-01].

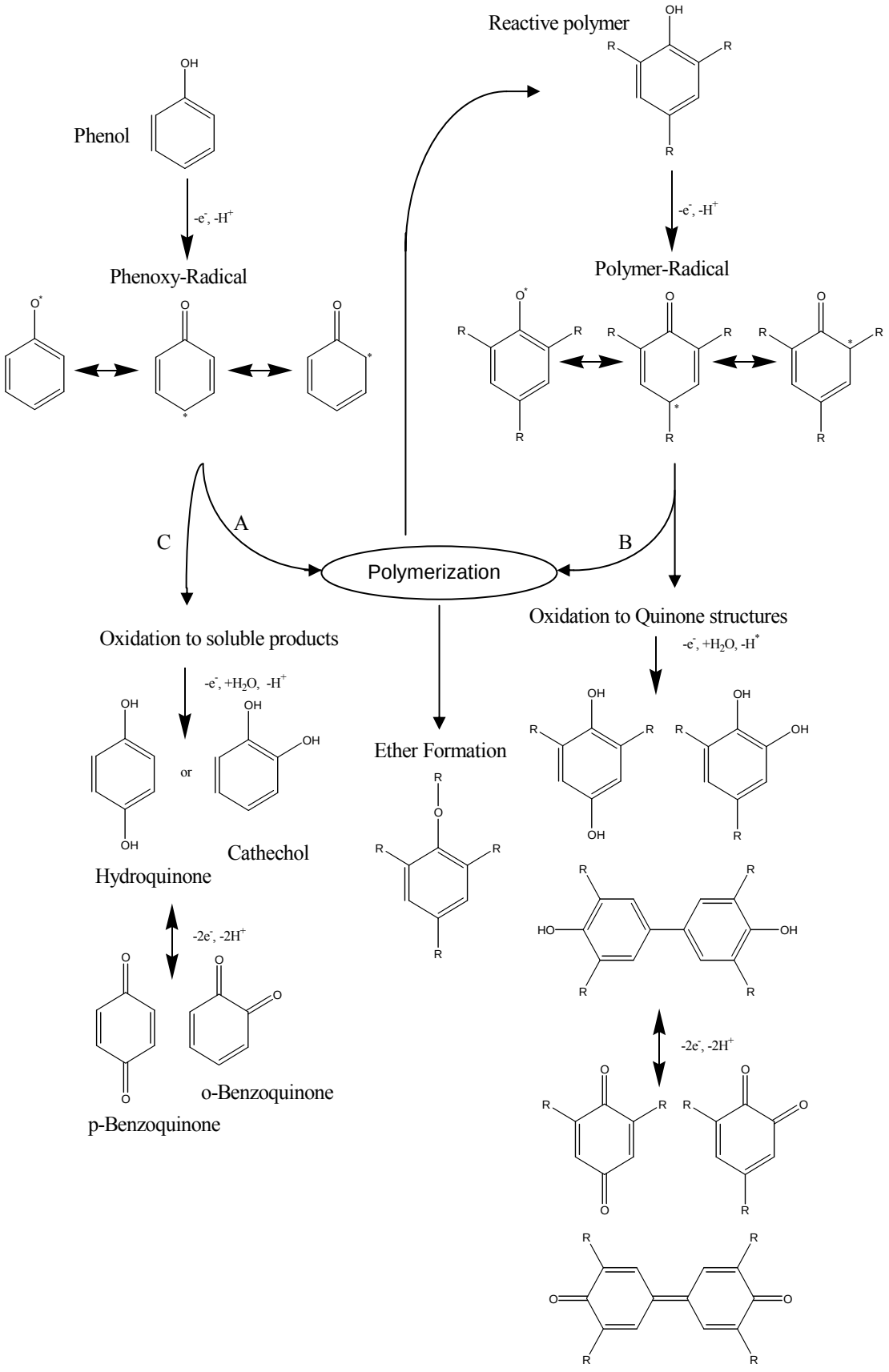

Fig. 1.7: Phenol oxidation and polymerization pathway. [GATT-93, GATT-93b]

In chapter 10, the electrochemical oxidation of 4-chlorophenol with bare gold electrodes and electrodes electrochemically modified with CoTSPc or CuTSPc is discussed.

1.5 References

[AGUI-02] Aguirre M.J., Isaacs M., Armijo F., Basaez L., Zagal J.H., *Electroanalysis*, **2002**, 14, 356-362.

[ALTW-96] Altwicker E.R., *Chemosphere*, **1996**, 33, 1897-1904.

[AMIN-01] Amini M.K., Shahrokhian S., Tangestaninejad S., Mirkhani V., *Anal. Biochem*., **2001**, 290, 277-282.

[ANGE-92] Anger J., Heinzow B., Schaller K.H., Weltle D., Lehnert G., *Fresenius J. Anal. Chem.*, **1992**, 342, 433-438.

[AROC-86] Aroca R., Martin F., *J Raman Spectrosc*., **1986**, 17, 243-247.

[ARRI-94] Arrigan O., *Analyst*, **1994**, 119, 1953-1966.

[AZZA-00] Azzam M.O., Al-Tarazi M., Tahboub Y., *J. Hazardous Mat.*, **2000**, B75, 99-113.

[BARD-01] Bard A.J., Faulkner L.R., *Electrochemical Methods Fundamentals and applications*, second edition, Wiley, New York, **2001**.

[BEVE-67] Bevenue A., Beckman H., *Residue Rev.,* **1967**, 19, 83-134.

[BRAU-07] Braun A., Tscherniak J., *Ber. Dtsch. Chem. Ges.*, **1907**, 40, 271.

[BUTL-92] Butler E.C.V., Dal Pont G., *J. Chromatogr.*, **1992**, 609, 113-123.

[CAMP-05] Campillo N., Aguinaga N., Vinas P., Lopez-Garcia I., Hernandez-Cordoba M., *Anal. Chim. Acta*, **2005**, 552, 182-189.

[CHEB-97] Chebotareva N., Nyokong T., *J. Appl. Electrochem*., **1997**, 27, 975-981.

[CLAC-76] Clack D.W., Hush N.S., Woolsey I.S., *Inorg. Chim. Acta*, **1976**, 19, 129-132.

[CODO-03] Codognoto L., Machado S.A.S., Avaca L.A., *J. Appl. Electrochem.*, **2003**, 33, 951-957.

[CROS-81] Crosby D.G., *Pure Appl. Chem*., **1981**, 53**,** 1051-1080.

[DERU-88] De Ruiter C., Bohle J., De Jong G., Brinckman U., Frei W., *Anal. Chem.*, **1988**, 60, 666-670.

[DIRE-76] *Directive 76/160/EEC*, commission of the European Communities, Brussels, **1975**.

[DURS-97] Durst R.A., Bäumer A.J., Murray R.W., Buck R.P., Andrieux C.P., *Pure Appl. Chem.*, **1997**, 69, 1317-1323.

[DWD-80] *Drinking water directive 80/778/EEC*, Commission of the European communities, Brussels, **1980**.

[ELZI-86] Elzing A., Van Der Putten A., Visscher W., Barendrecht E., *J Electroanal. Chem.*, **1986**, 200, 313-322.

[EXON-84] Exon J.H., Henningsen G.M., Osborne C.A., Koller L.D., *J. Toxicol. Environ. Health*, **1984**, 14, 723-730.

[FICH-13] Fichter F., *Z. Electrochem.*, **1913**, 19, 781.

[FICH-14] Fichter F., *Ber.*, **1914**, 47, 2003.

[FICH-16] Ficher F., *Bull.Soc. Chem.*, **1916**, 19, 281.

[FICH-19] Fichter F., *Helv. Chim. Acta.*, **1919**, 2, 583.

[FINK-00] Finklea D.K., *Self-Assembled Monolayers on Electrodes*, in Encyclopedia of Analytical Chemistry, Vol. 11, ed. Meyers R.A., Wiley, New York, **2000**.

[GALC-95] Galceran M.T., Jauregui O, *Anal. Chim. Acta*, **1995**, 304, 75-84.

[GATT-92] Gattrell M., Kirk D.W., *J. Electrochem. Soc*, **1992**, 139, 2736-2744.

[GATT-93] Gattrell M., Kirk D.W., *J. Electrochem. Soc.*, **1993**, 140, 903-911.

[GATT-93b] Gattrell M., Kirk D.W., *J. Electrochem. Soc.*, **1993**, 140, 1534-1540.

[GHOR-96] Ghorishi S.B., Altwicker E.R., *Chemosphere*, **1996**, 32, 133-144.

[GRIV-03] Griveau S., Gulppi M., Pavez J., Zagal J.H., Bedioui F., *Electroanalysis*, **2003**, 15, 779-785.

[HELL-00] Hell K., Altwicker E.R., Stieglitz L., Addink R., *Chemosphere*, **2000**, 40, 995-1001.

[HITC-95] Hitchman M.L., Spackman R.A., Ross N.C. and Agra C., *Chem. Soc. Rev.,* **1995**, 24(6),423-430.

[KATO-85] Kato M., Nishioka Y., Kaifu K., Kawamura K., Ohno S., *Appl. Chem. Lett.,* **1985**, 86, 196-197.

[KINA-81] Kinae N, Kashizume T, Makita T, Tomita I, Kimura I, Kanamori H., *Water Res.*, **1981**, 15, 17-24.

[KOIL-79] Koile R.C., Johnson D.C., *Anal. Chem.*, **1979**, 51, 741–744.

[KUDE-88] Kuder J. E., *J. Imaging Sci.* **1988**, 32, 51-56.

[KUTN-98] Kutner W.O., Wang J., L'Her M., Buck R.P., *Pure Appl. Chem.*, **1998**, 70, 1302-1318.

[KWAK-91] Kwakman P.J.M., Kamminga D.A., Brinkman U.A.T., De Jong G.J., *J. Chromatograph.*, **1991**, 553, 345-356.

[LABU-00] Labuda J., Vanickova M., Buckova M., Korgova E., *Chem. Papers*, **2000**, 54, 95-103.

[LEPR-82] Lepri L, Desideri P.G., Heimler D, *J. Chromatograph.*, **1982**, 248, 308-311.

[LEVE-87] Lever A.B.P., *Chemtech*, **1987**, 17, 506-510.

[LEZN-89] Leznoff C. C., Lever A. B. P., *Phthalocyanines Properties and Applications Vol. 1.*, VCH Publishers, New York, **1989**.

[LEZN-93] Leznoff C. C., Lever A. B. P., *Phthalocyanines Properties and Applications Vol. 3.*, VCH Publishers, New York, **1993**.

[MAFA-97] Mafatle T., Nyokong T., *Anal. Chim. Acta*, **1997**, 354, 307-314.

[MAGD-02] Magdesieva T.V., Zhukov I.V., Kravchuk D.N., Semenikhin O.A., Tomilova L.G., Butkin K.P., *Russ. Chem. Bull.*, **2002**, 51, 805-812.

[MARE-00] Maree S., Nyokong T., *J. Electroanal. Chem.*, **2000**, 492, 120-127.

[MUNA-05] Muna G.W., Quaiserova-Mocko V., Swain G., *Anal. Chem.*, **2005**, 77, 6542-6548.

[MURR-87] Murray R.W., Ewing A.G., Durst R., *Anal. Chem.*, **1987**, 59, A379-&.

[NYOK-03] Nyokong T., Vilakazi S., *Talanta*, **2003**, 61, 27-35.

[ONI-01] Oni J., Nyokong T., *Anal. Chim. Acta*, **2001**, 434, 9-21.

[ONI-02] Oni J., Westbroek P., Nyokong T., *Electroanalysis*, **2002**, 14, 1165-1168.

[ONI-03] Oni J., Westbroek P., Nyokong T., *Electroanalysis*, **2003**, 15, 847-854.

[OZOE-01] Ozoemena K., Westbroek P., Nyokong T., *Electrochem. Comm.*, **2001**, 3, 529-534.

[OZOE-06] Ozoemena K.I., Nyokong T., *Electrochem. Acta*, **2006**, 51, 5131-5136.

[PERA-04] Pera-Titus M., Garcia-Molina V., Banos M.A., Gimenez J. and Esplugas S., *Appl. Catalysis B: Environmenal*, **2004**, 47, 219-256.

[QI-95] Qi X.Y., Wang G.J., Zhang W.D., Ye X.K., Wu Y., *Chem. J. Ch. Univ.*, **1995**, 16, 791-795.

[REAL-81] Realini P.A., *J. Chromatogr. Sci.*, **1981**, 19, 124-129.

[ROLL-68] Rollman L.D., Iwamoto R.T., *J. Am. Chem. Soc.*, **1968**, 90, 1455.

[RUAN-93] Ruana J., Urbe I., Borrull F., *J. Chromatograph., A*, **1993**, 665, 217-226.

[SARK-85] Sarkka J., *Chemosphere*, **1985**, 14, 469-491.

[SATE-01] Saterlay A.J., Foord J.S., Compton R.G., *Electroanalysis*, **2001**, 13, 1065-1070.

[SAVI-92] Savinova E.R., Yashnik S.A., Savinov E.N., Parmon V.N., *React. Kinet. Catal. Lett*., **1992**, 46, 249-254.

[SIAN-05] Siangproh W., Chailapakul O., Laocharoensuk R., Wang J., *Talanta*, **2005**, 67, 903-907.

[SIMI-83] Simic-Glavaski B., Zecevic S., Yeager E., *J. Electroanal. Chem*., **1983**, 150, 469-479.

[SISW-06] Siswana M, Ozoemena K.I., Nyokong T., *Talanta*, 69, 1136-1142.

[SOUT-01] Southampton electrochemistry group, *Instrumental methods in electrochemistry*, Horwood Publishing Ltd., **2001**.

[STAF-97] Stafford U., Gray K.A., Kamat P.V., *J. Catalysis*, **1997**, 167, 25-32.

[SULI-06] Suliman F.E.O., Al-Kindi S.S., Al-Kindy S.M.Z., Al-Lawati H.A.J., *J. Chromatogr. A*, **2006**, 1101, 179-184.

[TEMO-89] Temofonte T. A., Schoch K. F., *J. Appl. Phys.*, **1989**, 65, 1350-1355.

[TERA-02] Terashima C., Rao T.N., Sarada B.V., Tryk D.A., Fujishima A., *Anal. Chem.*, **2002**, 74, 895-902.

[THAM-02] Thamae T., Westbroek P., Nyokong T., *Microchim. Acta*, **2002**, 40, 233-239.

[TONO-03] Tonokura K., Nakamura T., Koshi M., *Anal. Sci.*, **2003**, 19, 1109-1113

[URET-01] Ureta-Zanartu M.S., Bustos P., Diez M.C., Mora M.L., Gutierrez C., *Electrochim. Acta*, **2001**, 46, 2545-2551.

[URET-02] Ureta-Zanartu M.S., Bustos P., Berrios C., Diez M.C., Mora M.L., Gutierrez C., *Electrochim. Acta*, **2002**, 47, 2399-2406.

[URET-03] Ureta-Zanartu M.S., Berrios C., Pavez J., Zagal J., Gutierrez C., Marco J.F., *J. Electroanal. Chem.,* **2003**, 553, 147-156.

[VENI-94] Veningerova M., Prachar V., Uhnak J., Lukacsova M., Trnovec T., *J. Chromatograph., B*, **1994**, 657, 103-110.

[VILA-01] Vilakazi S., Nyokong T., *J Electroanal. Chem*., **2001**, 512, 56-63.

[VLAR-04] *Bijlage bij het besluit van de Vlaamse regering van 1 juni 1995 houdende algemene en sectorale bepalingen inzake milieuhygiëne*, **2004**.

[VUOR-85] Vuorinen P.J., *Chemosphere*, **1985**, 14, 1729-1740.

[WAGN-74] Wagnerova D.M., Scherwtnerova E., Veprek-Siska J., *Collection Czechoslov. Chem. comm.*, 1974, 39, 1980-1988.

[WALD-03] Waldner G., Pourmodjib M., Bauer R. and Neumann-Spallart M., *Chemosphere*, **2003**, 50, 989-998.

[WANG-91] Wang J., *Electroanalysis*, **1991**, 3, 255-259.

[WEBB-65] Webber J.H., Busch D.H., *Inorg. Chem.*, **1965**, 4, 469-471.

[WEBE-99] Weber R., Hagenmaier H., *Chemosphere*, **1999**, 38, 529-549.

[WHO-89] *Chlorophenols Other Than Pentachlorophenol (Environmental Health Criteria, 93)*, WHO, Geneva, **1989**.

[ZAGA-77] Zagal J.H., Sen R.K., Yeager E., *J Electroanal. Chem.*, **1977**, 83, 207-213.

[ZAGA-99] Zagal J.H., Gulppi M.A., Caro C.A., Cardenas-Jiron I., *Electrochem. Comm.*, **1999**, 1, 389-393.

[ZILO-06] Zilouei H., Guieysse B., Mattiasson B., *Process Biochem.*, **2006**, 41, 1083-1089.

Chapter 2:
Formation of phthalocyanine thin films on gold electrodes

The electrochemical behavior and properties of gold electrodes, modified with phthalocyanines have been studied intensively in our laboratory in the past [DEWA-04, DEWA-05, DEWA-05b, DEWA-05c]. To modify the electrodes, in this work, three different techniques were selected: immersion, drop-drying and electrodeposition. In this chapter these three preparation methods are shown. Moreover, for the preparation of the electrodes, the electrodeposition and the study of the target molecules, cyclic voltammetry has been used. Therefore, in the first section of this chapter the principles of cyclic voltammetry are explained. In the second section, the electrochemical cell configuration used to perform the cyclic voltammetry is described and in the third section the modification procedure of the three electrochemical techniques is dicussed.

2.1 Cyclic voltammetry [OLDH-94, KISS-96, SOUT-01, BARD-01]

2.1.1 Principle

Cyclic voltammetry (CV) is an extension of linear sweep voltammetry (LSV). [BARD-01, OLDH-94, KISS-96, SOUT-01]. In linear sweep voltammetry, the potential is varied as a function of time in one direction between the limits E_1 and E_2 at a known scan rate, v.

In cyclic voltammetry, the waveform is initially the same as in LSV, but upon reaching the potential E_2 (vertex potential), the direction of the sweep is reversed (usually at the same scan rate) instead of terminated. When the initial potential, E_1, has been reached again, there are several possibilities: the potential sweep may be halted, reversed, or alternatively continued further to value E_3. In both LSV and CV experiments, the cell current is recorded as a function of the applied potential resulting in a voltammogram. The potential-time waveforms used in cyclic

voltammetry are shown in Fig. 2.1. In what follows, the current-potential behavior is described for two different situations.

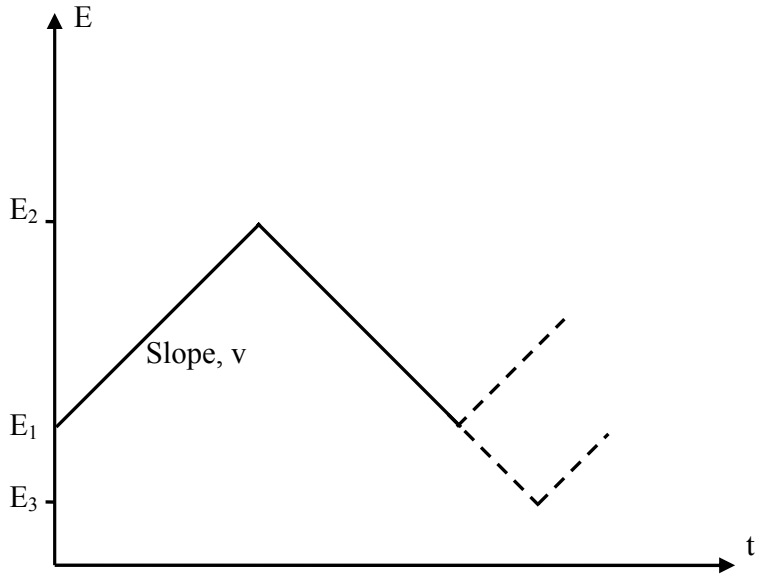

Fig. 2.1: Potential-time profiles for cyclic voltammetry. After [SOUT-01]

2.1.2 Reaction of a particle in solution

Let us first consider a simple reversible reaction where a reducing agent R is oxidized to an oxidizing agent O as described by Eq. 2.1 with a stationary electrode configuration assuming semi-infinite linear diffusion and assume that only R is initially present in solution.

$$R - ne^- \leftrightarrow O \qquad \text{(Eq. 2.1)}$$

(Charges have been omitted for the clarity of the presentation.)

At the moment oxidation starts, two competitive effects occur. The first is an increase in the oxidation rate of R which causes an increase in current. At the same moment, the concentration of R decreases from its bulk value in order to satisfy the Nernst equation and a concentration gradient is set up. As a result, a current proportional to the value of this new concentration at the electrode surface flows in the external circuit. Once this gradient exists, it does not remain constant but starts to

relax owing to diffusion. At the same moment the electrode potential still changes and therefore the surface concentration of R further decreases until it effectively reaches zero. Once the concentration of R reaches zero at the electrode surface, the concentration gradient starts to decrease, due to the relaxation effect and hence the current flowing must decrease. Overall, this behavior gives rise to a peak shaped current-potential response as shown in Fig 2.2.

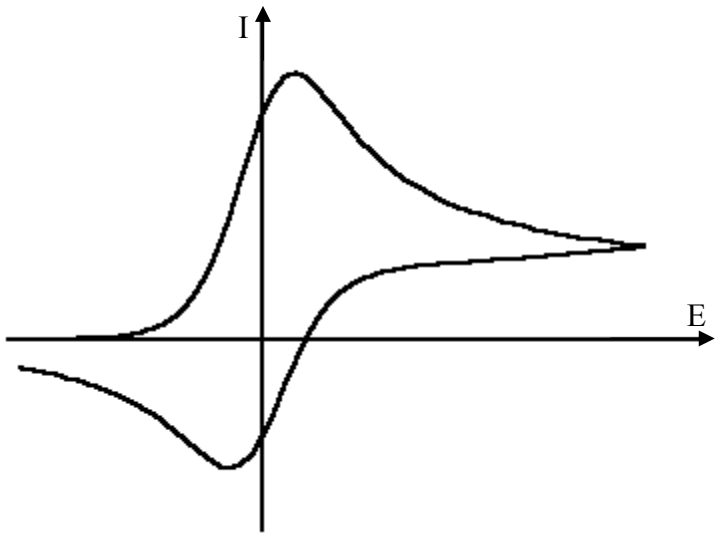

Fig 2.2: Cyclic voltammogram for a reversible process. After [SOUT-01]

After reaching the vertex potential, there is a significant concentration of O present near the electrode and O is still formed in the beginning of the reverse sweep until the potential has reached a value high enough to start the reduction of O near the electrode. This results in an increase in the cathodic current and a change of polarity of the total current. Using similar arguments as were used for the forward sweep, it can be shown that the current on the reverse sweep will also exhibit a peaked response though of opposite sign. The peak current of the oxidation as well as the reduction is given by the Randles-Sevcik equation shown in Eq. 2.2 [BARD-01].

$$I_p = (2.69 \times 10^5) n^{3/2} A c_i D_i^{1/2} v^{1/2} \qquad \text{(Eq. 2.2)}$$

where I_p is the peak current in A, n the number of electrons involved in the electrode reaction, A the surface area in cm^2, c_i the concentration of species i in mol cm^{-3}, D_i the diffusion coefficient of species i in cm^2 s^{-1} and v the scan rate in V s^{-1}.

In the case of the reversible system discussed above, the electron transfer rates at all potentials are significantly greater than the rate of mass transport, and therefore Nernstian equilibrium is always maintained at the electrode surface. When the rate of electron transfer is insufficient to maintain the surface equilibrium, then the shape of the cyclic voltammogram changes. The most noticeable effect is the increase between the peak potential of the oxidation process and the peak potential of the reduction process which is called the peak separation. The peak current of an irreversible system is given by Eq. 2.3 [BARD-01]

$$I_p = (2.99 \times 10^5)\alpha^{1/2} A c_i D_i^{1/2} v^{1/2} \qquad \text{(Eq. 2.3)}$$

where the symbols are as for Eq. 2.2 and α the transfer coefficient.

It is quite common for a process that is reversible at low scan rates to become irreversible at higher ones after passing through a region known as *quasi-reversible* at intermediate values. This transition occurs when the relative rate of the electron transfer with respect to that of mass transport becomes insufficient to maintain Nernstian equilibrium at the electrode surface (Fig. 2.3).

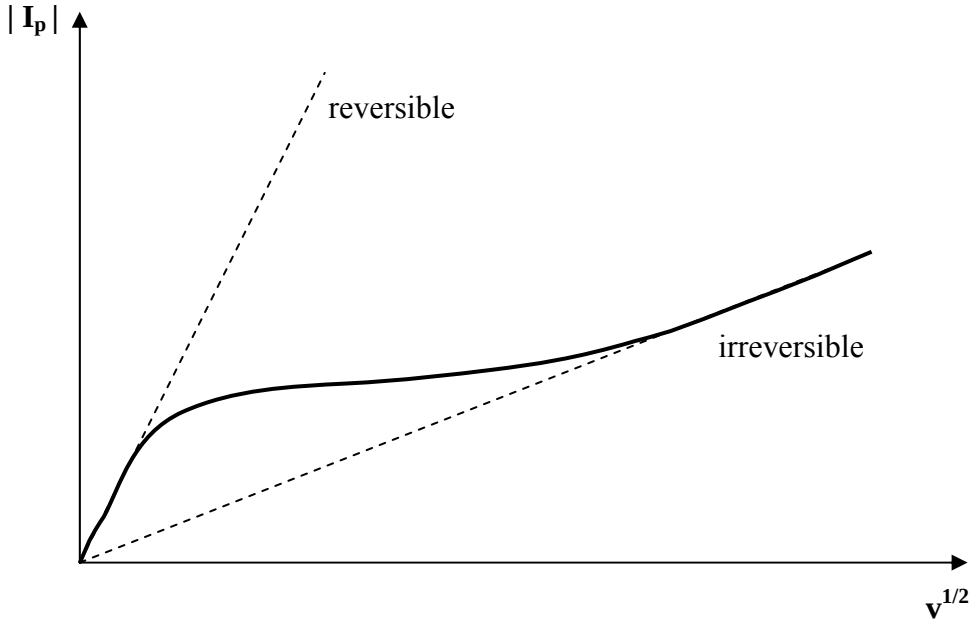

Fig. 2.3: Plot of the transition from reversible to irreversible behavior with increasing sweep rate. After [SOUT-01]

For this work, the most important feature of CV is that the peak current is proportional to the concentration of the reactive component in solution. This makes the quantitative determination of the concentration of a target molecule (in this case 4-Cp (see chapter 10)) possible after a calibration curve has been established.

2.1.3 Reaction of an adsorbed particle

The current-potential behavior of electrode reactions can be affected quite significantly by the adsorption of R or O. The interpretation of these curves is more complicated than those involving only dissolved species. Therefore, adsorption is an effect to be avoided if possible. However, adsorption of a species is sometimes a prerequisite for rapid electron transfer and can be of major importance in processes of practical interest. The negative as well as the positive effects of adsorption are observed in literature and fields adjacent to the research described in this work. It is indeed described that phthalocyanines are electrochemically adsorbed on a gold electrode and can be used as electron transfer mediator [DEWA-05c]. During the oxidation of chlorophenol, however, there is a decrease of current with time due to the fouling of the electrode, which is not wanted [URET-01].

Because of the above mentioned complexity of the adsorption processes, the reader is referred for a complete theoretical description to the literature [NOEL-90]. Only the simplest case is considered here, where only the adsorbed forms of R or O are electroactive in the potential range under investigation; where there are no mutual lateral interactions between R nor between O and where adsorbed R produces adsorbed O with no adsorption or desorption occurring during the scan. These are the conditions for the so called Langmuir isotherm, an adsorption isotherm introduced by Bard to describe the adsorption process in an electrochemical system. [BARD-01]

The analysis of such a system is fairly straightforward as mass transport reactions can be ignored. If the electron transfer is reversible then a cyclic voltammogram as shown in Fig. 2.4 will be obtained. The major difference when compared to a voltammogram for a reaction in which both product and reactant are soluble (Fig. 2.2) is that the peaks are sharp and symmetrical and the current rises from essentially zero to a peak value and then falling again to zero. There is little or no peak separation and the charges associated with anodic and cathodic processes are equal. The symmetrical peak arises because of the fixed amount of reactant. Only R

on the surface at the start of the sweep can be oxidized. The actual value of I_P depends on the amount of adsorbed R or O and in a case Langmuir equilibrium is assumed given by Eq. 2.4.

$$I_P = \frac{n^2F^2}{4RT} vA\Gamma_O^* \qquad \text{(Eq. 2.4)}$$

where I_P is the peak current in A, n the number of electrons involved in the electrode reaction, F the Faraday constant in C mol^{-1}, R the universal gas constant in J mol^{-1} K^{-1}, T the temperature in K, v the scan rate in V s^{-1}, A the surface area in cm^2 and Γ_O^* the surface excess of the adsorbed species in mol cm^{-2} before the reaction starts.

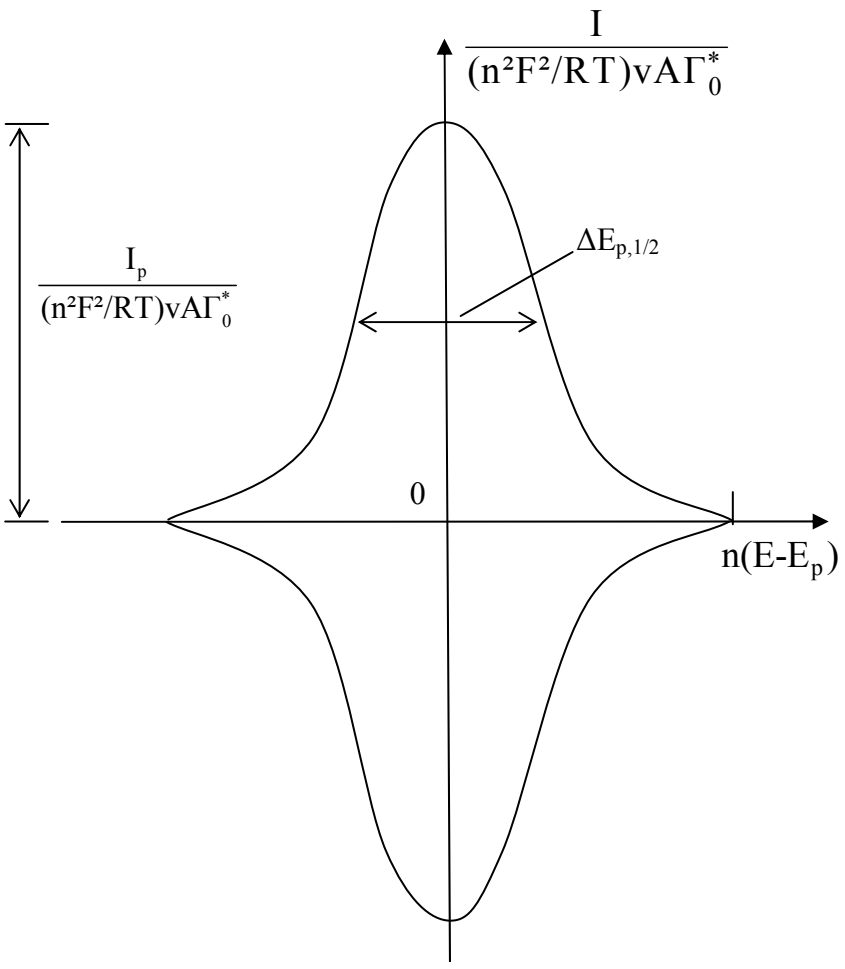

Fig. 2.4: Cyclic voltammatric curve for oxidation of absorbed R and subsequent reduction. After [BARD-01]

The peak current, and also the current at each point of the wave, is proportional to v, in contrast to the $v^{1/2}$ dependence observed for Nernstian waves of diffusing species (Eq. 2.2). The proportionality between I and v is the same as that observed for a purely capacitive current, and this fact has led to some treatments of adsorption in terms of pseudocapacitances. The area under the reduction wave, corrected for any residual current, represents the charge required for the full reduction of the layer, that is, $nFA\Gamma_O^*$.

For non Nernstians systems the shape of the cyclic voltammogram changes. For an irreversible case the forward peak ceases to be symmetric (Fig. 2.5), and there is no reverse peak. The peak current is given by Eq. 2.5

$$I_P = \frac{\alpha F^2 A v \Gamma_O^*}{2.718RT} \qquad \text{(Eq. 2.5)}$$

where the symbols are as for Eq. 2.4 and α the transfer coefficient.

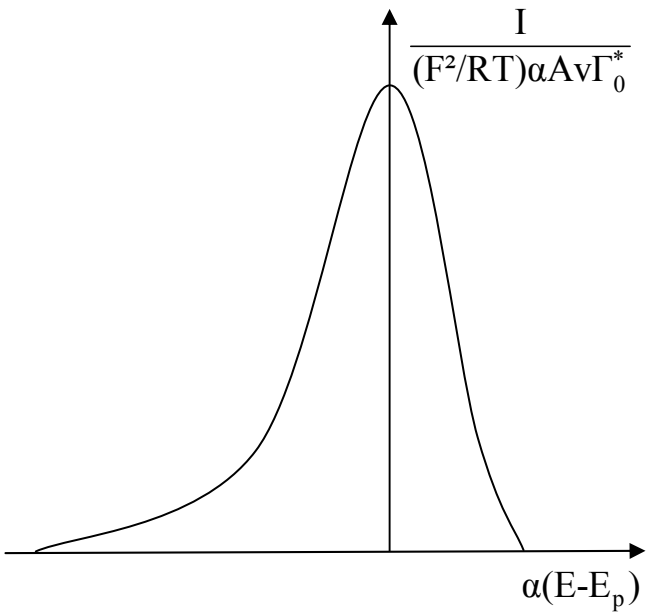

Fig. 2.5:Voltammogram for a system where adsorbed R is irreversibly oxidized. After [BARD-01]

For quasi-reversible reactions there will be a reverse peak but both peaks will be asymmetric and the peak potentials will not be coincident. For a more detailed description, there is referred to literature [LAVI-74, LAVI-74b, SRIN-68].

2.2 Electrochemical cell [SOUT-01]

The electrochemical cell consists primarily of the electrodes and the electrolyte, together with a container. For the cyclic voltammetry measurements three electrodes are commonly used: a working electrode which defines the interface under study, a reference electrode which maintains a constant reference potential, and a counter electrode which supplies the current. A potentiostat connected with the electrodes and a computer is used to control the measurements.

During this work, a small cylindrical container made from glass was used with a volume of 40 mL. The container is closed with a lid containing four holes. Three of these holes were used for the electrodes and the fourth one was used for the insertion of a glass tube which makes the bubbling of the solution with nitrogen gas possible. It is indeed important that the measurements are performed in an oxygen free environment since the oxygen reduction interferes with other electrochemical processes and it influences the electrode properties significantly (see later).

A saturated calomel electrode (SCE) with two compartments (Radiometer) was used as the reference electrode during this work. This is probably the most widely used reference electrode and has a reference potential of 0.241 V vs. standard hydrogen electrode. [SOUT-01]

The purpose of the counter electrode is to supply the current required by the working electrode without in any way limiting the measured response of the cell. It is essential that the electrode process is the decomposition of the electrolyte medium or the oxidation/reduction of a component of the electrolyte and that it has a large surface area compared to the working electrode so that the current flows without the need of a large overpotential. In this case, a carbon counter electrode purchased from Le Carbonne Lorraine was used.

The gold electrodes were purchased from Bioanalytical systems (BAS) (West Lafayette, USA). They are small disc electrodes with a diameter of 1.6 mm. The polycrystalline gold is encapsulated in PCTFE (polychlorotrifluoroethylene), which is

resistant towards the majority of the aqueous solutions [BAS-06]. A metal pin is attached at the back side of the gold electrode to make electrical contact possible. The gold electrodes were pretreated by mechanical and electrochemical polishing to create a reproducible surface. First the electrode surface was scoured briefly on 1200 grit SiC-emery paper to obtain a fresh surface. To smooth this relatively rough surface it was further subjected to sequential polishing on a polishing cloth covered with alumina (Buehler) powder of 1, 0.3, 0.05 μm for 5, 10 and 20 minutes respectively. To remove any adherent Al_2O_3 particles the electrode surface was rinsed thoroughly with doubly deionised water and cleaned in an ultrasonic bath (Branson 3210) for 2 minutes. Finally the electrode was pretreated electrochemically by scanning in a $NaOH/Na_2HPO_4$ pH 12 buffer solution, between -1.2 and 0.6 V vs. SCE until 5 subsequent cyclic voltammograms (scans) were identical [DEWA-04].

As indifferent electrolyte, a pH 12 buffer solution was purchased from VWR International. The cobalt(II) tetrasulphophthalocyanine tetrasodiumsalt.$2H_2O$ (CoTSPc) has been purchased from the Rhodes University of Grahamstown, Eastern Cape, South Africa (Department of Chemistry). Other suppliers of CoTSPc are Porphyrin Systems (Lübeck, Germany) and Mid-Century (Posen, USA). Unless otherwise noted, CoTSPc from South-Africa has been used for the experiments. The 3,4',4'',4''' copper(II) tetrasulphophthalocyanine tetrasodiumsalt.$2H_2O$ (CuTSPc) has been purchased from Sigma Aldrich (USA). Suppliers of copper(II) tetrasulphophthalocyanine tetrasodiumsalt.$2H_2O$ with the sulphonic groups randomly placed on the phthalocyanine structure are Mid-Century (Posen, USA) and Sigma Alldrich (USA). Unless otherwise noted, 3,4',4'',4''' copper(II) tetrasulphophthalocyanine tetrasodiumsalt.$2H_2O$ from Sigma-aldrich has been used for the measurements. The target molecule, 4-chlorophenol, has been purchased from VWR International (Leuven, Belgium). All species used during this work are at least of analytical grade.

A PGSTAT 20 potentiostat from ECO Chemie (the Netherlands) controlled by a GPES 4.9 software package [ECOC-96] running on a Pentium II computer was used to record the CV curves.

2.3 Electrochemical modification techniques

The first modification technique ("immersion method") involved the immersion of a gold electrode in a CoTSPc or CuTSPC pH 12 buffer solution for 120 minutes. After the modification, the electrode was scanned in a pH 12 buffer solution without CoTSPc or CuTSPc in order to study the electrochemical behavior of the modified electrode and to obtain information about the amount of CoTSPc or CuTSPc deposited on the gold surface.

In the second technique ("drop-drying method"), the gold electrode was modified by depositing a 20 μL droplet of a CoTSPc or CuTSPc pH 12 buffer solution on its surface. When the solution was dried, the modified electrode was scanned in a pH 12 buffer solution without CoTSPc or CuTSPc.

During the third modification procedure ("potential cycling method"), a gold electrode was modified with CoTSPc or CuTSPc by recording successive cyclic voltammetric scans (100 scans) in a potential window from -1.2 to 0.6 V versus SCE in a pH 12 buffer solution containing CoTSPc or CuTSPc. After completion of the electrochemical deposition experiment, the modified electrode was further scanned in the buffer solution in the absence of CoTSPc or CuTSPc.

2.4 References

[BARD-01] Bard A.J., Faulkner L.R., *Electrochemical Methods Fundamentals and applications*, second edition, Wiley, New York, **2001**.

[BAS-06] Bioanalytical systems website, *www.bioanalytical.com/products/ec/sve.html*

[DEWA-04] De Wael K., Westbroek P., Temmerman E., *J. electroanal. Chem.*, **2004**, 567, 167-173.

[DEWA-05] De Wael K., Westbroek P., Bultinck P., Depla D., Vandenabeele P., Adriaens A., Temmerman E., *Electrochem. Comm.*, **2005**, 7, 87-96.

[DEWA-05b] De Wael K., Westbroek P., Adriaens A., Temmerman E., *Electrochem. solid st.*, **2005**, 8(4), C65-C68.

[DEWA-05c] De Wael K., Westbroek P., Temmerman E., *Electroanal.*, **2005**, 17, 263-268.

[ECOC-96] Eco Chemie B.V., User manual for General purpose Electrochemical System for Windows (version 4.9), Utrecht, **1996.**

[KISS-96] Kissinger P.T., Heineman W.R., *Laboratory techniques in electrochemical chemistry*, second edition, Marcel Dekker, New York, **1996**.

[LAVI-74] Laviron E., *J. Electroanal. Chem.*, **1974**, 52, 355-393.

[LAVI-74b] Laviron E., *J. Electroanal. Chem.*, **1974**, 52, 395-402.

[NOEL-90] Noel M., Vasu K.I., *Cyclic Voltammetry and the Frontiers of Electrochemistry*, Aspect Publications, London, **1990**.

[OLDH-94] Oldham H.B., Myland J.C., *Fundamentals of electrochemical science*, Academic Press, New York, **1994**.

[SOUT-01] Southampton electrochemistry group, *Instrumental methods in electrochemistry*, Horwood Publishing Ltd., **2001**.

[SRIN-68] Srinivasan S., Gileadi E., *Electrochim. Acta*, **1968**, 13, 721.

[URET-01] Ureta-Zanartu M.S., Bustos P., Diez M.C., Mora M.L., Gutierrez C., *Electrochim. Acta*, **2001**, 46, 2545-2551.

Chapter 3:
Spectroscopic characterization

Three spectroscopic techniques, synchrotron micro X-ray fluorescence spectroscopy (SR-XRF), X-ray photoelectron spectroscopy (XPS) and UV-Vis spectroscopy have been used to study the modified gold electrodes and the phthalocyanine solutions used during the modification. Since SR-XRF has been used for a detailed study of the micro-structure and the heterogeneity of the phthalocyanine thin films in this work, it is discussed in this chapter in detail. This discussion covers in the first section a brief historical description of X-rays and the electromagnetic spectrum, followed by an overview of the characteristics of synchrotron induced X-rays and the interaction of X-rays with matter. In the second section of the chapter, the principle of X-ray fluorescence (XRF) spectroscopy is explained, followed by a theoretical overview on the X-ray resonant Raman scattering (XRRS) which was found to be an important interference in case of XRF-measurements on CuTSPc thin films. In the fourth section, the synchrotron facility used at HASYLAB (Hamburg, Germany) and the experimental setup used in this work are shown. In the fifth section, a description of the fundamental parameter method used for the quantification of the XRF data is given. In the final section, the two other spectroscopic techniques, XPS and UV-Vis are briefly described.

3.1 X-rays [VANG-01]

X-rays were discovered in 1895 by Wilhelm Conrad Röntgen. It is electromagnetic radiation having wavelengths roughly within the range from 0.005 to 10 nm. At the short-wavelength end, X-rays overlap with γ-rays, and at the long-wavelength end, they approach the ultraviolet radiation (Fig. 3.1). X-ray fluorescence spectroscopy (XRF) is based on the use of X-ray excitation to induce element specific fluorescence in the X-ray regime within the irradiated sample. XRF provides the identification of the chemical elements present in the sample by means of their characteristic X-ray energies or wavelengths. The method allows the quantification of

a given element by first measuring the emitted characteristic line intensity and then relating this intensity to element concentration. While the roots of XRF go back to the early part of this century with the classic work of Henry Mosely in 1912, it is only during the last 35 years that the technique has gained major significance as a routine means of analysis. [JENK-99]

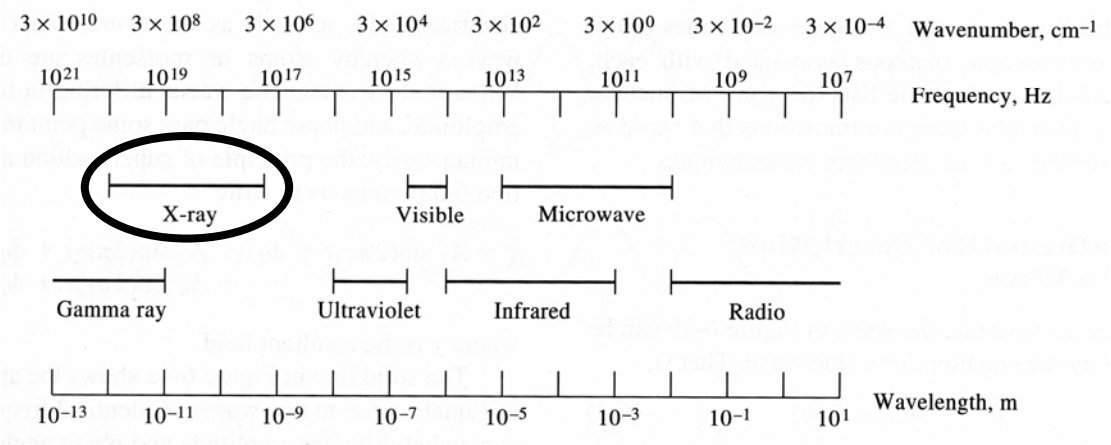

Fig. 3.1: Overview of the electromagnetic spectrum. After [SKOO-97]

3.1.1 Synchrotron induced X-rays

In the present work, X-rays (or synchrotron radiation) produced by a synchrotron source have been used for analysis. It has been known for almost 100 years that the acceleration of a charged particle results in the radiation of electromagnetic energy, which is the principle of the generation of synchrotron radiation in facilities called synchrotron storage rings. A synchrotron storage ring consists of a near-circular vacuum tube in which 'bunches' of high-energy electrons or positrons are stored as they circulate near the velocity of light under the control of synchronized electromagnetic fields. The electrons/positrons are guided through the ring by steering, focusing and bending magnets and the energy loss is compensated by the input from radiofrequency cavities. Each bending magnet perturbs the electron/positron path from a straight line into a circular arc by an inward centripetal force. As each 'bunch' of charged particles is accelerated inwards, an instantaneous jet of 'white' electromagnetic radiation (mainly tuned for the X-ray regime) is emitted along the forward tangent in the form of a fan emanating from each bending magnet.

In the 1960s the first generation of synchrotrons were developed as 'colliders' for high energy physics. The second generation, the so-called 'dedicated' synchrotron sources were built in the 1970s and 1980s when storage rings were optimized as source for synchrotron radiation. In the 1990s, the third generation of synchrotrons started their operation (ESRF, APS, Spring 8) providing X-rays sources of much higher brilliance and intensity from high performance storage rings. The high-performance was derived from two developments: the optimized magnetic lattice design that increases the brilliance, and the use of insertion devices (wigglers and undulators placed between the bending magnets) as the main source of synchrotron radiation which provide increased flux density. [CHUN-00]

The synchrotron produced X-ray beams have unique properties that make them desirable for use. One of the main advantages of synchrotron X-ray beams is associated with their uniquely high intensity, which is orders of magnitude higher than that produced by conventional X-ray sources, such as X-ray tubes. They have a continuous energy distribution whit a maximum intensity at the critical photon energy so that monoenergetic/tunable beams can be produced over a wide range of energies by the use of monochromators. The emitted radiation is highly polarized in the plane of the electron or positron beam orbit, which is extremely important for background reduction in synchrotron radiation induced X-ray emission (see §2.4) type experiments in particular. The X-rays are emitted in a continuous band in the horizontal direction but are highly collimated in the vertical direction. It is therefore possible to produce intense beams with little angular divergence. The source size is small and, as a result, the production of intense beams of small area is feasible. The synchrotron source is a pulsed source because the electrons or positrons form bunches which need short time to pass the bending magnet or its aperture. The X-rays are produced in narrow bursts, less than 1 ns in width, and have a time between pulses of around 20 ns or more.

The main parameters of interest in defining a synchrotron source are the magnitude of the stored electron/positron current, the source brightness (photons s^{-1} $mrad^{-2}$ per 1% bandwidth) or the brilliance (brightness normalized for the area of the source) [KOCH-83] and its machine energy. Typically, currents are in the range from 100 to 1000 mA [CHUN-00]. The most important parameters of the DORIS III synchrotron storage ring at HASYLAB (Hamburg, Germany), used during this research (see section 3.4), are given in table 3.1

Table 3.1: Most important parameters of the DORIS III synchrotron ring at HASYLAB (Hamburg, Germany). After [HASY-06]

Positron energy:	4.45 GeV
Initial positron beam current	140 mA
Bunch separation	192 ns
Critical photon energy from bending magnets	16.6 keV
Brightness (at around 8 keV)	3 x 10^{14} photons s^{-1} $mrad^{-2}$ per 1% bandwidth

3.1.2 Interaction of X-rays with matter

During the interaction of X-rays with matter, there are three important interaction types: photoelectric effect, Rayleigh (elastic) and Compton (inelastic) scattering [VINC-99]. The photoelectric effect involves the absorption of a photon by fully transferring its energy to an inner-shell electron, which becomes energetically possible when the energy of the exciting photon is higher than the binding energy of the electron in question. This results in the ejection of the electron (photoelectron) from the absorbing atom leaving the atom in an electronically excited level. The kinetic energy of the ejected photoelectrons is given by the difference between the incident photon energy and the atomic binding energy of the electron.

Rayleigh scattering is an elastic process by which photons are scattered by bound atomic electrons and in which the atom is neither ionized nor excited. The incident photons are scattered with unchanged frequency/energy and with a definite phase relation between the incoming and scattered waves.

Compton scattering is an inelastic scattering interaction of a photon with a free or a weakly bound electron that is considered to be at rest. In this case the energy of the incoming photon is partially tranferred to the scattering electron, resulting in a reduced energy of the scattered photon as a function of scattering-angle. The weak binding of electrons to atoms may be neglected since the momentum transferred to the electron greatly exceeds the momentum of the electron in the bound state. [VANG-01]

When a narrow, parallel, and monochromatic beam with intensity I_0, passes through homogenous matter with density ρ and thickness t (Fig. 3.2), the transmitted intensity I is given by the exponential Lambert-Beer law (Eq. 3.1) [GAUG-03]

$$I = I_0 \, e^{-\mu\rho x} \qquad \text{(Eq. 3.1)}$$

where I is the transmitted intensity, I_0 the incident intensity, μ the mass attenuation coefficient in $cm^2 \, g^{-1}$, ρ the density of the material in $g \, cm^{-3}$ and x the thickness of the absorber in cm.

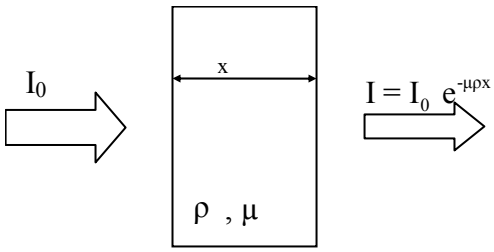

Fig. 3.2: Absorption of X-rays by matter. After [GAUG-03]

The number of photons (intensity) is reduced by passage through matter but their energy is generally unchanged. The term μ is called the mass attenuation coefficient. The product of μ with ρ gives μ_L, which is called the linear absorption coefficient (cm^{-1}). The absorption length λ is the inverse of μ_L. The term μ(E) is often also called the mass absorption coefficient for X-ray absorption at energy E. This value increases with increasing atomic number (Z) indicating that low Z-materials attenuate X-rays of a given energy less than high Z-elements. A given material will in general attenuate high energy (i.e. hard) X-rays less than low energy (i.e. soft) X-rays, except in the vicinity of the so-called absorption edges where μ(E) shows strong discontinuities, i.e., sudden increase ("jumps") as a given photoelectric absorption process becomes energetically allowed. These absorption edges correspond to the binding energies of given atomic electronic shells. [JENK-99, GAUG-03]

When the photoelectric effect, the Compton and Rayleigh scatter are taken into account, the mass attenuation coefficient can be calculated from their respective attenuation coefficients (Eq. 3.2).

$$\mu = \tau_Z + \sigma_{R,Z} + \sigma_{C,Z} \qquad \text{(Eq. 3.2)}$$

where μ is the total mass attenuation coefficient and τ_Z, $\sigma_{R,Z}$ and $\sigma_{C,Z}$ in $cm^2\ g^{-1}$ are the mass attenuation coefficients according to the photoelectric effect, Rayleigh and Compton scatter respectively.

The values of τ_Z, $\sigma_{R,Z}$ and $\sigma_{C,Z}$, can be calculated by using compiled data libraries, such as the Evaluated Photon Data Library, '97 Version (EDPL97) [CULL-97]. The photoelectric effect, the Rayleigh and Compton scattering can take place respectively with the transition probabilities P:

$$P_{photo}(E,Z) = \frac{\tau_Z(E)}{\mu(E)} \qquad \text{(Eq. 3.3)}$$

$$P_{Rayleigh}(E,Z) = \frac{\sigma_{R,Z}(E)}{\mu(E)} \qquad \text{(Eq. 3.4)}$$

$$P_{Compton}(E,Z) = \frac{\sigma_{C,Z}(E)}{\mu(E)} \qquad \text{(Eq. 3.5)}$$

where the same symbols have been used as in the previous equation. [VINC-04]

If the absorber is a chemical compound or a mixture, its mass attenuation coefficient can be obtained from the coefficients μ_i for the constituent elements according to the weighted average, as given in Eq. 3.6.

$$\mu = \sum_{i=1}^{n} W_i\ \mu_i \qquad \text{(Eq. 3.6)}$$

where μ is the mass attenuation coefficient in $cm^2\ g^{-1}$, W_i is the weight fraction of the *i*th element and n is the total number of elements in the absorber.

For situations more complicated than the narrow-beam geometry, the attenuation is still basically exponential, but it is modified by two additional factors. The first is the so called geometry factor, depending on the source absorber geometry. The other factor, often called the buildup factor, takes into account secondary photons produced in the absorber, mainly the result of one or more Compton scatters, which finally reach the detector. [VANG-01]

3.2 Principle of XRF [VANG-01, GAUG-03, JENK-99]

Fig. 3.3 shows the principle of the X-ray fluorescence phenomenon. As a first step of this process, an inner shell electron is ejected by the incident photon in the X-ray region (photoelectric effect) leaving the atom in an excited state. During the relaxation process, an electron transition takes place from a higher energy level to fill the created vacancy as a result of the photoelectric process, which in turn results in the emission of a so-called X-ray fluorescence photon or may result in the emission of a so-called Auger-electron (radiationless relaxation). The energy of the emission line can be calculated as the difference between two energy terms, each term corresponding to a definite state of the atom. If E_1 and E_2 are the values representing the energies of the corresponding levels, the frequency ν of an X-ray line is given by Eq. 3.7.

$$\nu = \frac{E_1 - E_2}{h} \qquad \text{(Eq. 3.7)}$$

where E_1 and E_2 are the respective energies of the corresponding electronic levels of the given transition in eV, h Planck's constant (4.136×10^{-15} eV s) and ν in s^{-1} the frequency of the emitted photon. The energy of the given transition (hν) is characteristic to the element in question, making elemental analysis by XRF possible.

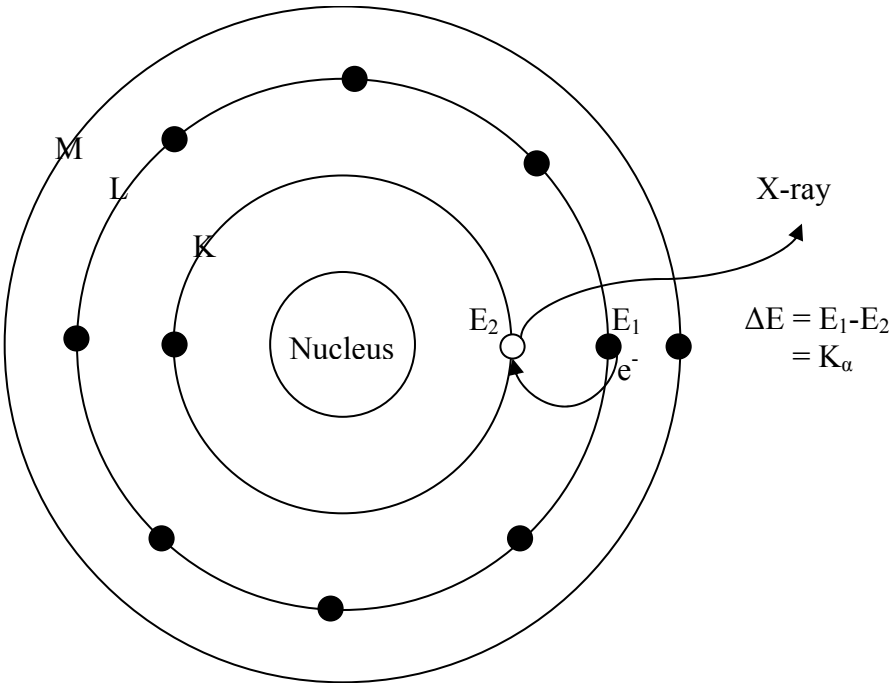

Fig. 3.3: Principle of X-ray fluorescence. After [JANS-04]

Each element present in the specimen will produce a series of characteristic lines as well as scattered radiation, making up a polychromatic emission spectrum of characteristic radiation superimposed on a scattered continuum coming from the specimen. The systematic (IUPAC) notation of the X-ray line arising from a vacancy in the K-shell of an atom, which is filled by an electron originally belonging to the L_3 shell of that atom, is the K-L_3 transition. This transition is more commonly referred to as the $K_{\alpha 1}$ line (Siegbahn nomenclature); similarly, fluorescent X-rays resulting from L_3-M_5 transition are better known as $L_{\alpha 1}$-photons. Table 3.2 lists a number of observed X-ray lines and their corresponding IUPAC and Siegbahn names.

Mosely first established the relationship between the wavelength λ of a characteristic X-ray photon and the atomic number Z of the excited element. Mosely's law is written as:

$$1/\lambda = K(Z-s)^2 \qquad \text{(Eq. 3.8)}$$

where λ is the wavelength in cm, Z is the atomic number, s is the screening constant which takes a value close to one and K is a constant which has a different value for each of the line series considered.

Table 3.2: Principal X-ray lines (IUPAC and Siegbahn notations). After [GAUG-03]

Series	IUPAC name	Siegbahn name
K-lines	$K\text{-}L_3$	$K_{\alpha 1}$
	$K\text{-}L_2$	$K_{\alpha 2}$
	$K\text{-}M_3$	$K_{\beta 1}$
	$K\text{-}M_2$	$K_{\beta 3}$
L_3-lines	$L_3\text{-}M_5$	$L_{\alpha 1}$
	$L_3\text{-}M_4$	$L_{\alpha 2}$
	$L_3\text{-}N_{5,4}$	$L_{\beta 2,15}$
	$L_3\text{-}M_1$	L_1
	$L_3\text{-}N_1$	$L_{\beta 6}$
L_2-lines	$L_2\text{-}M_4$	$L_{\beta t}$
	$L_2\text{-}N_4$	$L_{\gamma 1}$
	$L_2\text{-}M_1$	L_{η}
	$L_2\text{-}O_1$	$L_{\gamma 6}$
L_1-lines	$L_1\text{-}M_3$	$L_{\beta 3}$
	$L_1\text{-}M_2$	$L_{\beta 4}$
	$L_1\text{-}N_3$	$L_{\gamma 3}$
	$L_1\text{-}N_2$	$L_{\gamma 2}$
M-lines	$M_5\text{-}N_7$	$M_{\alpha 1}$
	$M_5\text{-}N_6$	$M_{\alpha 2}$
	$M_5\text{-}O_6$	$M_{\beta 1}$

Every single atom has a number of available electrons that can take part in the transfer and, since millions of atoms are typically involved in the excitation of a given specimen, all possible de-excitation routes are taken. These de-excitation routes can be defined by a simple set of selection rules that can be applied for the majority of the observed wavelengths. The selection rules or beyond the scope of this research and there is referred to more specialized literature [VANG-01].

Another important aspect is that an excited atom may return to a state of lower energy by ejecting one of its own electrons from a less tightly bound state instead of the emission of fluorescent photon. This radiationless transition is called the Auger effect, and the ejected electrons are called the Auger electrons. Generally, the probability of the Auger effect increases with a decrease in the difference of the

corresponding energy states, and it is the highest for low-Z elements. An important consequence of the Auger effect is that the actual number of emitted fluorescent X-ray photons produced from an atom is less than expected, because a vacancy in a given shell might be filled by a nonradiative transition. The probability that the vacancy in an atomic shell or subshell is filled through a radiative transition is called the fluorescence yield ω, which has tabulated values for the various (sub)shells for all atoms in the periodic table.

3.3 X-ray resonant Raman scattering

While the Raman scattering in molecules is a well-known effect and a well-established technique in the optical wavelength range, the resonant inelastic scattering character in the X-ray regime were inner-core excitations are involved has only been demonstrated on solid targets by Sparks in 1974 [SPAR-74]. This X-ray resonant Raman scattering (XRRS) occurs when the energy of the incident X-ray radiation is smaller than the binding energy of an inner shell of the target atom and the principle is shown in Fig. 3.4. It is seen in this figure that the binding energy of an inner shell electron is a Lorentzian due to the core hole lifetime broadening centered around the energy $\hbar\Omega_K$, the binding energy of the K electrons, with a FWHM Γ_K [UDAG-94]. Due to this lifetime broadening, when the energy of the incident X-ray radiation is approaches the binding energy of an inner shell of the target atom, there is a finite probability to excite the K-shell electrons and to create a virtual core hole in an inner shell. The corresponding electron is excited into the continuum. The created virtual core hole is subsequently filled by an electron from a higher shell, followed by the emission of a photon yielding a final stage which is characterized by a core hole in a higher shell, an electron in the continuum and the emitted ("scattered photon"). When the energy of the exciting radiation is close to that of an adsorption edge of the atom, the process shows resonant behavior and is called the XRRS process [BRIA-89]. A more detailed theoretical description of this process there can be found in the literature [SIMI-90, SUOR-79, MANN-97].

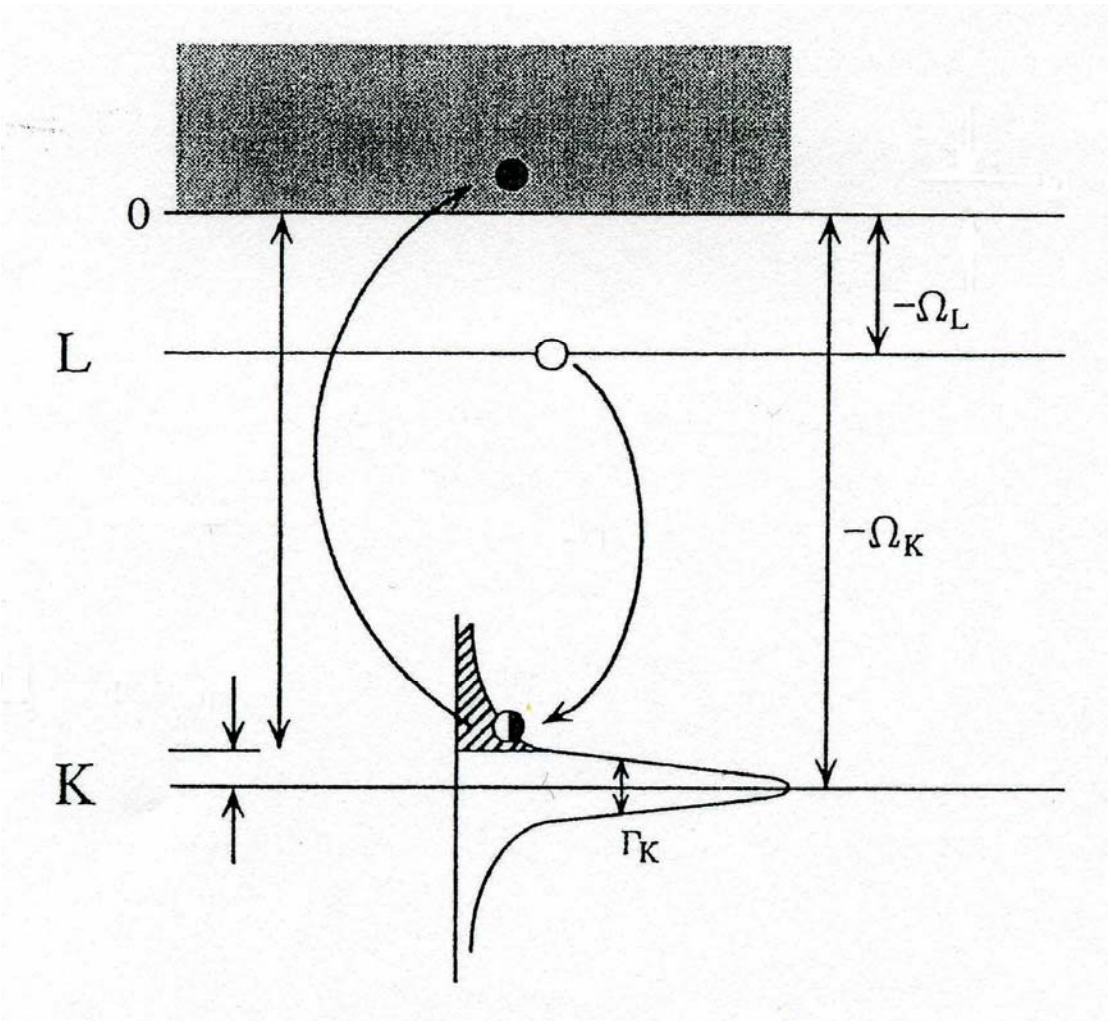

Fig. 3.4: A schematic energy diagram of the X-ray resonant Raman scattering process.

The practical importance of the XRRS process has been documented in the determination of ultra-trace-impurities on substrates, such as during the detection of low Z elements (e.g. Al, oxides) in Si wafers [BAUR-00, BAUR-01, STRE-03, SZLA-05], Pt in ancient gold [GUER-05] and Ni in Cu substrates [ZARK-06]. For these cases the energies of the fluorescence lines of the impurities are just below the absorption edge of the main substrate element. The exciting photon energy is selected just below the absorption edge of the main substrate element to avoid the excitation of the substrate fluorescence lines which will otherwise dominate the X-ray fluorescence spectrum. In this way an additional strong background peak is caused by the XRRS process which results in a considerable overlap between the XRRS peak and the fluorescence lines of the impurities. This affects the detection limits (DLs) as well as the quantification of the impurities. The latter can be improved by the determination

of the cross sections associated with the background distribution of the interfering XRRS process [ZARK-06, MULL-06].

3.4 Experimental setup at Beamline L [VINC-99]

The synchrotron micro X-ray Fluorescence (SR-XRF) experiments were performed at Beam Line L of the second generation DORIS III storage ring, HASYLAB (Hamburg, Germany). This beamline is dedicated to micro XRF measurements using either white or monochromatic bending magnet excitation and mono- or poly capillary focusing, with routinely available beam sizes of 10 to 30 μm. Fig. 3.5a shows the experimental arrangement used during our scanning micro XRF experiments and Fig. 3.5b shows a photo of the setup. [FALK-01, PROO-03]

At beamline L, the primary X-ray beam is generated by a 1.2 T bending magnet source which, given the machine energy of 4.45 GeV, provides a polychromatic spectral distribution with a critical energy of 16.6 keV. After initial low-energy filtering and collimation, the beam is monochromatized by a Si(111) fixed exit monochromator ($\Delta E/E \approx 10^{-4}$) or by Ni/C multilayer monochromator ($\Delta E/E \approx 10^{-2}$) and further collimated by a motorized cross-slit system. [HASY-06]

After monochromatization, the beam is focused by a monolithic polycapillary half lens (X-ray Optical System Inc.), designed specifically for parallel primary beams and hence suitable for the focusing of low divergence synchrotron beams. A beam size of ~ 20 μm (FWHM) was obtained at the energy range of 8.0 ± 0.1 keV and 9.3 ± 0.1 keV which was used to excite selectively the Co $K_{\alpha,\beta}$ and Cu $K_{\alpha,\beta}$ fluorescent lines without exciting the Au L lines of the (spectroscopically infinitely thick) gold substrate. The transmission efficiency is around 45% and the gain in flux density (= transmission efficiency * input area / beam cross section at the focal point) is around 2000 at the applied energies yielding fluxes of 10^{10}-10^{11} photons s^{-1} per 1% bandwidth [HASY-06]. The nominal working distance of the polycapillary optic was 5 mm and an energy dispersive Si-VORTEX detector with an active area of 50 mm^2 was used. [PROO-03]

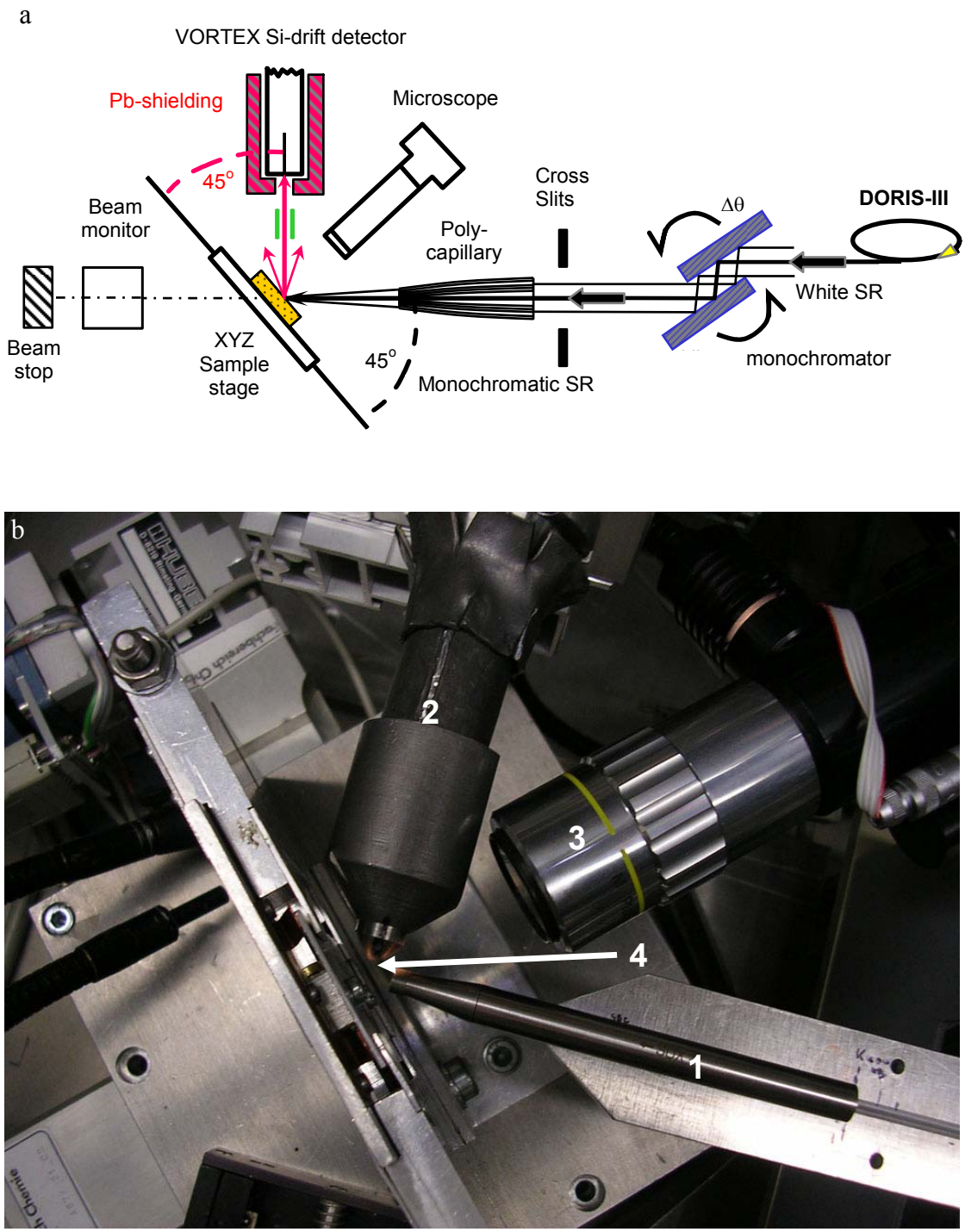

Fig. 3.5: Schematic representation (a) and picture (b) of the experimental setup at beamline L with in (b) (1) the poly capillary, (2) the detector, (3) the microscope and (4) the sample. After[FALK-01, PROO-03]

Experimental difficulty of the MTSPc thin film uniformity studies included the determination of low amounts of Co or Cu (~0.1 – 0.5 pg, assuming a 20 µm beam) in the presence of Rayleigh, Compton and Au X-ray resonant Raman peaks. The problems with the Compton and Rayleigh peaks have been greatly reduced by the fact

of using highly (linearly) polarized monochromatic SR under 90˚ excitation/detection geometry in the plane of linear-polarization. While a photoelectric/fluorescence interaction results in the isotropic emission of characteristic radiation, scattering interactions produce photons having highly anisotropic angular distributions, therefore the ratio of fluorescence/scatter intensities can be strongly influenced by the choice of excitation/detection geometry. Quantitatively, the intensity of Rayleigh/Compton scattered radiation can be characterized by the so-called differential scattering cross-sections $d\sigma/d\Omega$ (see Eq. 3.9 and 3.10), which characterize the angular distribution of the scattered photons. For the description for a linearly polarized photon beam, the local coordinate system is chosen in such a way that the photon beam (having an initial propagation vector k_0) travels along the Z-axis prior to the interaction and its (net) electric field vector ε_0 is parallel with the X-axis (Fig. 3.6). After the scattering event, the new direction of photon propagation is characterized by the (unit) propagation vector k_1 and the net electric vector ε_1. [VINC-99]

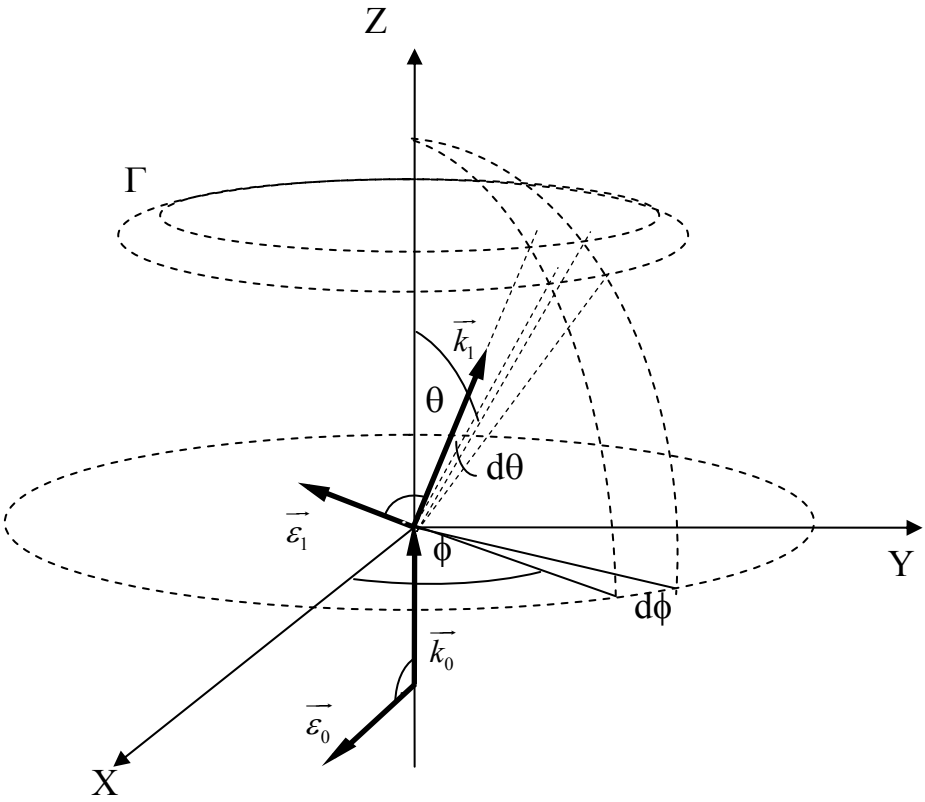

Fig. 3.6: The coordinate system attached to the photon used to describe the scattering phenomenon. [VINC-99]

In case of linearly polarized radiation having a degree of polarization p with respect to the reference plane XZ (Fig. 3.6), the expression for the Rayleigh ($d\sigma_R/d\Omega$) and Compton ($d\sigma_C/d\Omega$) differential scattering cross-sections are, respectively, given by:

$$\frac{d\sigma_R}{d\Omega}(\theta,\varphi,E) = \frac{d\sigma_T}{d\Omega}(\theta,\varphi)F^2(x,Z)$$

$$= \frac{r_e^2}{2}\left[2\text{-}\sin^2\theta\times(1\text{-}p+2p\cos^2\varphi\right]F^2(x,Z) \quad \text{(Eq. 3.9)}$$

$$\frac{d\sigma_C}{d\Omega}(\theta,\varphi,E) = \frac{d\sigma_{KN}}{d\Omega}(\theta,\varphi,E)S(x,Z)$$

$$= \frac{r_e^2}{2}\left(\frac{E}{E_0}\right)^2\left[\frac{E}{E_0}+\frac{E_0}{E}\text{-}\sin^2\theta\times(1\text{-}p+2p\cos^2\varphi)\right]S(x,Z)$$

(Eq. 3.10)

where $d\sigma_T/d\Omega$ denotes the Thomson and $d\sigma_{KN}/d\Omega$ the Klein-Nishina differential cross-section [HANS-86]. F(x,Z) and S(x,Z) are the atomic form factor and the incoherent scattering function, respectively [HUBB-75], for an element with atomic number Z, $x(Å^{-1}) = \sin(\theta/2)E\,(keV)/12.39$ is the momentum transfer of the photon and r_e is the classical electron radius.

Eq. 3.9 and 3.10 show that $d\sigma_R/d\Omega = 0$ and that $d\sigma_C/d\Omega$ reaches a minimum for p=1, $\theta = 90°$ and $\varphi = 0°$. The latter inquires that when the angle between the incoming beam and the detector in the plane of the synchrotron (assuming p = 1) is 90°, the Rayleigh scatter will theoretically be 0 and the Compton scatter will reach its minimum. The degree of linear polarization of the SR-beam emitted by bending magnet source at Beamline L is only 94-95 % and the angle between the incoming beam and the scattering angle is not exactly 90° for the complete detector surface, inplying that there will be an influence of the Rayleigh and Compton scatter.

During the CoTSPc/CuTSPc uniformity studies, 21 x 21, 31 x 31 or 41 x 41 scanning XRF maps were recorded with typically 20 μm step size, using a data collection time of 10-20 s per data point. To determine the level of uniformity of the deposited CoTSPc or CuTSPc thin film, the scanning and subsequent data reduction

has been based on the strategy of Kempenaers et al. [KEMP-00, KEMP-02]. This feature, however, is discussed in more detail in chapter 8.

During the X-ray Resonant Raman study 300 s spectra were collected at energies varying from 9200 eV to 11700 eV. Monochromatization occurred using the Si(111) monochromator and a beamsize of 20 μm was used at a fixed position on the modified gold electrodes.

3.5 Quantification of the Co or Cu thin films [VANG-01, VINC-05]

The quantification of XRF involves the conversion of the measured fluorescent intensities to the concentration of the analyte with the measured intensities corrected for background and line overlap. To determine the net-peak intensities of the Co-K_α or Cu-K_α signal in the measured XRF spectra, the non linear least squares fitting software AXIL [VEKE-94] was used. Pure thin Co (thickness 10 μm) and Cu (thickness 1 μm) foils were used as standards.

The quantification is based on the fundamental parameter method where only the primary fluorescence of monochromatic radiation is taken into account. The secondary radiation is not taken into account since the investigated CoTSPc and CuTSPc films are very thin, pure Co and Cu foils are used as standards and monochromatic excitation energies just above the excitation energy of Co and Cu and below the excitation energy of Au-L lines are used. This results in a low amount of secondary photons with energies above the adsorption edge of Co or Cu in the samples or standards suppressing the chance of having secondary fluorescence. Let the intensity of an incident parallel beam, which strikes the surface of a specimen with an angle α, with energy E_0 at the surface be given by I_0 (E_0). The beam is considered to extend to infinity in all three dimensions and is gradually absorbed by the specimen. At a layer at depth z (Fig. 3.7) below the surface, the remaining fraction of the intensity I_0 (E_0) is given by the Lambert-Beer law:

$$I=I_0 e^{-\mu(E_0)\,\rho x} \qquad \text{(Eq. 3.11)}$$

where I is the transmitted intensity, I_0 the incident intensity, $\mu(E_0)$ the mass attenuation coefficient at energy E_0 in $cm^2\ g^{-1}$ and the other symbols as defined before.

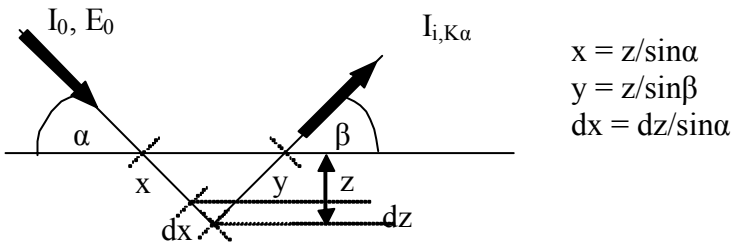

Fig. 3.7: Schematic representation of the geometry involved in the calculation of primary fluorescence emission. After [VANG-01]

The mass attention coefficient $\mu(E_0)$, is calculated for all the elements in the specimen which means that all the mass attenuation coefficients for all elements j present in the specimen are taken into account, each multiplied with its mass fraction W_j

$$\mu(E_0) = \sum_{i=1}^{n} \mu_i(E_0) W_i \qquad \text{(Eq. 3.12)}$$

where $\mu(E_0)$ is the mass attenuation coefficient at energy E_0 in $cm^2\ g^{-1}$, W_i is the weight fraction of the *i*th element and n is the total number of elements in the sample.

The fraction of the incident beam absorbed by the sample in the layer between x and x + dx is given by

$$dI = I\,\mu(E_0)\,\rho\,dx \qquad \text{(Eq. 3.13)}$$

where the symbols are as for Eq. 3.11.

The probability that the absorbed photon results in a K shell excitation of element *i* is given by

$$P_{i,K} = W_i \ \tau_{i,K}/\mu(E_0) \qquad \text{(Eq. 3.14)}$$

where W_i is the weight fraction of the analyte *i* in the interval between x and x+dx, $\tau_{i,K}$ is the photo-electric attenuation coefficient according to the K shell interactions with the analyte *i* at energy E_0.

The photoelectric attenuation coefficient for the K shell excitation of analyte *i* $\tau_{i,K}$ at energy E_0 can be approximated by means of the jump ratio J_K. This jump ratio is the ratio of the photoelectric attenuation coefficient just above (τ_+) and the photoelectric attenuation coefficient just below (τ_-) the K adsorption edge ($J_K = \tau_+/ \tau_-$). Only a fraction of the photons which are absorbed by a given element creates vacancies in the K shell. This fraction is given by $(J_K - 1)/ J_K$, where J_K is the absorption jump ratio of the K shell of the element *i* under investigation. Therefore, $\tau_{i,K}$ is given by

$$\tau_{i,K} = \tau(E_0)\ (J_K - 1)/J_K \qquad \text{(Eq. 3.15)}$$

where $\tau_{i,K}$ is the photoelectric attenuation coefficient for K shell excitation of analyte *i* at energy E_0, $\tau(E_0)$ is the photoelectric attenuation coefficient expressed in $cm^2\ g^{-1}$ and J_K is the jump ratio.

The fraction of K vacancies emitting X-rays in the interval between x and x+dx is given by the fluorescence yield $\omega_{i,K}$ and the fraction of K_α photons in the total of X-rays emitted for the analyte *i* is given by the transition probability $P_{i,K\alpha}$.

The combination of Equations 3.11, 3.13 and 3.14, show that the K_α fluorescence intensity of element *i* generated in the interval (x, x+dx) can be given by

$$\begin{aligned} dI^*_{i,K\alpha} &= I_0 e^{-\mu(E_0)\rho x}\ \mu(E_0)\rho dx\ \frac{W_i \tau_{i,K}}{\mu(E_0)}\ P_{i,K\alpha}\ \omega_{i,K} \\ &= I_0 e^{-\mu(E_0)\rho x}\ W_i \tau_{i,K}\ P_{i,K\alpha}\ \omega_{i,K}\ \rho\ dx \\ &= I_0 e^{-\mu(E_0)\rho x}\ W_i\ Q_{i,K\alpha}\ \rho\ dx \end{aligned} \qquad \text{(Eq. 3.16)}$$

where the same symbols are used as in Eq. 3.11, Eq. 3.13 and Eq. 3.14 with $Q_{i,K\alpha}$ the element dependent production cross section in $cm^2\ g^{-1}$.

The characteristic photons given by Eq. 3.16 are isotropically emitted in all directions, without a preferential direction. Only a fraction is emitted towards the detector. If the solid angle subtended by the detector is given by Ω_{det} (expressed in sterradians), then the detected fraction is given by $\Omega_{det}/4\pi$. The angle Ω_{det} should be small enough so that the beam can be considered to be a parallel beam leaving the specimen at an angle defined by β with the surface. The fraction of the characteristic photons with energy E_1 emitted towards the detector, which is not absorbed over the distance y in the specimen is given by the Lambert-Beer law. This, together with Eq. 3.16 yields that the detected K_α intensity of analyte *i* from a depth (z, z+dz) is given by

$$
\begin{aligned}
dI_{i,K\alpha} &= dI^{*}_{i,K\alpha}\,\frac{\Omega_{det}}{4\pi}\,e^{-\mu(E_1)\rho y} \\
&= I_0\,\frac{\Omega_{det}}{4\pi}\,e^{-\mu(E_0)\rho x}\,e^{-\mu(E_1)\rho y}\,W_i\,Q_{i,K\alpha}\,\rho\,dx \\
&= I_0\,\frac{\Omega_{det}}{4\pi}\,e^{\underbrace{-(\mu(E_0)/\sin\alpha+\mu(E1)/\sin\beta)}_{\chi}\rho z}\,W_i\,Q_{i,K\alpha}\,\rho\,dx \\
&= I_0\,\frac{\Omega_{det}}{4\pi}\,W_i\,Q_{i,K\alpha}\,e^{-\chi\rho z}\,\rho\,dz/\sin\alpha \\
&= I_0\,G\,W_i\,Q_{i,K\alpha}\,e^{-\chi\rho z}\,\rho\,dz \qquad \text{(Eq. 3.17)}
\end{aligned}
$$

where all symbols are as in Eq. 3.16 with Ω_{det} the solid angle as seen by the detector system expressed in streradians, G the geometry factor and χ given in $cm^2\ g^{-1}$.

The geometry factor G is given by

$$
G = \frac{\Omega_{det}}{4\pi\sin\alpha} \cong \frac{1}{4\pi\sin\alpha}\,\frac{A_{det}}{D^2} \qquad \text{(Eq. 3.18)}
$$

where A_{det} is the active detector surface in cm^2 and D is the distance between the specimen and the detector in cm.

The variable χ is given by

$$\chi = \mu(E_0)/\sin\alpha + \mu(E1)/\sin\beta \qquad \text{(Eq. 3.19)}$$

where all symbols are as in Eq. 3.17 and χ is given in $cm^2\ g^{-1}$.

Integration over the sample thickness T gives the total detected intensity $I_{i,K\alpha}$

$$I_{i,K\alpha} = \int_0^T dI_{i,K\alpha} = I_0\ G\ W_i\ Q_{i,K\alpha}\rho \int_0^T e^{-\chi\rho z}\ dz$$

$$= I_0\ G\ W_i\ Q_{i,K\alpha}\ \frac{1-e^{-\chi\rho t}}{\chi}$$

$$= I_0\ G\ W_i\ Q_{i,K\alpha}\ \rho\ T\ \frac{1-e^{-\chi\rho T}}{\chi\ \rho\ T}$$

$$= I_0\ G\ W_i\ Q_{i,K\alpha}\ \rho\ T\ A_{corr} \qquad \text{(Eq. 3.20)}$$

where all symbols are as in Eq. 3.17, T is the sample thickness in cm and A_{corr} is the absorption correction factor.

The above equation corresponds to the fluorescence intensity detected by an ideal detector, having a quantum efficiency of 1. This approximation holds for the energy range represented by the Co and Cu lines.

The absorption correction A_{corr} is a correction for the matrix effects and is $0 < A_{corr} < 1$. For a very thin sample ($T << 1/\chi\rho$) as is the case for the CoTSPc and CuTSPc thin films the total detected intensity is given by

$$I_{i,K\alpha} = I_0\ G\ W_i\ Q_{i,K\alpha}\ \rho\ T \qquad \text{(Eq. 3.21)}$$

where all the symbols are as in Eq. 3.17.

In this work, pure Co or Cu foils were used as standards to calculate the Co or Cu surface concentrations on the gold electrodes. From Eq. 3.20, it can be derived that

for a standard, the intensity of the of the detected fluorescence line can be calculated as

$$I_{s,K\alpha} = I_{0,s}\ G\ W_s\ Q_{s,K\alpha}\ \rho_s\ T_s\ A_{corr,s} \qquad \text{(Eq. 3.22)}$$

where all the symbols are as in Eq. 3.17 for a standard.

The surface concentration S_u of the Co and Cu can be calculated from Eq. 3.21 and is given by

$$S_u = I_{u,K\alpha}/(I_{0,u}\ G\ W_u\ Q_{u,K\alpha}) \qquad \text{(Eq. 3.23)}$$

where all the symbols are as in Eq. 3.21 and $S_u = W_u\ \rho\ T$ is the surface concentration of the unknown on the electrode in g cm^{-2}.

Since the same experimental setup has been used for the standards as for the unknowns, G is identical for both measurements. The element dependent production cross section $Q_{i,K\alpha}$ is only dependent on the analyte element so it is the same for both the standard and the unknown. W_s is 1 since pure foils have been used as standards. Taking this into account, the surface concentration of the unknown is given by

$$S_u = \frac{I_u}{I_{0,u}} \frac{I_{0,s}}{I_s}\ \rho_s\ T_s\ A_{corr,s} \qquad \text{(Eq. 3.24)}$$

where all the symbols are as for Eq. 3.17 and 3.23.

3.6 Other spectroscopic techniques

3.6.1 X-ray photoelectron spectroscopy [WHIT-84]

X-ray photoelectron spectroscopy (XPS) (sometimes referred to as electron spectroscopy for chemical analysis (ESCA)) [WHIT-84] is based on the photoelectric effect. During XPS measurements, the energy of the ejected electrons into vacuum is

studied [SOMO-94]. It is a surface specific technique with typical escape depths of 100 to 500 nm and it allows the oxidation state of the studied elements can be determined. Therefore, it is a useful technique for the study of gold electrodes modified with CoTSPc or CuTSPc.

The XPS measurements in this research were performed with a Perkin-Elmer Phi ESCA 5500 system equipped with a monochromated 450 W Al K_α source. The base pressure of the system was 1 x 10^{-7} Pa. Experiments were recorded with a 220 W source power and an angular acceptance of ± 7°. The analyzer axis made an angle of 45° with the specimen surface. The XPS data analysis was performed with the XPS Peak 4.1 program while a Shirly function was used to subtract the background.

3.6.2 UV-Vis spectroscopy [GAUG-03]

As described in chapter one, phthalocyanines are UV-Vis active since the Q and the B band show absorption, respectively at 600-700 nm and 300 nm. Moreover it is described in literature that it is a useful technique for the determination of the monomer-dimer equilibrium of the phthalocyanines in solution since there is a blue shift of the absorption peaks for the transition of monomer to dimer [YANG-85, CAMP-02, ABRA-04]. Therefore, it is used to determine the monomer-dimer equilibrium in solution of the different phthalocyanine species under investigation in this research. In the case UV-Vis measurements are described, the Lambert-Beer law is normally described as

$$A = \varepsilon c l \qquad \text{(Eq. 3.25)}$$

where A is the absorbance, ε the molar absorption coefficient in L mol^{-1} cm^{-1}, c the concentration in mol L^{-1} and l the path length in cm^{-1}.

In this work ε_M is used for the molar absorption coefficient of monomer species and ε_D for the dimer species.

These UV-Vis measurements are performed with a Varian Cary 3E spectrophotometer (Instrument version 8.01) (Palo Alto, Canada) or with a Specors 200 spectrophotometer (Analytical Jena, Germany).

3.7 References

[ABRA-04] Abramczyk H., Szymczyk I., Waliszewska G., Lebioda A., *J. Phys. Chem. A*, **2004**, 108, 264-274.

[BAUR-00] Baur K., Kerner J., Brennan S., Singh A., Pianetta P., *J. Appl. Phys*, **2000**, 88, 4642-4647.

[BAUR-01] Baur K., Brennan S., Burrow B., Werho D., Pianetta P., *Spectrochim. Acta Part B*, **2001**, 56, 2049-2056.

[BRIA-89] Briand J.P., Simionovici A., Chevallier P., Indelicato P., *Phys. rev. lett.*, **1989**, 62, 2092-2095.

[CAMP-02] Camp P.J., Jones A.C., Neely R.K., Speirs N.M., *J. Phys Chem. A*, **2002**, 106, 10725-10732.

[CHUN-00] Chung F.H., Smith D.K., *Industrial Applications of X-ray Diffraction*, Marcel Dekker, New York, **2000**.

[CULL-97] Cullen D.E., Hubbell J.H., Kissel L., Lawrence *Livermore National Laboratory Report UCRL-50400*, Vol. 6, Rev. 5, **1997**.

[FALK-01] Falkenberg G., Clauss O., Swiderski A., Tschentscher Th., *X-Ray Spectrom.*, **2001**, 30, 170-173.

[GAUG-03] Gauglitz G., Vo-Dihn T., *Handbook of Spectroscopy Vol. 1*, Wiley-VCH, Weinheim, **2003**.

[GUER-05] Guerra M.F., Calligaro T., Radtke M., Reiche I., Reisemeier H., *Nucl. Instr. and Meth. in Phys. Res. B*, **2005**, 240, 505-511.

[HANS-86] Hanson A.L., *Nucl. Instrum. Methods A*, **1986**, 243, 583-598.

[HASY-06] Hasylab website, *www-hasylab.desy.de/facility/doris/parameters.htm*

[HUBB-75] Hubbel J.H., Veigele W.J., Briggs A., Brown R.T., Cromer D.T., Howerton R.J., *J. Phys. Chem. Ref. Data*, **1975**, 4, 471.

[JANS-04] Janssens K., *Comprehensive Analytical Chemistry* Ed. Barcelo D., *Volume XLII Non-destructive Microanalysis of cultural heritage materials*, Ed. Janssens K., Van Grieken R., Elsevier Science B.V., Amsterdam, **2004**.

[JENK-99] Jenkins R., *X-ray fluorescence spectrometry second edition*, John Wiley & Sons, New York, **1999**.

[KEMP-00] Kempenaers L., Vincze L, Janssens K., *Spectrochim. Acta Part B*, **2000**, 55, 651-669.

[KEMP-02] Kempenaers L., Janssens K., Vincze L., Vekemans B., Somogyi A., Drakopoulos M., Simionovici A., Adams F., *Anal. Chem.,* **2002**, 74, 5017-5026.

[KOCH-83] Koch E.E., Eastman D.E., Farge Y., *Handbook on synchrotron radiation*, Volume 1A, Ed. Koch E.E., North-Holland Publishing Company, Amsterdam, **1983**.

[MANN-97] Manninen S., *Radiat. Phys. Chem.*, **1997**, 50, 77-89.

[MULL-06] Müller M., Beckhoff B., Ulm G., *Phys. Rev. A*, **2006**, 74, 012702.

[PROO-03] Proost K., Vince L., Janssens K., Gao N., Bulska E., Schrein M., Falkenberg G., *X-Ray Spectrom.*, **2003**, 32, 215-222.

[SIMI-90] Simionovici A., Briand J.P., Indelicato P., Chevallier P., *Phys Rev. A*, **1990**, 41, 3707-3715.

[SKOO-97] Skoog D.A., Holler F.J., Nieman T.A., *Principles of instrumental analysis fifth edition*, Thomson Learning Inc., USA, **1997**.

[SOMO-94] Somorjai G.A., *Introduction to Surface Chemistry and Catalysis*, John Whily & Sons, New York, **1994**.

[SPAR-74] Sparks C.J., *Phys. Rev. Lett.,* **1974,** 33, 262-265.

[STRE-03] Streli C., Pepponi G., Wobrauschek P., Beckhoff B., Ulm G., Pahlke S., Fabry L., Ehmann Th., Kangieβer B., Malzer W., Jark W., *Spectrochim. Acta Part B*, **2003**, 58, 2113-2121.

[SUOR-79] Suortti P., *Phys. Status Solidi B-Basic Solid State Phys*., **1979**, 91, 657-666.

[SZLA-05] Szlachetko J., Berset M., Dousse J. Cl., Fennane K., Szlachetko M., Barret R., Hoszowska J., Kubala-Kukus A., Pajek M., *Nucl. Instr. and Meth. in Phys. Res. B*, **2005**, 238, 353-356.

[UDAG-94] Udagawa Y., Hayashi H., Tohji K., Mizushima T., *J. Phys. Soc. Jap.,* **1994**, 64, 1713-1720.

[VANG-01] Van Grieken R., Markowicz A., *Handbook of X-ray Spectrometry,* second edition, Marcel Dekker, New York, **2001**.

[VEKE-94] Vekemans B., Janssens K., Vincze L., Adams F., Vanespen P., *X-ray Spectrom*., **1994**, 23, 278-285.

[VINC-99] Vincze L., Janssens K., Vekemans B., Adams F., *Spectrochim. Acta Part B*, **1999**, 54, 1711-1722.

[VINC-02] Vincze L., Wei F., Proost K., Vekemans B., Janssens K., He Y., Yan Y. and Falkenberg G., J. Anal. At. Spectrom., **2002**, 17, 177-182.

[VINC-04] Vincze L., Janssens K., Vekemans B. and Adams F., *X-ray Spectrometry: Recent Technological Advances*, Ed. Tsuji K., Injuk J., Van Grieken R., John Wiley & Sons, New York, **2004**.

[VINC-05] Vincze L., *Chemical analysis by X-ray Spectroscopy*, course at University of Ghent, **2005**.

[WHIT-84] White R.E., Bockris J.O., Conway B.E., Yeager E., *Comprehensive Treatise of Electrochemistry, Vol. 8*, Plenum Press, New York, **1984**.

[YANG-85] Yang Y.C., Ward J.R., Seiders R.P., *Inorg. Chem.,* **1985**, 24, 1765-1769.

[ZARK-06] Zarkadas Ch., Karydas A.G., Müller M., Beckhoff B., *Spectrochim. Acta Part B*, **2006**, 61, 189-195.

Chapter 4:
Earlier published results and objectives of this work

As already mentioned in chapter 3, the electrochemical behavior and properties of gold electrodes, modified with phthalocyanines have been studied extensively in our research group in the past [DEWA-04, DEWA-05, DEWA-05b, DEWA-05c]. In the first section of this chapter these results are briefly described in order to fit this work into context. In the second section of this chapter the objectives of this work are listed.

4.1 Earlier published results

The modification procedure of gold electrodes with cobalt tetrasulphophthalocyanine (CoTSPc) and copper tetrasulphophthalocyanine (CuTSPc) consists of three steps. The first step is the mechanical and electrochemical preparation of the gold electrode as discussed in chapter 2. In section 4.1.1, a short overview of the most important electrochemical characteristics of a gold electrode in pH 12 buffer solution is given. The second step encompasses the electrodeposition of CoTSPc or CuTSPc at a gold electrode in a pH 12 buffer solution by recording successive voltammetric scans between 0.6 and -1.2 vs. SCE. In the third step, the modified electrode is brought back in the pH 12 buffer solution, this time without CoTSPc or CuTSPc, and again cyclic voltammetric scans are recorded between 0.6 – 1.2 V vs. SCE. In the following sections, the published results according to this modification procedure will be discussed.

4.1.1 Voltammetric behavior of a bare gold electrode

As already mentioned in chapter 2, all gold electrodes are pretreated in a similar way to make reproducible measurements possible. As described by De Wael et al. the electrochemical pretreatment encompasses the scanning in a pH 12 buffer

solution, between -1.2 and 0.6 V vs. SCE until 5 subsequent scans are identical. [DEWA-04]. Fig. 4.1 shows the 20th scan of a bare gold electrode in the presence (curve 1) and the absence of oxygen (curve 2, the solution has been bubbled during 20 minutes with nitrogen gas). At 0.4-0.6 V vs. SCE the gold surface is oxidized with the formation of gold(I)hydroxide (AuOH) and Au(II) oxide (AuO, α-oxides). The reduction peak at 0.13 V vs. SCE can be explained as the reduction of the oxides formed during the oxidation [ABDE-01]. Curve 1 of Fig. 4.1 shows an extra reduction process around -0.19 V vs. SCE. This peak has been attributed to the reduction of oxygen present in the solution. Since important electrochemical processes related to phthalocyanine occur in this potential region of this reduction, all solutions were made oxygen free by bubbling the solution with nitrogen gas.

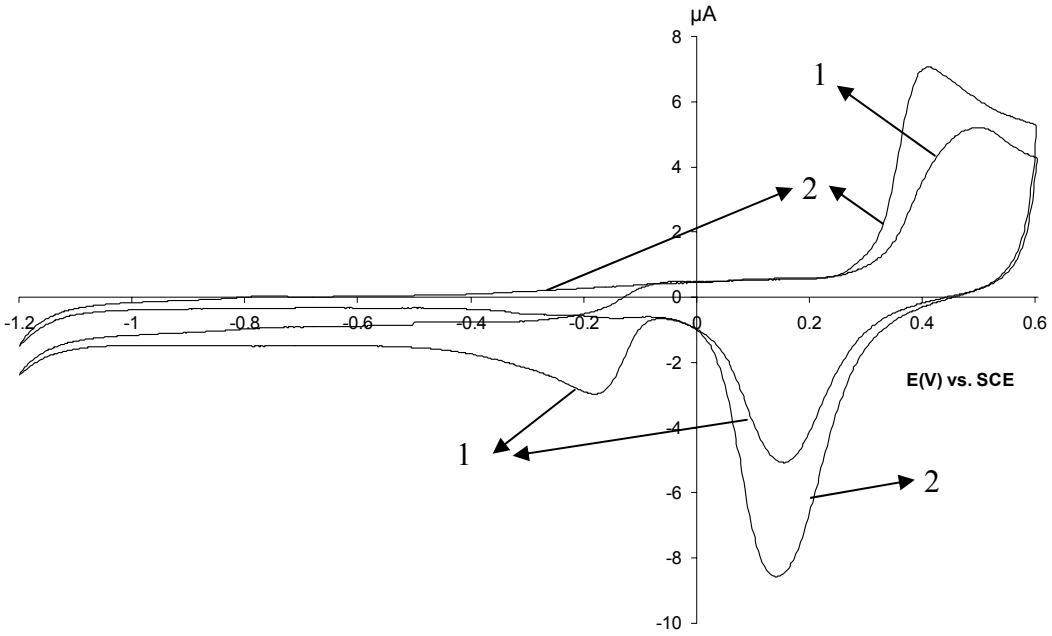

Fig. 4.1: Cyclic voltammogram of a bare electrode in pH 12 buffer solution in oxygen rich (curve 1) and free (curve 2) environment between 0.6 and -1.2 V vs. SCE and scan rate 50 mV s^{-1}.

Fig. 4.2 zooms in on the cathodic region of the cyclic voltammogram shown in Fig. 4.1 (curve 2), revealing small peaks visible at potentials of -0.75 V, -0.3 V, -0.18 V and -0.05 V vs. SCE. While these currents below the main monolayer region were first attributed to impurity effects [WOOD-76], it has been postulated in the late eighties of last century that they are caused by a phenomenon known as premonolayer oxidation/reduction in which reactive metal adatoms (Au*) can be oxidized/reduced at potentials well below that required for regular monolayer oxide formation (in this case

below 0.4 V vs. SCE) [BURK-86]. These adatoms are single adsorbed atoms outside the surface lattice structure [BUDE-96]. They are characterized by a high energy which causes a small and variable electrochemical response since most of the metal atoms at the interface revert to a high bulk lattice metal coordination state (Au_l) [BURK-89].

$$Au^* \leftrightarrow Au_l \qquad \text{(Eq. 4.1)}$$

These adatoms, however, can be generated at interfaces by cycling over the regular monolayer oxidation and reduction stage of the metal (as is the case in this research) resulting in the roughening of the gold surface. These adatoms and their hydrous oxide species can play a vital role in noble metal electrocatalysis [TREV-89, BURK-92, BURK-94, BURK-02]. The redox transitions at the lowest potentials (-0.75 and -0.3 V vs. SCE) can be attributed to Au^*/Au(I) transitions and those at the higher potentials (-0.05 and -0.18 V vs. SCE) can be attributed to Au^*/Au(III) hydrous oxide transitions [BURK-89,ABDE-01].

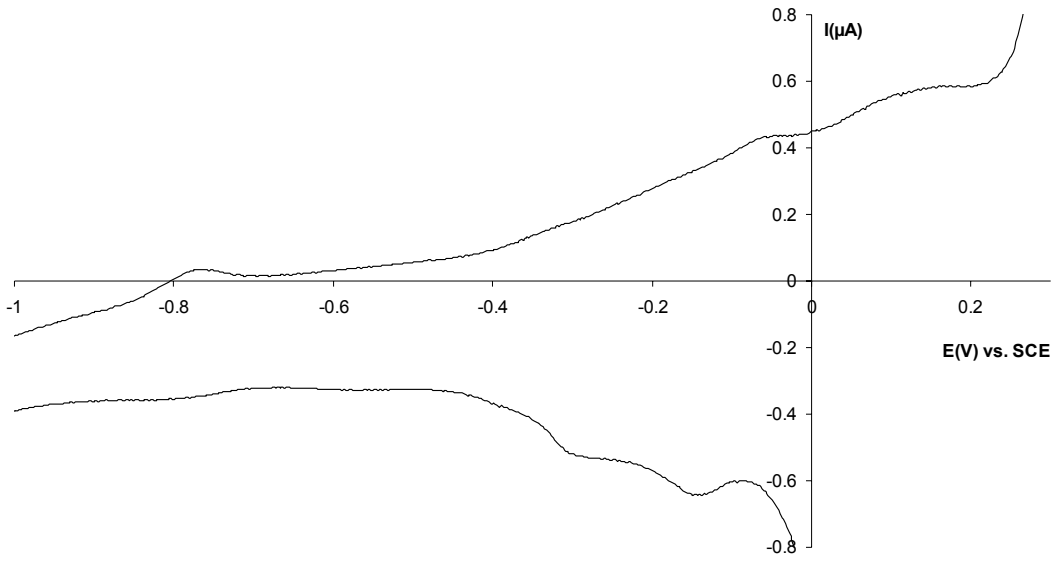

Fig. 4.2: Enlargement of the premonolayer region of the cyclic voltammogram of a bare gold electrode in a pH 12 buffer solution in oxygen free environment shown in Fig. 4.1.

4.1.2 Modification of a gold electrode with CoTSPc [DEWA-04]

Fig. 4.3 shows some of the first 20 cyclic voltammetry scans recorded at a gold electrode in a pH 12 buffer solution (curve 1) and in a solution containing 8.07 mmol L^{-1} CoTSPc (curves 2-7) [DEWA-04]. In curve 1 of Fig. 4.3 an oxidation peak I_a at 0.38 V vs. SCE and a reduction peak I_c at 0.13 V vs. SCE can be observed, attributed to the oxidation of the gold surface and reduction of the gold oxide formed during surface oxidation (see § 4.1.1). In curves 2-7 it can be seen that two new oxidation peaks at -0.05 V (II_a) and 0.24 V vs. SCE (III_a) occur and that the peak attributed to gold oxide formation (I_a) decreases markedly. Another three reduction peaks are observed, the first one at -0.41 V (II_c) and a third peak at -1.15 V vs. SCE (IV_c) grow with increasing scan number, the peak maximum of the second reduction peak with a value around -0.8 V vs. SCE (III_c) shifts towards more negative potentials during the first five scan before also the peak maximum starts to decrease. The increase of the oxidation peaks II_a and III_a and the reduction peaks II_c and IV_c and the decrease of the gold oxide reduction peak I_c continue until scan 20. Continuation of the scanning beyond scan 20 results in different behavior. It is remarkable for scan 20 that the charge related to the two oxidation waves (II_a and III_a) and the charge related to the reduction wave (II_c) are almost the same. For peak I_c a higher charge has been obtained and therefore, it is supposed that peak I_c at scan 20 is not only due to the fraction of the gold surface that is still uncovered and able to be oxidized and reduced but that this peak is the return peak of the oxidation peak (III_a). Taking this into account, a surface covering of 95 % CoTSPc can be calculated after 20 scans. It can be concluded that peaks I_c and III_a in scan 20 are related to the same reversibly behaving redox system.

It is also important to note that for peak III_c the peak potential shifts towards more negative potentials without a decrease in peak current in the first scans. Only after a few scans the peak height starts to decrease and simultaneously peak IV_c starts to grow. This indicates that the decrease of peak III_c and increase of peak IV_c are related to each other.

The increase with scan number of the peaks II_a, III_a and II_c is due to the deposition of CoTSPc at the gold surface. With each scan, the amount of deposited CoTSPc increases, which results in higher peaks because more adsorbed CoTSPc is present at the surface in the next scan. This feature also explains the gradual decay of

peak I_c. Covering the gold surface with CoTSPc prevents its oxidation and reduction, therefore the gold oxide formation and reduction peaks (I_a and I_c) decrease.

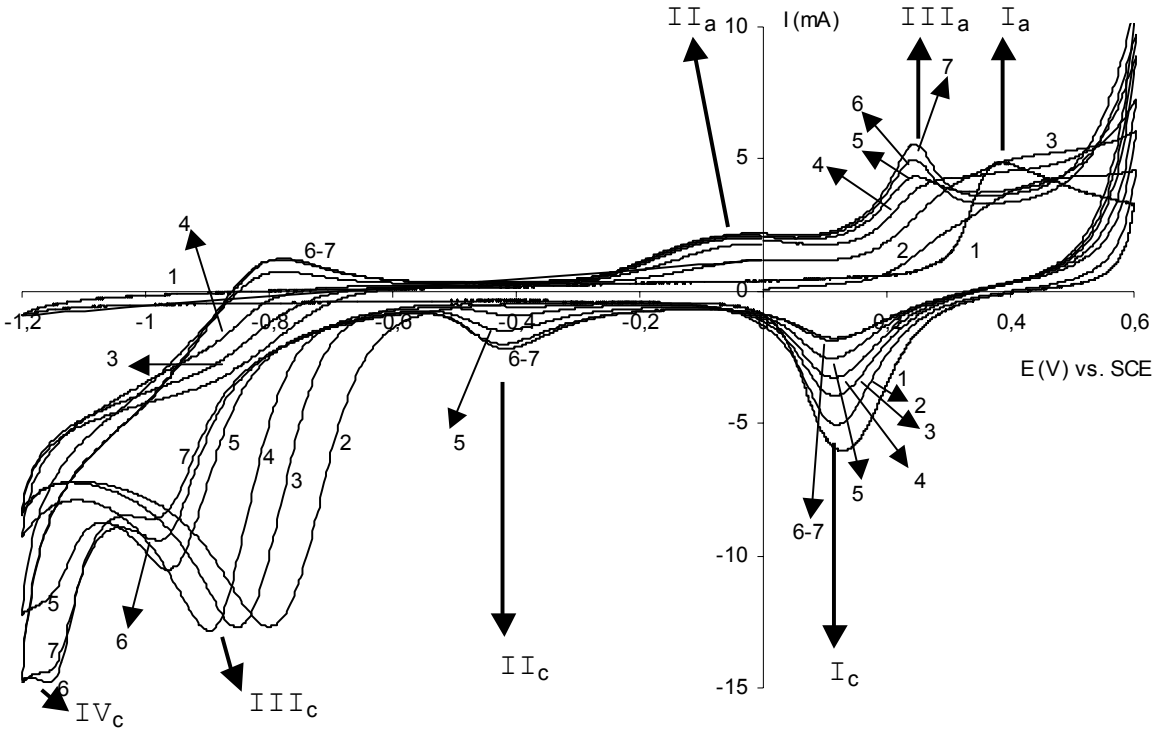

Fig. 4.3: Cyclic voltammograms recorded at a gold electrode in pH 12 buffer solution in the absence (after 20 scans) (curve 1) and presence (curves 2-7) of 8.07 x 10^{-3} mol L^{-1} CoTSPc at a scanrate of 50 mV s^{-1} as a function of scan number. Scan numbers are (2) 1; (3) 2; (4) 5; (5) 10; (6) 15 and (7) 20. [DEWA-04]

Fig. 4.4 shows curves obtained during the following 100 scans, from scan 20 (curve 1) to scan 120 (curve 11). It can be seen that both oxidation peaks (II_a and III_a) and reduction peak II_c, and the associated charges, decrease with increasing scan number. This indicates that CoTSPc initially adsorbed at the electrode surface is again released. A possible explanation is given by the reorganization of the deposited thin films to obtain a thermodynamically more stable condition. At the same time, a third oxidation peak (IV_a) is observed which increases with scan number. Its peak potential is dependent initially on scan number, and eventually becomes independent on scan number.

Another observation in Fig. 4.4 is that the reduction peak III_c increases markedly, combined with a shift of peak potential towards less negative potentials. It can be seen that, simultaneously with the increase of peak III_c, the fourth peak IV_c

decreases, which in fact is the opposite effect of that observed in the first 20 scans. This confirms the interrelationship between the increased/decreased peaks III_c and IV_c. With continued scanning, eventually reduction peak IV_c disappears completely.

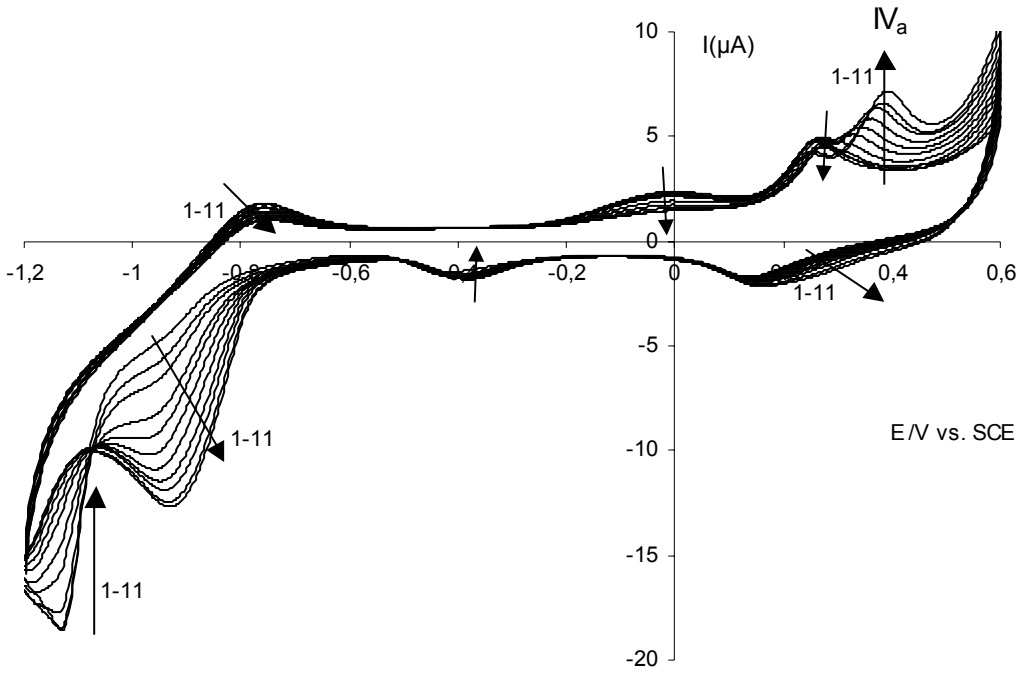

Fig. 4.4: Cyclic voltammograms recorded at a gold electrode in pH 12 buffer solution in the presence of 8.07 x 10^{-3} mol L^{-1} CoTSPc at a scan rate of 50 mV s^{-1} as a function of scan number. Scan numbers are(1) 20; (2) 30; (3) 40; (4) 50; (5) 60; (6) 70 and (7) 90; (8) 90; (9) 100; 10 (110) and (11) 120.[DEWA-04]

It has been shown that the peaks II_a, III_a, I_c and II_c correspond to adsorbed CoTSPc, while peaks III_c and IV_c are attributed to the reaction of CoTSPc in solution. The peaks II_a and II_c are attributed to Co(II)/Co(I) redox system, while the oxidation and reduction peaks III_a and I_c correspond to Co(III)/Co(II). The first system behaves quasi reversibly, the second one is a reversible redox system.

The charges of peaks II_a, III_a and II_c, which first increase with growing scan number, become constant around scan 20 and start to decrease. These variations are attributed to changes in the adsorption configuration of the molecule. While the thin films are formed, it is supposed that a mixture of flat and perpendicularly oriented molecules are deposited. This process is kinetically controlled, explaining the relatively chaotic orientation of the CoTSPc molecules. However, from a thermodynamic point of view, flat oriented molecules (columnar aggregates) are more stable [DEWA-04]. Once saturation of the electrode with CoTSPc is obtained (in scan

20), a reorganization of the thin film takes place from a mixture of flat and perpendicularly oriented molecules towards flat molecules only. To obtain this situation a fraction of initially adsorbed CoTSPc molecules should desorb from the surface to allow others to obtain the flat configuration, explaining the small decrease of the exchanged charge under the peaks. This is reflected by the decrease of the current of reduction peak IV_c and the formation of the third oxidation peak (IV_a). However, both peaks and also peak III_c are to large to be explained by the reduction or oxidation of adsorbed CoTSPc only. It is assumed that this is the result of an electrocatalytic reaction, such as reaction with CoTSPc in solution. This is confirmed by the fact that these peaks disappear when the modified electrode is scanned in a pH 12 buffer solution without CoTSPc. [DEWA-04]

In a later stadium of the research in our research group, the explanation of the peaks has changed and in this work, this new explanation will be followed. In this case, the for this work important reduction peak II_c has been attributed to the Co(III)/ Co(II) reduction of CoTSPc adsorbed on the gold electrode and oxidation peak III_a has been designated to the Co(II)/Co(III) oxidation of the adsorbed CoTSPc and peak II_a has been attributed to the ring oxidation of CoTSPc in solution. [DEWA-05d]

The long term stability of the electrode also has been investigated. This research shows that it takes a considerable period of time before the electrode obtains a stable voltammetric curve (e.g. 960 scans in 8.07×10^{-3} mol L^{-1} CoTSPc). These slow changes in electrode surface conditions are related to the gradual increase in the fraction of gold adatoms at the surface of the modified electrode. The reaction of the adsorbed CoTSPc on the surface has shifted towards the potential of a gold adatom reduction (curve 1, Fig. 4.5). [DEWA-05b]

When the CoTSPc concentration during the modification is changed, similar results were obtained. The same peaks were observed and they also appeared/disappeared as a function of scan number but the number corresponding with the break in the trend of the behavior depends on CoTSPc concentration. Moreover it is clear that the time (or scan number) needed to obtain maximum coverage is dependent on the CoTSPc concentration in solution. This is shown in Fig. 4.6.

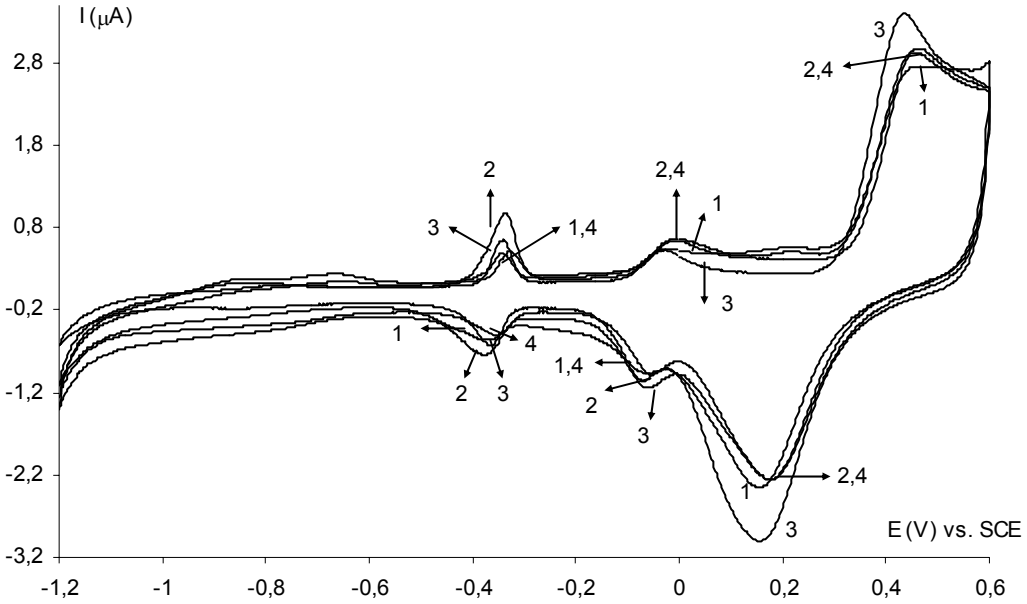

Fig. 4.5: Cyclic voltammograms of long-term continuous cyclic voltammetric scanning experiments recorded at gold electrodes modified with MTSPc in a pH 12 buffer solution containing 8.1 mmol L^{-1} MTSPc. Shown is scan 960 of (1) CoTSPc; (2) iron tetrasulphophthalocyanine (FeTSPc); (3) CuTSPc and (4) Alumina tetrasulphophthalocyanine (AlTSPc). [DEWA-05b]

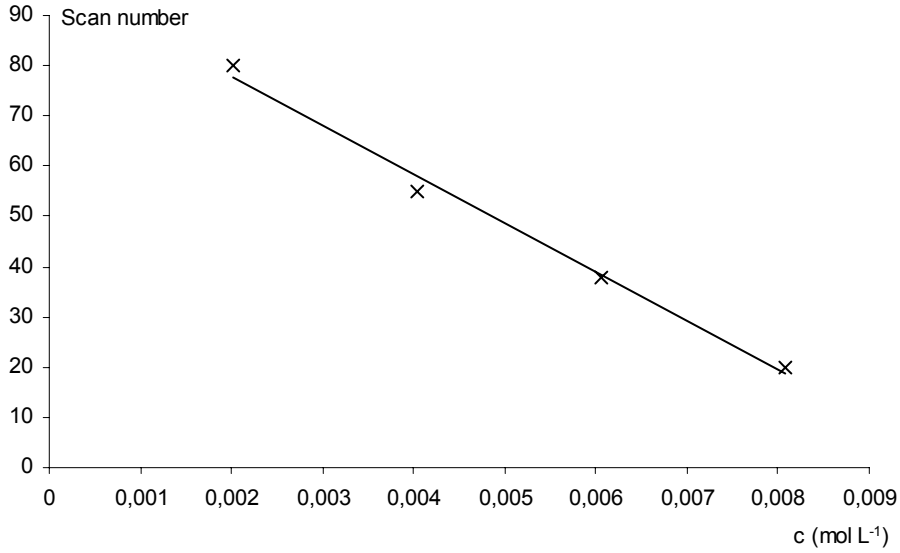

Fig. 4.6: Relationship between scan number and CoTSPc concentration at which different behavior of the CoTSPc thin film formation is observed at a gold electrode in pH 12 buffer solution. [DEWA-04]

Spectroscopic proof of the adsorption of CoTSPc on a gold electrode has been given with Raman and X-ray photoelectron spectroscopy (XPS). The XPS results show that after modification, 94.3 % of the surface is covered with CoTSPc and that

about 90 % of the Co in the CoTSPc is in the Co(II) state. The other 10 % are in oxidation stage 0 or +III.

The results shown in this section are obtained for the modification of a gold electrode with CoTSPc purchased from Mid-Century. This company went bankrupt in 2004. So another supplier had to be found. The results with the CoTSPc purchased from the Rhodes University in South Africa, are similar. Only the moment of break in trend is different. These differences and the possible explanation will be discussed in chapters 5 and 6.

4.1.3 Modification of a gold electrode with CuTSPc [DEWA-05]

The electrodeposition of CuTSPc, with the sulphonic groups randomly spread over the phthalocyanine ring, purchased from Mid-Century on a gold electrode has been described by De Wael et. al. [DEWA-05]. Fig. 4.7 shows some of the 120 cyclic voltammetric scans recorded at a gold electrode in pH 12 buffer solution (curve 1) and a solution containing 8.00 x 10^{-3} mol L^{-1} CuTSPc purchased from Mid-Century. The peaks corresponding to the oxidation of the gold surface (I_a) and the reduction of the gold oxide formed during surface oxidation (I_c), decrease when the electrode potential is cycled. This is, analogous to CoTSPc, a first indication of adsorption, as covering the gold surface with CuTSPc prevents its oxidation and subsequent reduction. The decrease of the gold oxidation and reduction processes is small which indicates that the amount of adsorbed CuTSPc is quite low. There is only a small shift in peak potential during the decrease of signals I_a and I_c, thus these peaks were only attributed to the gold processes. As there is no interference with other 'adsorption' peaks, the decrease of processes I_a and I_c gives an idea about the coverage. Comparison of the charge under the peak associated with the gold reduction (I_c) after 120 scans in a CuTSPc solution (curve 10) with the charge of the same reduction process in curve 1 of Fig. 4.7 (in the absence of CuTSPc), leads to a coverage of 18.3 %.

In curves 2-10 it can be seen that a new oxidation peak, at about -0.29 V and a new reduction peak, at about -0.36 V vs. SCE, occur. Both signals grow during the first 100 scans. The increase with increasing scan number is due to the deposition of CuTSPc on the gold surface. With each scan the amount of deposited CuTSPc increases, which results in higher peak currents because more adsorbed CuTSPc is present at the surface in the next scan. After scan 100, the oxidation and the reduction

processes at -0.29 V and -0.36 V vs. SCE stabilize. In other words there is, as for CoTSPc, an evolution to a fixed peak height or charge that corresponds to a well-defined amount of adsorbed CuTSPc (inset Fig. 4.7). It is also important to note that the rate of decrease of peak I_c, is equal to the rate of increase of the processes at -0.29 and -0.36 V vs. SCE. The oxidation and reduction peaks at -0.29 V and -0.36 V vs. SCE are attributed to the Cu(II)TSPc/Cu(I)TSPc redox system.

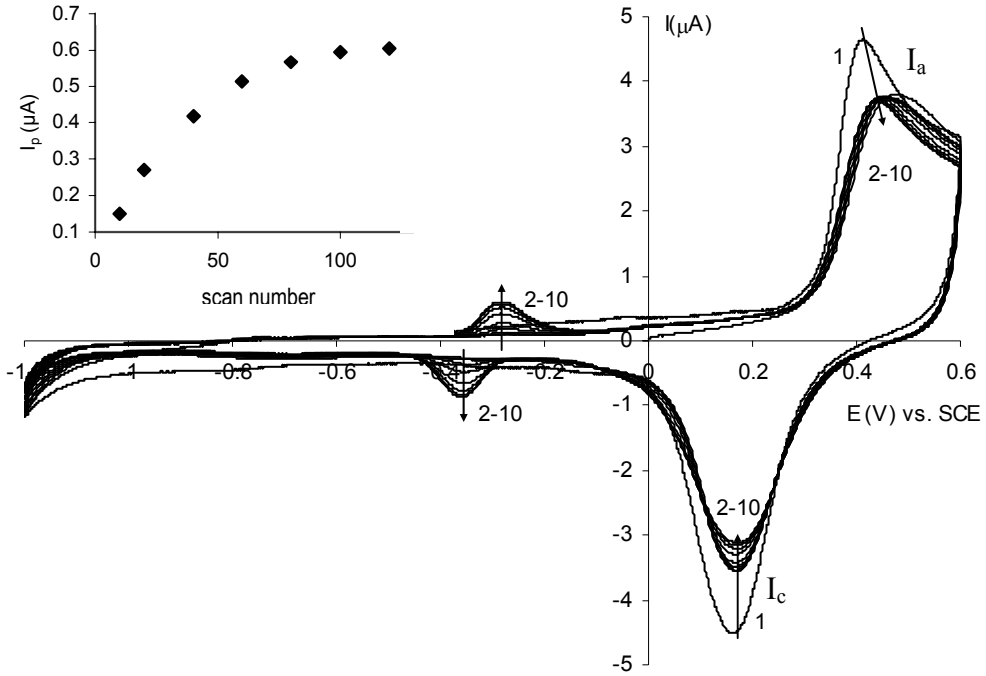

Fig. 4.7: Cyclic voltammograms recorded at a gold electrode in a pH 12 buffer solution in the absence (curve 1) and presence (curve 2-10) of 8.00 x 10^{-3} mol L^{-1} CuTSPc at a scan rate of 50 mV s^{-1} as a function of scan number. Scan numbers are (2) 1; (3) 2; (4) 10; (5) 20; (6) 40; (7) 60; (8) 80; (9) 100 and (10) 120. Inset: Relationship between peak current of the process at -0.29 V vs. SCE and scan number. [DEWA-05]

As for CoTSPc the long term stability of the CuTSPc modified electrode has been investigated and a shift of the potential to the adatom oxidation/reduction process has been noticed.

The presence of CuTSPc on the gold electrodes has been proven with Raman spectroscopy and with XPS. Based on the atomic concentration, obtained from the XPS data, a coverage value of 20.6 % has been calculated.

The electrodeposition of the CuTSPc purchased from Sigma-Aldrich (sulphonic acid groups at the positions 3,4',4'',4''') is quite different from the one described here. The description and interpretation of these data is given in chapter 7.

4.2 Objectives of this work

The past work has been focussed on the electrochemical characterization of gold electrodes modified with CoTSPc, CuTSPc, AlTSPc or FeTSPc and on the electrochemical processes that take place during the modification procedure. In this study, the aim is expanded. Besides the study of electrochemical properties on different metallophalocyanines, also the heterogeneity and the morphology of the modified gold electrode surfaces were taken into account using SR-XRF. Emphasis has been laid on the following phtalocyanines: CoTSPc and CuTSPc.

The heterogeneity and morphology of the CoTSPc and CuTSPc thin films, were studied for three different modification procedures (immersion, drop-drying and electrodeposition). In addition CoTSPc and CuTSPc purchased from different suppliers were tested, voltammetric scan numbers during the electrochemical modification procedure were varied and different phthalocyanine concentrations were used during the modification. The information received from the electrochemical and SR-XRF data was linked with XPS and UV-Vis data, which enabled us to derive the percentage of coverage of the gold electrodes with CoTSPc or CuTSPc and to determine the monomer dimer equilibrium in the phthalocyanine solutions. This way, a better understanding of the modification process and the thin film buildup was obtained and the modification procedure could be optimized.

In addition, the modified gold electrodes were used for the oxidation of 4-Cp, a chemical pollutant. Moreover, the oxidation behavior towards the oxidation of 4-Cp of the modified gold electrodes was linked with the thin film buildup of the CoTSPc and CuTSPc thin films on the gold electrode. In this way, a first step to the development of an electrochemical sensor for the detection of chlorophenols in waste waters using gold electrodes modified with water soluble phthalocyanines was set.

4.3 References

[ABDE-01] Abdelsalam M.E., Denuault G., Baldo M.A., Bragato C., Daniele S., *Electronanal*., **2001**, 13, 289-294.

[BUDE-96] Budevski E., Staikov G., Lorenz W.J., *Electrochemical Phase Formation and Growth An Introduction to the Initial Stages of Metal Deposition*, VCH, Weinheim, **1996**.

[BURK-86] Burke L.D., Cunnane V.J., *J. electroanal. Chem*., 1986, 210, 69-94.

[BURK-89] Burke L.D., O'Leary W.A., *J. Appl. Electrochem.*, **1989**, 19, 758-767.

[BURK-92] Burke L.D., O'Sullivan J.F., *Electrochim. Acta*, **1992**, 37, 585-594.

[BURK-94] Burke L.D., *Electrochim. Acta*., **1994**, 39, 1841-1848.

[BURK-02] Burke L.D., Ahern A.J., O'Mullane A.P., *Gold Bull.*, **2002**, 35, 3-10.

[DEWA-04] De Wael K., Westbroek P., Temmerman E., *J. electroanal. Chem.*, **2004**, 567, 167-173.

[DEWA-05] De Wael K., Westbroek P., Bultinck P., Depla D., Vandenabeele P., Adriaens A., Temmerman E., *Electrochem. Comm.*, **2005**, 7, 87-96.

[DEWA-05b] De Wael K., Westbroek P., Adriaens A., Temmerman E., *Electrochem. solid st.*, **2005**, 8(4), C65-C68.

[DEWA-05c] De Wael K., Westbroek P., Temmerman E., *Electroanal.*, **2005**, 17, 263-268.

[DEWA-05d] De Wael K., *Elektrochemische studie van een goudelektrodeoppervlak gemodificeerd door het immobiliseren van transitiemetaalion-ftalocyanines en –porfyrines*, PhD. **2005**, chapter 5, 65-126.

[TREV-89] Trevor D.J., Chidsey C.E.D., Loiacono D.N., *Phys. Rev. Letters*., **1989**, 62, 929-932.

[WOOD-76] Woods R., in *Electroanalytic chemistry*, Vol. 9, Ed; by Bard A.J., Dekker M., New York, **1976**, 1-162.

Articles

Chapter 5:
Modification of gold electrodes with cobalt tetrasulphophthalocyanine: a comparison of different immobilization techniques

In this chapter the aim is focused on the immobilization characteristics of CoTSPc on gold electrodes. Different modification techniques, such as the immersion of the electrode in a CoTSPc solution, the drop drying, and the potential cycling method (all of them described in chapter 2) were used to produce modified gold electrodes. In the first section of this chapter, the experimental conditions used are described. The second part makes a detailed comparison between the above mentioned modification techniques with respect to the resulting Co thin film properties on the electrode surface. The latter is based on both electrochemical and scanning synchrotron micro X-ray fluorescence (SR-XRF) data. In addition, scanning SR-XRF analyses were performed to determine the level of uniformity of the deposited thin film. This nondestructive, quantitative characterization of CoTSPc deposition on gold electrodes by means of scanning SR-XRF has never been described before and can be in general used for thin film characterization. The third section of the chapter discusses the degree of CoTSPc aggregation, which was studied by performing UV-Vis absorption spectroscopy analyses. A remarkable observation was the difference in dimer-monomer equilibrium for the CoTSPc samples purchased from different suppliers, Midcentury, Porphyrin Systems and Rhodes University of Grahamstown. The influence of the dimerization of CoTSPc on its electrochemical behavior at gold electrodes is described in the fourth section of this chapter after which conclusions are drawn.

5.1 Experimental conditions

Gold electrodes were modified with CoTSPc using the three modification procedures described in chapter 2. The modification was performed with a 6×10^{-3} mol L^{-1} CoTSPc pH 12 buffer solution after which the modified electrodes were voltammetric scanned between -1.2 and 0.6V vs. SCE in a phthalocyanine free buffer solution. To calculate the cobalt surface concentration, the charge of the Co(III)/ Co(II) reduction peak in this phthalocyanine free buffer solution (II_c in Fig. 5.2) was determined in the cyclic voltammogram using the GPES 4.9 software package and has been calculated according to Eq. 5.1

$$c = \frac{n\,Q\,M_{Co}}{F\,A} \qquad \text{(Eq. 5.1)}$$

where c is the cobalt surface concentration in g cm^{-2}, n the number of electrons exchanged during the reduction process, Q the charge according to the Co(III)/Co(II) reduction peak in C, M_{Co} the relative atomic mass of Co which equals 58.93 g mol^{-1}, F Faraday's constant which equals 96485 C mol^{-1} and A the surface area of the gold electrode in cm^2.

The modified electrodes were also studied with scanning SR-XRF performed at Beam Line L of the DORIS-III storage ring, HASYLAB (see section 3.4). This beamline is dedicated to micro XRF experiments using either white or monochromatic bending magnet excitation and mono- or polycapillary focusing, with routinely available beam sizes of 10-30 μm. Chapter 3 has listed the experimental arrangements used (Fig. 3.5). For this set of experiments, the beam was monochromatized by a Si(111) fixed-exit monochromator ($\Delta E/E \approx 10^{-4}$) and further collimated by a motorized cross-slit system after initial low-energy filtering and collimation. After monochromatization, the beam was focused by a monolithic polycapillary half-lens (X-ray Optical Systems Inc.), designed specifically for parallel primary beams and hence suitable for the focusing of low-divergence synchrotron beams. A microbeam size of ~20 μm (FWHM) was obtained at the excitation energy range of 7.7-8.0 keV, which was used to excite selectively the Co $K_{\alpha,\beta}$ fluorescent

lines without exciting Au L lines from the (spectroscopically infinitely thick) gold substrate. The nominal working distance of the polycapillary optic was 5 mm.

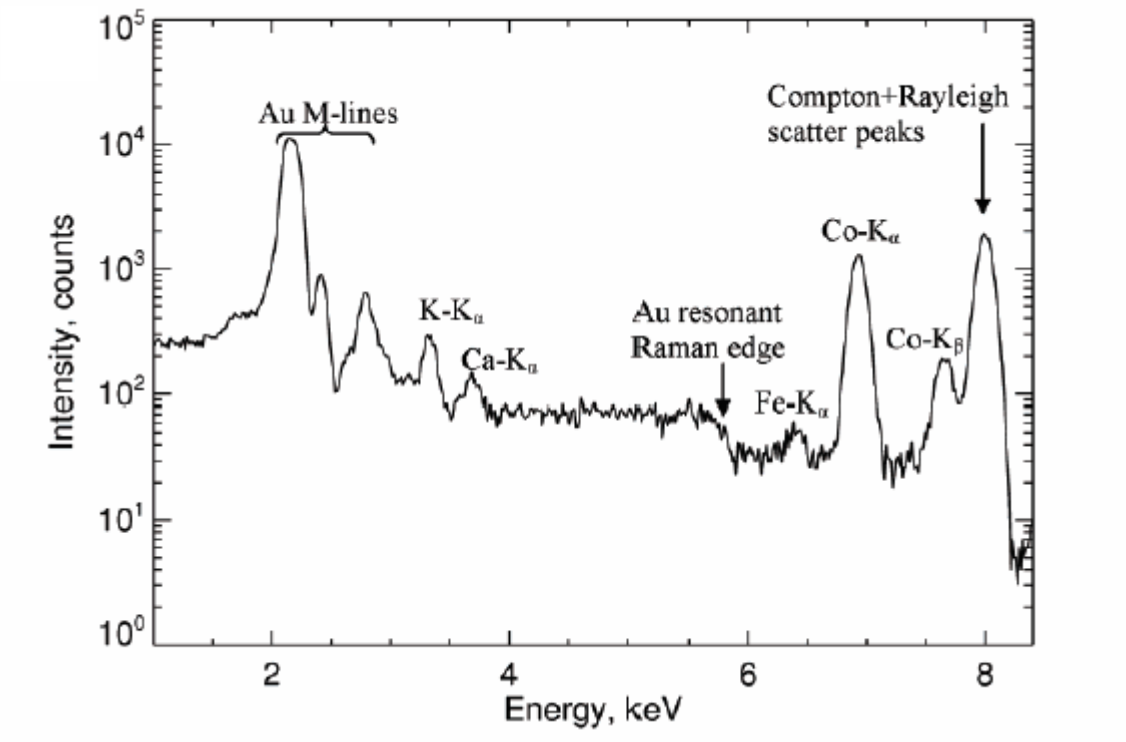

Fig.5.1: Typical XRF spectrum measured at this instrument for a gold electrode corresponding to a measuring time of 500 s.

As already mentioned in chapter 3, experimental difficulty of the CoTSPc thin film uniformity studies included the determination of low amounts of Co (~0.1-0.5 pg, assuming a 20 μm incident beam) in the presence of partially overlapping Compton and Au X-ray resonant Raman peaks. In Fig. 5.1 a typical SR-XRF spectrum measured at Beam Line L for a gold electrode modified with CoTSPc corresponding to a measuring time of 500 s is shown. The most important peaks, as there are, the K-K_α, Ca-K_α, Fe-K_α, Co-K_α, Co-K_β are indicated together with the Au M-lines, the Au-resonant Raman edge and the Compton and Rayleigh scatter peaks. During the CoTSPc uniformity studies, 21 × 21 or 41 × 41 scanning XRF maps were recorded with typically 20-μm step size, using a data collection time of 10-20 s per data point. The non linear least square fitting software AXIL [VEKE-94] was used to determine the net-peak intensities of the Co-K_α in the measured XRF spectra. Absolute detection limits for Co were estimated to be 7-8 ng cm^{-2} using a measuring time of 20 s. To

determine the level of uniformity of the deposited CoTSPs thin film, the scanning and subsequent data reduction strategy described by Kempenaers et al. has been applied [KEMP-02].

The UV-Vis measurements were performed with a Varian Cary 3E spectrophotometer (Instrument version 8.01) (Palo Alto, Canada).

5.2 Comparison of different electrochemical modification techniques

The data in Fig. 5.2a, corresponding to the electrode immersion method, show the growth of the $Co(III)_{ads}$/ $Co(II)_{ads}$ redox couple during the first 20 voltammetric scans in the buffer solution after the modification, which implies that some of the CoTSPc is adsorbed onto the gold surface. The peaks at -0.335 (II_c) and 0.236 V (II_a) versus SCE reflect the reduction/ oxidation behavior of adsorbed Co(III)TSPc and Co(II)TSPc. The peaks attributed to a ring reaction of adsorbed CoTSPc appear at ~ -0.9 V versus SCE and are indicated by III_a in Fig. 5.2a.

Another observation that provides evidence for adsorption is the decrease of the relatively broad AuO formation peak around 0.5 V versus SCE (Ia) (curve 1 vs. curve 2-7 in Fig. 5.2a) and its related reduction signal at 0.15 V versus SCE (Ic) as described in chapter 4. As the gold surface is covered with CoTSPc, the oxidation and reduction of the gold(oxide) surface is prevented. A remarkable result is the growth of the CoTSPc-related adsorption peaks during the first 10 voltammetric scans. After these 10 voltammetric scans, a stable cyclic voltammogram is observed. This growth with increasing voltammetric scan number is probably associated with the transformation of a heterogeneous surface thin film into a homogeneous surface condition as indicated by the scanning SR-XRF uniformity studies discussed below. The charge under the Co(III)/Co(II) adsorption reduction peak (II_c), based on voltammetric scan 20, is equal to 2.4 ± 0.3 μC, which corresponds to an adsorbed cobalt surface density of ~0.074 μg cm^{-2} (Table 5.1). It is also remarkable that the reduction peak I_c increases with growing voltammetric scan number during the first 10 voltammetric scans after the modification (curve 2-7 in Fig. 5.2a). This can be explained by the electrochemical reactivation of the gold. This effect is indeed also seen when a bare gold electrode, after electrochemical activation, is immersed in a pH

12 buffer solution for two hours and then voltammetric scanned again in a pH 12 buffer solution in the given potential window.

A similar electrochemical behavior is shown when a modified electrode is created by the drop drying method. Fig. 5.2b represents the evolution of the Co(III)/Co(II)-related adsorption peaks during the first 20 voltammetric scans when the modified CoTSPc gold electrode is voltammetric scanned in a blank buffer solution after the drop drying process. The charge under the Co(III)/Co(II) adsorption peak, again based on voltammetric scan 20, is equal to 3.2 ± 0.2 μC, which corresponds to a cobalt surface density of 0.098 μg cm^{-2} (Table 5.1). The increase of reduction peak I_c (curve 2-7 in Fig. 5.2b) can also be explained by the electrochemical reactivation of the gold after the drop drying, as is the case for the immersion method. Comparison of the two above-mentioned modification techniques leads to the conclusion that more CoTSPc is adsorbed onto the electrode surface when modifying by drop drying. This is due to the intensive contact between the droplet and the electrode and the intensive drying process.

Table 5.1. Electrochemical and SR-XRF Data[a]

Modification techniques	**Charge (μC)**	**Surface concentration (μg cm^{-2})**	**Mean Co-K_α**	**δ_{Co}/I_{Co} x100 (%)**	**Total surface concentration derived by SR-XRF (μg cm^{-2})**
Immersion	2.4±0.2	0.074	135.4	28.4	0.08±0.02
Drop drying	3.2±0.2	0.098	192.7	37.4	0.14±0.05
Potential cycling	3.6±0.2	0.110	2036.7	31.6	3.3±1.0

[a] *The first three columns show the electrochemical data concerning the three modification techniques: the charge due to the Co(III)/Co(II) reduction peak and the calculated cobalt surface concentration. The last three columns show the SR-XRF data, respectively, the mean Co K_α intensity, its relative standard deviation, and the total cobalt surface concentration.*

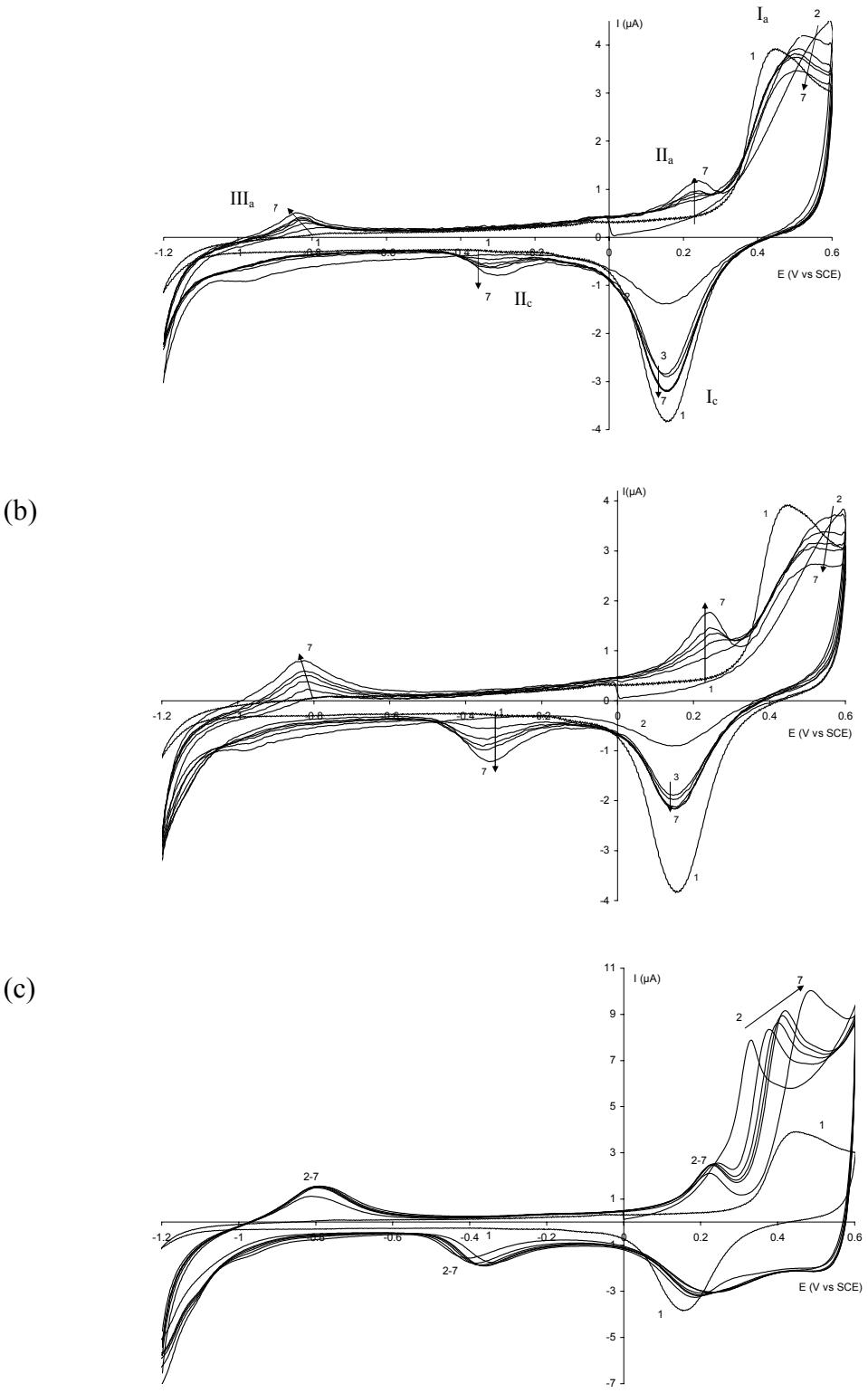

Fig.5.2: Current-potential curves recorded at a gold electrode in a pH 12 buffer solution (1) and voltammetric scanning of the modified electrode in a pH 12 buffer solution (2-7). Voltammetric scan numbers: (2) 1, (3) 3, (4) 5, (5) 7, (6) 10, and (7) 20. Different modification techniques: electrode immersion (a), drop drying (b), and potential cycling (c).

The recorded cyclic voltammograms corresponding to the potential cycling method are shown in Fig. 5.2c. The first voltammetric scan already shows that the charges of the adsorption processes reach their maximum value. This means that there is no change in the surface condition, as will be explained below when dealing with the spectroscopic analysis of the modified electrodes. The charge under the Co(III)/Co(II) adsorption reduction peak is equal to 3.6 ± 0.2 μC, which corresponds to an adsorbed Co surface concentration value of 0.110 μg cm^{-2} (Table 5.1). Curves 2-7 show that a new oxidation peak shifts from 0.3 to 0.45 V versus SCE during the first 20 voltammetric scans. It is hypothesized that this oxidation peak is caused by the electrocatalytic oxidation of hydroxide ions in the pH 12 buffer solution.

Micro SR-XRF measurements were performed to provide further experimental evidence of the formation of an adsorbed CoTSPc thin film at the gold electrodes and to study the uniformity of the formed thin film quantitatively. Fig. 5.3 shows the measured elemental maps and the corresponding intensity distribution of the detected Co K_α (Fig. 5.3a, immersion; b, drop drying; c and d, potential cycling) obtained by SR-XRF measurements after normalization with the gold M line. These figures not only provide evidence of the occurrence of adsorbed CoTSPc but also give an estimate of the amount of adsorbed CoTSPc. The total surface concentrations derived by SR-XRF are shown in Table 5.1 together with the surface concentrations derived from the electrochemical data. Comparison of the surface concentrations derived from both techniques shows that there is a discrepancy between the calculated surface concentrations. This discrepancy can be explained by a different electrochemical activity of the CoTSPc monomer and dimer species (see further). Only CoTSPc monomer species appear to be electrochemically detected and not the dimer species. When it is assumed that CoTSPc dimers are present on the modified electrode in any circumstance, but that these compounds are not electrochemically active, they will not be electrochemically detected. In contrast, the XRF measurements are able to detect all kind of cobalt species, monomers as well as dimers. Therefore, the XRF signal includes both the monomer and the dimer signal leading to significant higher amounts of cobalt.

On the basis of Fig. 5.3, it can be concluded that when cycling the gold electrode in a Co(II)TSPc pH 12 buffer solution during 100 voltammetric scans in a potential window from -1.2 to 0.6 V versus SCE (Fig. 5.3c), the amount of adsorbed CoTSPc is much larger than in the case of the two other techniques (Fig. 5.3a and b).

The normalized intensity is much higher (more than a 10-fold) in the case of potential cycling. The relative standard deviation calculated from the relative FWHM of the histograms and the calculated Co surface concentration values calculated by the fundamental parameter method (see chapter 3) are presented in Table 5.1.

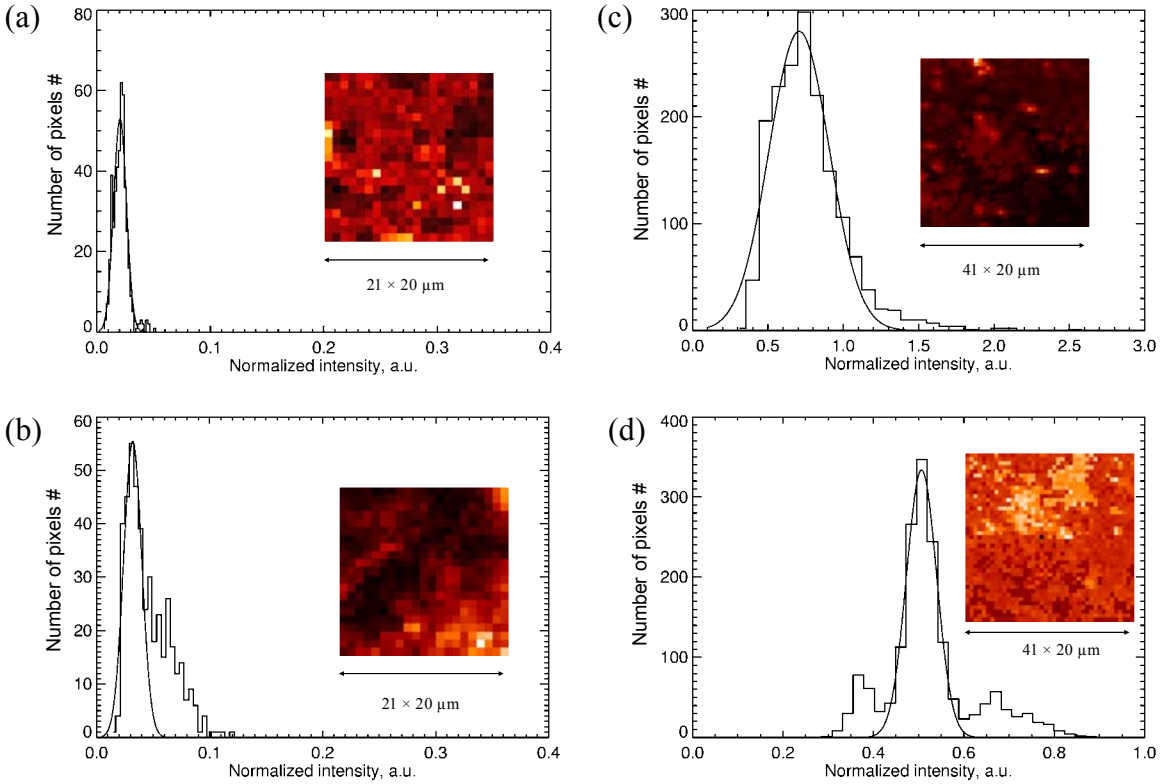

Fig. 5.3: Elemental map and intensity distribution of cobalt on a gold electrode modified by three different modification techniques: electrode immersion (a), drop drying (b), and potential cycling during 100 subsequent voltammetric scans with 20 voltammetric scans in pH 12 buffer after modification (c) and without 20 voltammetric scans in pH 12 buffer after modification (d). The XRF maps consists of a 21 × 21 or 41 × 41 raster using 20 µm step size in both X and Y directions.

A similar experiment was performed to investigate the influence of cycling in a blank buffer solution during 20 voltammetric scans (after the modification) on the homogeneity of the adsorbed CoTSPc thin film. A gold electrode, modified by recording 100 voltammetric scans in a pH 12 buffer solution containing 6×10^{-3} mol L^{-1} CoTSPc was rinsed with buffer solution and directly analyzed by SR-XRF. The voltammetric scanning in a pH 12 buffer solution after the modification was now skipped in the procedure. The elemental map and the matching histogram obtained by SR-XRF measurements after normalization with the gold M line, are presented in Fig. 5.3d. The histogram shows a more heterogeneous distribution of Co. This means

that the voltammetric scanning step in the buffer solution (after modification) is needed to obtain a homogeneous adsorbed CoTSPc thin film. This hypothesis can also be used to explain the increase of the peak current of peaks II_a, III_a and II_c with growing voltammetric scan number for the adsorption processes in Fig. 5.2a and b. The increase reflects the transformation of a heterogeneous to a more homogeneous surface condition. The enhancement of homogeneity can be attributed to the fact that by cycling the potential the deposited thin films goes through different orientation stages until a thicker and more stable thin film is formed. In the latter situation, the flipping process from one orientation into another is no longer possible.

On the basis of the above-mentioned arguments, it can be concluded that the homogeneity is clearly enhanced by the subsequent voltammetric scanning in the buffer solution after the modification. As there is more CoTSPc adsorbed onto the surface, the deposition is more efficient. More information on this modification technique, also called electrodeposition, and on its use to create modified electrodes with important electrocatalytic properties can be found in chapter 4.

5.3 Dimerization of CoTSPc

It has been observed that the efficiency of electrodeposition highly depends on the degree of dimerization of CoTSPc. Prior to explaining this influence, the monomer-dimer equilibrium was studied. UV-visible absorption spectra of tetrasulphophthocyanines have been described in terms of the monomer-dimer equilibrium [YANG-85, THAM-02, CAMP-02]. The absorption spectrum is dominated by the Q-band arising from π-π^* transitions. Within the Q-band, several peaks can be assigned to either free molecules or aggregates. In general, the aggregate peak is blue-shifted with respect to the monomer peak. Aggregation can be influenced by the pH, ionic strength, solvent, etc. Fig. 5.4 shows the UV-visible spectra obtained from the CoTSPc samples, obtained from three different manufacturers, in a pH 12 buffer solution in a concentration range from 2.5×10^{-6} to 2×10^{-5} mol L^{-1}. In this concentration range, a linear relationship between absorbance and concentration is observed. As the Lambert-Beer equation is no longer valid when the absorbance is higher then 3, the UV-Vis measurements can not be performed at the CoTSPc concentrations used during the modification process. Therefore, and since UV-Vis has

been used to study the monomer-dimer equilibrium in solution, only a hypothesis about the monomer-dimer equilibrium can be formulated for the CoTSPc concentrations used during the modification. In this case it has been assumed that the monomer-dimer equilibrium of the CoTSPc species purchased from the three different suppliers follow the same trend at the higher concentrations then the one detected with UV-Vis for the lower concentrations.

The monomer peak for the CoTSPc species in a pH 12 buffer solution is located at 661 nm, while the dimer peak is observed at 634 nm [THAM-02, CAMP-02]. Fig. 5.4a shows that the pH 12 buffer solution containing CoTSPc powder purchased from Rhodes University of Grahamstown consists of monomer species as well as dimers in a concentration range from 2.5×10^{-6} to 2×10^{-5} mol L^{-1}. Because of the higher absorbance for the monomer peak in the complete concentration range and because of the similarity of the molar absorption coefficient ε for the monomer and the dimer ($\varepsilon_M = 1.21 \times 10^5$ M^{-1} cm^{-1} and $\varepsilon_D = 7.7 \times 10^4$ M^{-1} cm^{-1} at 25 °C in water) [YANG-85], it can be stated that more monomers are present even at higher concentrations (e.g., 6×10^{-3} mmol L^{-1} for the modification technique). As can be seen in Fig. 5.4b, the sample purchased from Midcentury consists of a smaller percentage of dimers than the CoTSPc species purchased from the Rhodes University of Grahamstown. This means that the CoTSPc species can be found more in their monomer form. Therefore, it is evident that, for higher concentrations their will be some CoTSPc present in its monomer form. In contrast, the UV-visible spectrum of CoTSPc purchased from Porphyrin Systems (Fig. 5.4c) reveals that for the highest concentrations of CoTSPc more dimers than monomers are present in the pH 12 buffer solution. On the basis of this observation, it can be concluded that, at high concentrations, such as 6×10^{-3} mmol L^{-1}, aggregation will be completed and dimers are the dominant species.

When comparing the UV-visible spectra of all CoTSPc samples, it is clear that the monomer-dimer equilibrium is different. Based on Fig. 5.4, it is assumed that at high CoTSPc concentrations (e.g., 6×10^{-3} mmol L^{-1} for the modification technique) more dimers than monomers are formed in the case of Porphyrin Systems. For the CoTSPc sample, purchased from Midcentury and Rhodes University of Grahamstown, the figures show that even at high CoTSPc concentrations their will be more monomer species in the solution than is the case for the CoTSPc from

Phorphyrin Systems. In the next section, the influence of the monomer dimer equilibrium on the electrochemical behavior at gold electrodes will be discussed.

(a)

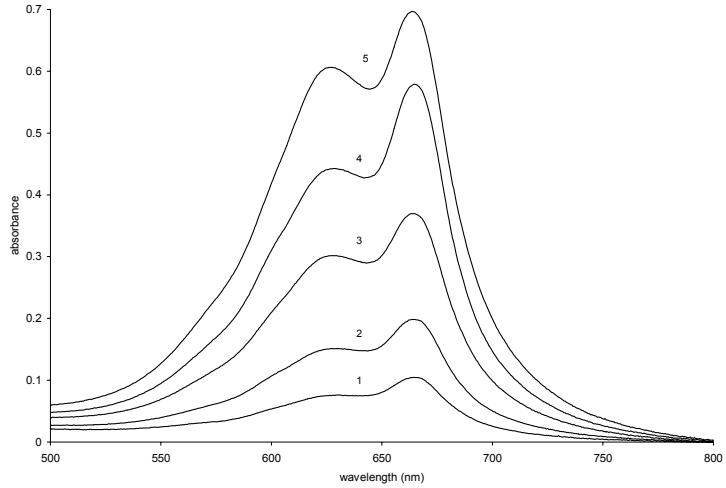

(b)

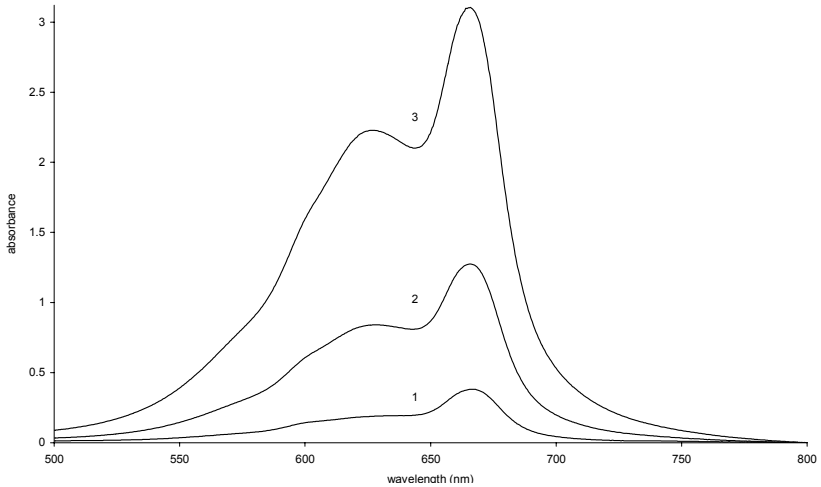

(c)

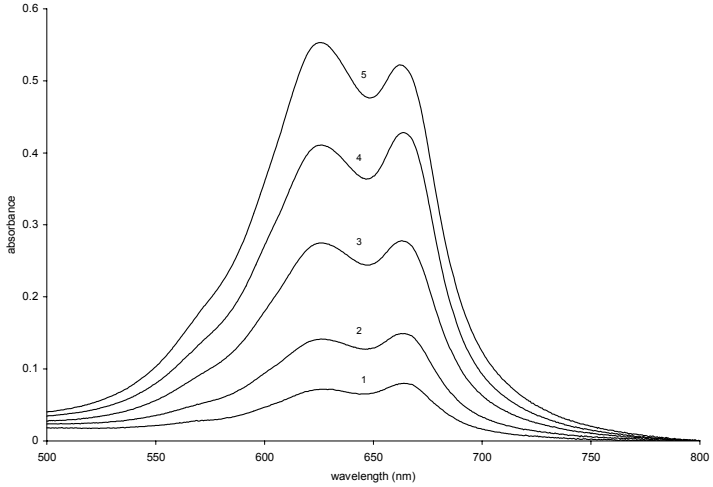

Fig. 5.4: Absorbance spectra of a pH 12 buffer solution containing different cobalt(II) tetrasulphophthalocyanine concentrations purchased from the following manufacturers. (a) Rhodes University: (1) 2.5 × 10^{-6}, (2) 5.0 × 10^{-6}, (3) 1.0 × 10^{-5}, (4) 1.5 × 10^{-5}, and (5) 2.0 × 10^{-5} mol L^{-1}. (b)Midcentury: (1) 4.4 × 10^{-6}, (2) 1.9 × 10^{-5}, and (3) 4.8 × 10^{-5} mol L^{-1}. (c) Porphyrin Systems: (1) 2.5 × 10^{-6}, (2) 5.0 × 10^{-6}, (3) 1.0 × 10^{-5}, (4) 1.5 × 10^{-5}, and (5) 2.0 × 10^{-5} mol L^{-1}.

5.4. Influence of the dimerization of CoTSPc on the electrodeposition at gold surfaces.

As described in section 5.2, the most efficient modification technique that leads to a homogeneous CoTSPc thin film onto the gold surface is achieved by electrodepostion. More precisely when the modification occurs by recording 100 successive cyclic voltammetric scans in a potential window from -1.2 to 0.6 V versus SCE in a pH 12 buffer solution containing 6×10^{-3} mol L^{-1} CoTSPc and when after the modification 20 subsequent voltammetric scans are recorded in the same potential window in a pH 12 buffer solution without CoTSPc. This modification method was now used for all CoTSPc samples.

The modification of gold electrodes with CoTSPc (Midcentury) has previously been described in detail in chapter 4, including the explanation of all peaks recorded in the corresponding CoTSPc pH 12 buffer solution. It was observed that the mechanism of the deposition can be considered as a multistep process. The initial deposition, from voltammetric scan 1 to the breaking point (point of maximum adsorption), is kinetically controlled resulting in a chaotic multilayer. After the breaking point, a slow reorganization of the chaotic multilayer occurs. The voltammetric scan related to the breaking point for the CoTSPc purchased from Midcentury is shown in Fig. 5.5, curve 2. It could be observed that the charge under the peak (II_c, see Fig. 4.3) associated with $CoTSPc_{ads}$ (taken at the breaking point, when deposition is virtually complete) is equal to 4.1 ± 0.2 μC. As already suggested by the differences in the measured UV-visible spectra corresponding to CoTSPc from Porphyrin Systems and Rhodes University of Grahamstown (Fig. 5.4), a different electrochemical behavior is expected when using CoTSPc from these suppliers.

Curve 3 in Fig. 5.5 represents the voltammetric scan related to the breaking point recorded in a pH 12 buffer solution containing 6×10^{-3} mol L^{-1} CoTSPc, purchased from Rhodes University of Grahamstown. The charge under the peak associated with $CoTSPc_{ads}$ reduction is equal to 3.7 ± 0.2 μC. This value for the charge, corresponding to the amount of adsorbed CoTSPc is somewhat lower than the value obtained from the Midcentury sample. This discrepancy can be explained by the difference in monomer-dimer equilibrium. Compared to CoTSPc from Rhodes University of Grahamstown, the monomer-dimer ratio is higher in the case of

Midcentury. As the amount of adsorbed CoTSPc is higher in the case of Midcentury, it can be concluded that only the monomer species of CoTSPc can be adsorbed onto the gold surface.

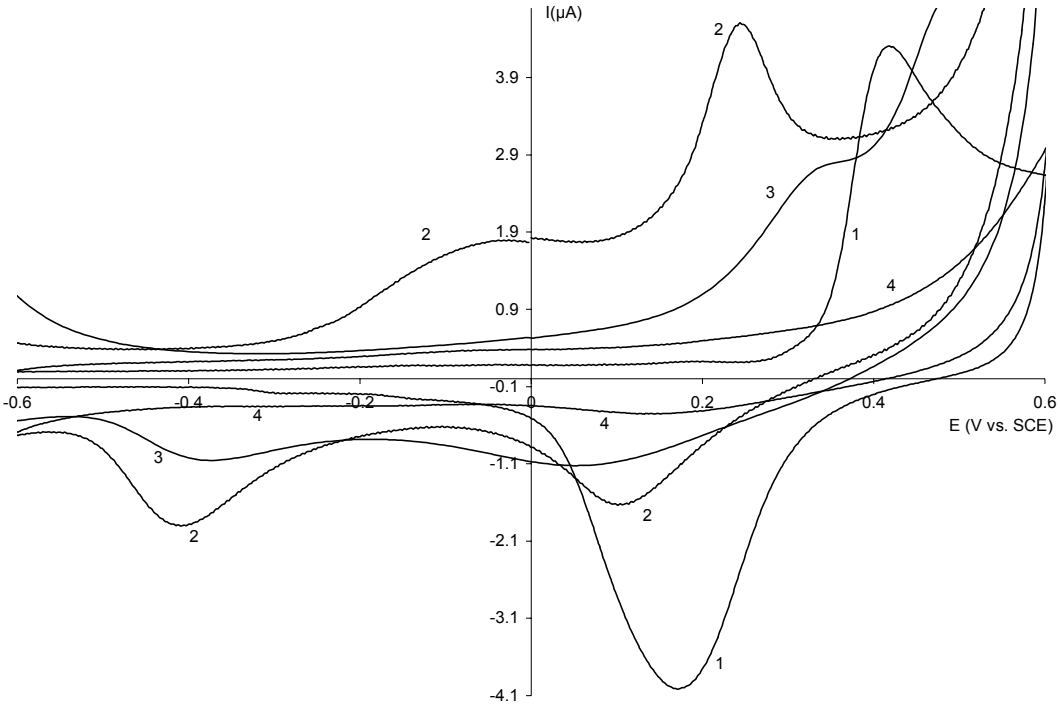

Fig. 5.5: Current-potential curves recorded at a gold electrode in a pH 12 buffer solution without CoTSPc (1) and the voltammetric scan measured at the breaking point of the voltammograms for the three different companies: Midcentury (2), Rhodes University (3), and Porphyrin Systems (4).

Curve 4 in Fig. 5.5 corresponds to voltammetric scan 20 recorded in a 6 mmol L^{-1} CoTSPc buffer solution purchased from Porphyrin Systems. As shown in Fig. 5.4c, the UV-visible spectrum indicates that principally dimers are present in the solution. Because the adsorption onto electrodes only takes place through the monomer species, no electrochemical adsorption reactions can be obtained. The electrode is surrounded by dimers; however, there is no specific bonding between the two resulting in an electrochemical signal. The presence of the electrochemical inactive CoTSPc dimer species near the gold electrode, however, might cause the disappearance of the gold oxidation and reduction peak (I_a and I_c).

5.5 Conclusions

A comparison of different surface modification techniques for gold electrodes with CoTSPc has been described in this chapter. Results have shown that performing successive cyclic voltammetric scans clearly leads to a more efficient deposition, which results in a uniformly adsorbed CoTSPc thin film. A study of the deposited CoTSPc thin film by scanning micro SR-XRF allowed us to derive the adsorbed Co surface concentration values and their relative standard deviations for the various surface modification techniques, which could be used to establish the optimum electrochemical deposition conditions for CoTSPc.

It was also observed that, depending on the monomer-dimer equilibrium of the CoTSPc solution, the electrochemical deposition can be influenced. In this chapter it is shown that only the monomer species of CoTSPc can be adsorbed electrochemically onto a gold surface.

5.6 References

[CAMP-02] Camp P.J., Jones A.C., Neely R.K., Speirs N.M., *J. Phys. Chem. A,* **2002**, 106, 10725-10732.

[KEMP-02] Kempenaers L., Janssens K., Vincze L., Vekemans B., Somogyi A., Drakopoulos M., Simionovici A., Adams F., *Anal. Chem.,* **2002**, 74(19), 5017-5026.

[THAM-02] Thamae M., Nyokong T., *Polyhedron,* **2002**, 21, 133-140.

[VEKE-94] Vekemans B., Janssens K., Vincze L., Adams F., Vanespen P., *X-ray Spectrom*., **1994**, 23, 278-285.

[YANG-85] Yang Y.-C., Ward J.R., Seiders R.P., *Inorg. Chem.,* **1985**, 24, 1765-1769.

Chapter 6:
Study of the electrodeposition of CoTSPc on gold electrodes as a function of voltammetric scan number

In the previous chapter, the immobilization characteristics of CoTSPc on gold electrodes with three different modification procedures were described. Based on the electrochemical, synchrotron micro X-ray fluorescence (SR-XRF) and UV-Vis data, it could be concluded that the electrodeposition of CoTSPc is the most efficient modification procedure and that the monomer-dimer equilibrium of CoTSPc in solution has a major influence on the modification. Therefore, in this chapter, cyclic voltammetry and scanning SR-XRF have been used to study the electrodeposition of CoTSPc on gold electrodes as a function of the voltammetric scan number. CoTSPc purchased from one single supplier was used (Rhodes University of Grahamstown, Eastern Cape, South Africa) to collect the data of this chapter. The experimental setup for the SR-XRF study is the same as described in chapter 5, thereby obtaining a similar SR-XRF spectrum as in Fig. 5.1. Also similar was the procedure to determine the level of uniformity of the deposited CoTSPs thin film and the subsequent data reduction strategy described by Kempenaers et al. [KEMP-02].

6.1 Study of the electrodeposition as a function of voltammetric scan number

This chapter discusses the electrochemical potential cycling method which is used to deposit a film of phthalocyanines onto a gold electrode. This technique enables one to control and characterize the formed thin film by following the potential and current during the deposition process as a function of the applied number of voltammetric scans. The modification was done by recording successive cyclic voltammetric scans in a potential window from -1.2 to 0.6 V vs. SCE (50 mV s^{-1}) during 100 voltammetric scans in a pH 12 buffer solution containing 6.0 mmol L^{-1}

CoTSPc. Fig. 6.1 shows a few of the 100 cyclic voltammetric scans subsequently and continuously recorded at a gold electrode in order to create an electrochemically modified CoTSPc gold electrode. A detailed explanation of all electrochemical processes can be found in chapter 4.

Only the reduction peak at -0.335 V vs. SCE ($Co(III)TSPc_{ads}/Co(II)TSPc_{ads}$) is relevant for this study. The charge related to this adsorption process, which first increases with growing number of voltammetric scans, becomes constant around voltammetric scan 17. This voltammetric scan is also called the breaking point, the voltammetric scan characterized by a maximum adsorption. Before the breaking point, the adsorption process is kinetically controlled resulting in a chaotic multilayer of CoTSPc molecules. Once the breaking point of deposited CoTSPc is reached (voltammetric scan 17), a reorganization of the chaotic multilayer takes place towards a more stable and ordered multilayer structure of CoTSPc molecules (columnar aggregates) (see chapter 4).

Table 6.1 shows the charges related to the $Co(III)_{ads}/Co(II)_{ads}$ reduction, after a background correction, indicating the increase of the charge with growing number of voltammetric scans before the breaking point and the stabilization after voltammetric scan 17. The lower value of the charge related to voltammetric scan 30 was not expected but can be attributed to the occurrence of impurities that alter the modification. The cobalt surface concentrations calculated from the electrochemical data as well as those derived from the XRF measurements are presented. The XRF measurements were performed after different number of voltammetric scans. The elemental maps of the deposited Co and the corresponding histograms of the detected Co-K_α intensities (Fig. 6.2a: voltammetric scan 5, 6.2b: voltammetric scan 10, 6.2c: voltammetric scan 17, 6.2d: voltammetric scan 30 and 6.2e: voltammetric scan 100), derived from the SR-XRF measurements after normalization using the gold M lines are presented in Fig. 6.2. The average cobalt intensity, its relative standard deviation and the average cobalt surface concentration is summarized in Table 6.1.

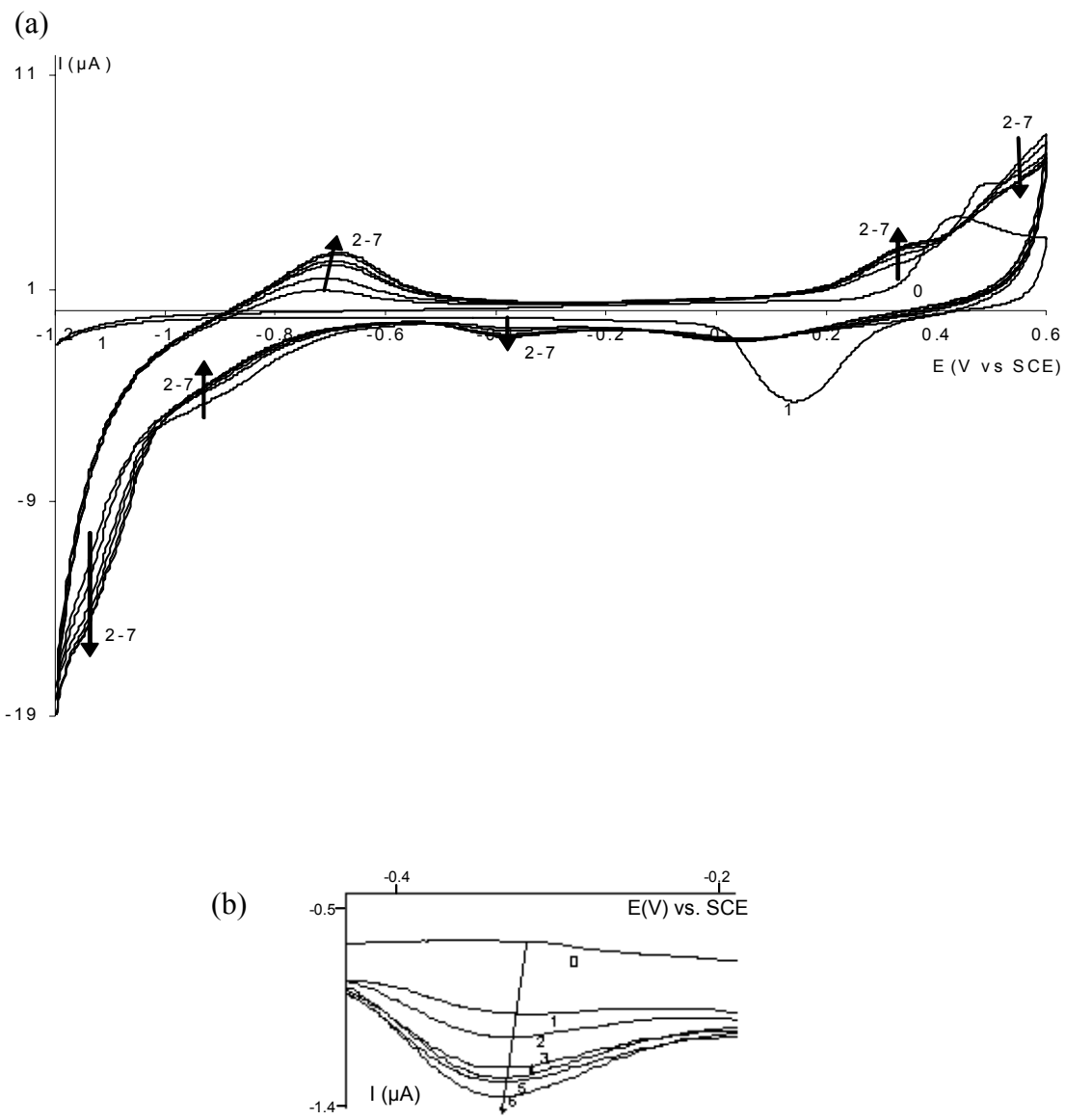

Fig. 6.1: (a) Current potential curves recorded at a gold electrode with a scan rate of 50 mVs^{-1} before (1) and after modification (2-7) with a subsequent number of cyclic voltammetric scans in a pH 12 buffer solution containing 6 mmol L^{-1} Co(II)TSPc. Number of modification scans are (2) 3, (3) 5, (4) 10, (5) 17, (6) 30 and (7) 100. (b) shows an enlarged view of the reduction process at -0.38 V vs SCE.

Table 6.1: Electrochemical and SR-XRF data[a]

Number of voltammetric scans	Charge (μC)	Surface concentration (μg cm^{-2}) measured by voltammetry	$<I_{Co}>$	$\delta_{Co}/\bar{I}_{Co}$ (%)	Surface concentration (μg cm^{-2}) measured by SR-XRF
5	3.3±0.2	0.100	201.0	18.9	0.17±0.03
10	3.8±0.2	0.115	663.8	10.5	0.44±0.05
17	3.9±0.2	0.118	511.3	16.0	0.38±0.06
30	3.5±0.3	0.106	1404.1	7.7	1.03±0.08
100	3.6±0.2	0.110	2036.7	31.6	3.30±1.00

[a] *First three columns show the electrochemical data respectively the number of modification scans in a pH 12 buffer solution containing 6 mmol L^{-1} CoTSPc, the charge due to the Co(III)/Co(II) reduction peak and the calculated surface concentration. The last three columns show the SR-XRF data respectively the average cobalt intensity, its relative standard deviation and the cobalt surface concentration.*

These figures (6.2a to 6.2e) not only provide evidence of the occurrence of adsorbed CoTSPc but also give an estimate of the amount of adsorbed CoTSPc. First, the surface concentrations based on the XRF data are significant higher than those obtained from the electrochemical data. Secondly, in contrast with the electrochemical data, it can be seen that the amount of cobalt keeps increasing even after voltammetric scan 17. Based on these observations, the discrepancy between both methods can be explained by the fact that only CoTSPc monomer species and not dimers can be electrochemically detected. As only monomer species adsorb onto the gold surface by potential cycling, a constant value for the charge is expected after voltammetric scan 17, even when dimers are also stacked around the adsorbed monomers. It is expected that CoTSPc dimers surround the modified electrode in any circumstances, but these compounds are not electrochemically active. In contrast, the XRF measurements are able to detect the total amount of both cobalt species, monomers as well as dimers. Therefore, the XRF signal which includes both the monomer as well as the dimer signals leads to significantly higher surface concentration of cobalt compared to the electrochemically detectable amount. The difference between the cobalt amount calculated from the XRF measurements (monomers and dimers) and the one obtained

from the electrochemical experiments (only monomers) gives an estimate of the amount of dimers. It can be seen in Fig. 6.3 that the number of CoTSPc dimers stacked around the modified electrode increases with voltammetric scan number. This means that in the beginning of the modification monomer species are adsorbed on the gold electrode. Once the monomers are adsorbed the dimers start to adsorb too since the electrodes is surrounded by monomers as well as dimers. After the breaking point only dimers are adsorbed.

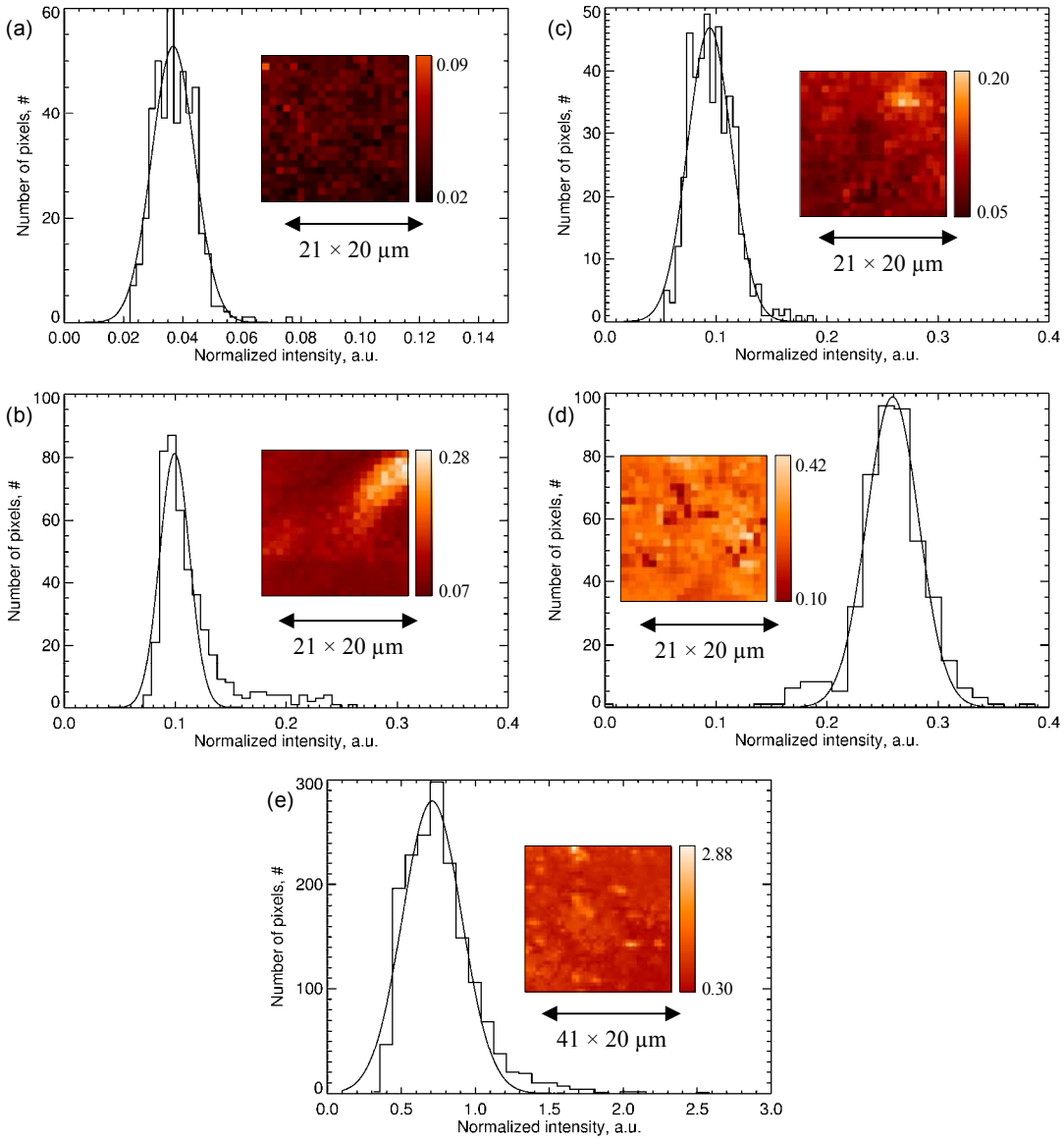

Fig. 6.2: Elemental map with the corresponding shale bar of deposited Co and the corresponding histogram of the detected Co-K_α line obtained from a modified gold electrode as a function of voltammetric scan number: 5 scans (a), 10 scans (b), 17 scans (c), 30 scans (d) and 100 scans (e). The XRF maps consist of a 21x21 or 41x41 raster using 20 µm step size in both X and Y direction.

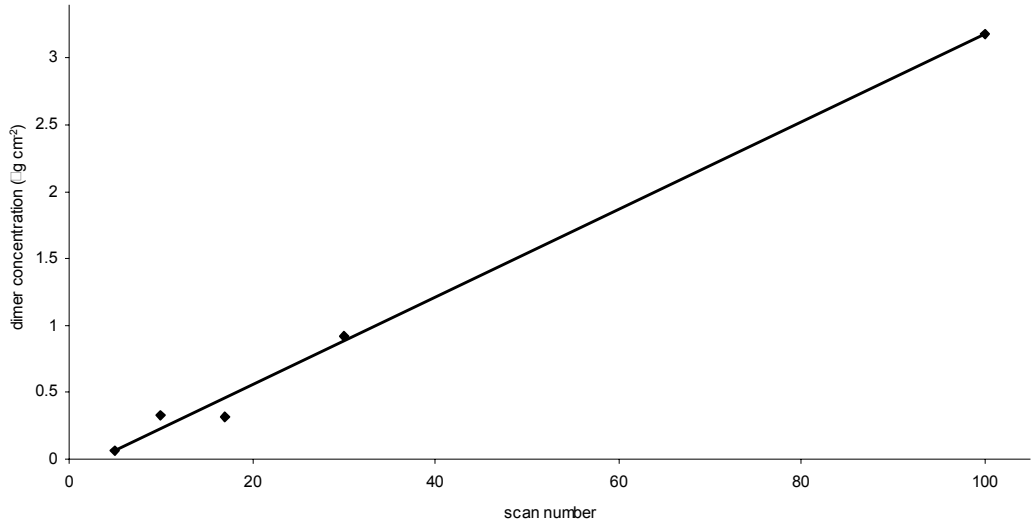

Fig. 6.3: Relationship between dimer concentration and number of voltammetric scans.

6.2 Conclusions

This chapter has provided a detailed study concerning the morphology and heterogeneity of the electrochemical deposited phthalocyanine thin film onto a gold electrode as a function of voltammetric scan number. The non-destructive characterization of CoTSPc deposited on a modified gold electrode was performed by means of synchrotron micro X-ray fluorescence. The electrochemical measurements and scanning micro SR-XRF allowed us to derive the adsorbed Co surface concentration values.

Results showed that only monomer CoTSPc species can be observed with electrochemical techniques. In contrast, XRF detects both the monomer as well as dimer species leading to significantly higher amounts of detected cobalt compared to values derived from electrochemical techniques. The difference between the Co surface concentration values obtained by the above techniques gives an estimate of the amount of CoTSPc dimers and it could be seen that at the start of the modification procedure the monomer species is the dominating species on the gold surface. With increasing voltammetric scan number, the amount of dimer species adsorbing on the electrode surface increases and after the breaking point, a high amount of electrochemical inactive species adsorbs on the electrode surface.

6.3 References

[KEMP-02] Kempenaers L., Janssens K., Vincze L., Vekemans B., Somogyi A., Drakopoulos M., Simionovici A., Adams F., *Anal. Chem.,* **2002**, *74(19)*, 5017-5026.

Chapter 7:
Characterization of 3,4',4'',4''' copper tetrasulphophthalocyanine modified gold electrodes

The two previous chapters have described the morphology and heterogeneity of CoTSPc thin films modified on gold electrodes. In this chapter, a detailed characterization of the modification of 3,4',4'',4''' – copper (II) tetrasulphophthalocyanine (3,4',4'',4'''-CuTSPc) is given. The latter was chosen to be studied in detail because preliminary results have shown a different electrochemical behavior in comparison to the electrochemical modification of gold electrodes with r-CuTSPc (copper tetrasulphophthalocyanine with the sulphononated groups randomly oriented on the phthalocyanine ring) as described in chapter 4.

The experimental conditions of the measurements are briefly described in the first section of this chapter. The second section describes the electrochemical behavior of 3,4',4'',4'''-CuTSPc and in the third section the electrochemical behavior of 3,4',4'',4'''-CuTSPc is compared with this of r-CuTSPc. The fourth section encompasses the comparison of the electrochemical behavior of 3,4',4'',4'''-CuTSPc with this of CoTSPc and in the fifth section the spectroscopic characterization (SR-XRF, XPS and UV-Vis) of the 3,4',4'',4'''-CuTSPc solutions and the thin films is given. The final section provides the conclusions of this chapter.

7.1 Experimental conditions

The study of the electrodeposition of 3,4',4'',4'''-CuTSPc on gold electrodes was done by recording 100 successive cyclic voltammetric scans in a potential window from -1.2 V to 0.6 V vs. SCE (50 mV s^{-1}) in a pH 12 buffer solution containing 4.0 mmol L^{-1} 3,4',4'',4'''-CuTSPc. Similar as in the precious chapters, the modified electrodes were studied in a phthalocyanine free pH 12 buffer solution.

UV-Vis measurements were performed with a Specors 200 spectrophotometer (Analytical Jena, Germany) for 3,4',4'',4'''-CuTSPc in solution and with a Varian Cary 3E spectrophotometer (Instrument version 8.01) (Palo Alto, Canada) for CoTSPc in solution. The latter technique was used to study the ratio of monomers and dimers present in solutions.

Additional XPS measurements were performed with a Perkin–Elmer Phi ESCA 5500 system equipped with a monochromated 450W Al K_α source. The latter experiments were performed to determine the coverage.

A morphology and heterogeneity study of the 3,4',4'',4'''-CuTSPc thin films was performed by SR-XRF on gold electrodes modified with 3,4',4'',4'''- CuTSPc by the three different modification techniques (immersion, drop-drying or electrodeposition) described in chapter 2. In addition, the variation of voltammetric scan numbers during electrodeposition from 5 to 100 voltammetric scans was studied with SR-XRF. The SR-XRF experimental setup was similar as described in the previous chapters. A Ni/C multilayer monochromater ($\Delta E/E \approx 10^{-2}$) was used and the surface concentrations from SR-XRF were derived by the fundamental parameter method as described in chapter 3. The copper concentrations were derived from the electrochemical data by using Eq. 5.1 (chapter 5) for the Cu(I)/Cu(II) oxidation process in phthalocyanine free buffer solution after modification (see chapter 4 and further in this chapter).

7.2 Electrochemical behavior of 3,4',4'',4'''-CuTSPc at a gold electrode

7.2.1 Behavior during electrochemical modification

Fig 7.1 shows a selection of the 100 cyclic voltammetric scans (i.e. scans 10, 20, 30, 40, 60, 80 and 100) recorded at a gold electrode in a pH 12 buffer solution (curve 1) and a solution containing 4.0 x 10^{-3} mol L^{-1} 3,4',4'',4'''-CuTSPc (curve 2-8). The voltammogram shows two well defined oxidation and reduction peaks. The oxidation peak (I_a) at 0.50 V vs. SCE electrode was previously explained as the oxidation of the gold surface and linked with the reduction process (I_c) at 0.15 V vs. SCE which was explained as the reduction of the gold oxides formed during surface oxidation (see

section 4.1.1). Besides these two peaks, new oxidation and reduction processes appear respectively at 0.05 V (X_a) and -0.1 V vs. SCE (X_c).

A first indication of adsorption is the decrease and the shift of the AuO formation peak around 0.5 V vs. SCE (I_a) and its related reduction signal at 0.15 V vs. SCE (I_c). The latter indicates that the 3,4',4'',4'''-CuTSPc molecules immobilized on the gold electrode prevent the oxidation and reduction of the gold surface. Similar to the electrochemistry of CoTSPc, the processes observed in the potential range from -0.4 to -1.2 V vs. SCE can be explained as ring processes of 3,4',4'',4'''-CuTSPc in solution (see chapter 4). A well-defined oxidation peak at 0.05 V (X_a) vs. SCE and a reduction peak at -0.1 V (X_c) vs. SCE can be explained as the oxidation and reduction of adsorbed 3,4',4'',4'''-CuTSPc as shown respectively in Eq. 7.1 and 7.2:

$$X_a: \text{Cu(I)TSPc}_{ads} \rightarrow \text{Cu(II)TSPc}_{ads} + e^- \qquad \text{(Eq. 7.1)}$$

$$X_c: \text{Cu(II)TSPc}_{ads} + e^- \rightarrow \text{Cu(I)TSPc}_{ads} \qquad \text{(Eq. 7.2)}$$

Both peaks grow during the first 100 voltammetric scans. This growth with increasing voltammetric scan number is due to the deposition of 3,4',4'',4'''-CuTSPc on the gold surface.

The variation of the peak current at -0.1 V vs. SCE as a function of the voltammetric scan number is represented in Fig. 7.2 (curve A). Based on the fact that the slope decreases as a function of voltammetric scan number, it can be stated that the adsorption becomes more difficult as a function of time. Curve B in Fig. 7.2 shows the relationship between the peak current of the reduction process at 0.15 V vs. SCE (I_c) and the voltammetric scan number. The slope of this curve decreases in a way similar to curve A. However, the shift in peak potential to less positive values (Fig. 7.1) is an indication that the process is not exclusively associated with the gold oxide reduction. The peak maximum shifts towards less positive potentials with increasing voltammetric scan number, despite the fact that the peak intensity decreases. An opposite effect is expected when the peak is only attributed to the gold oxide reduction. Therefore, the reduction process at 0.15 V vs. SCE can be explained as the gold oxide superimposed by another redox process. Probably an interference with the increasing peak X_c occurs. Another potential explanation of this phenomenon is the occurrence of an interference with the ring reduction of adsorbed 3,4',4'',4'''-CuTSPc.

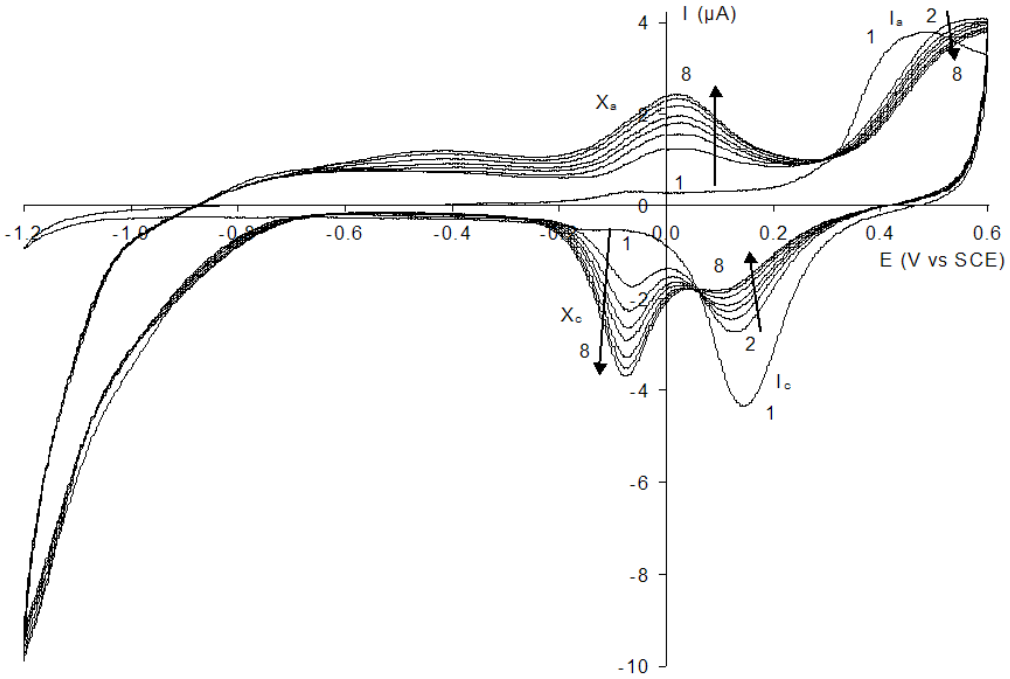

Fig. 7.1: Current-potential curves recorded at a gold electrode in a pH 12 buffer solution in the absence (1) and presence of 4.0 x 10^{-3} mol L^{-1} 3,4',4'',4'''-CuTSPc (2-8) at a scan rate of 50 mV s^{-1} and a temperature of 298.0 K as a function of voltammetric scan number. Voltammetric scan number is (2) 10, (3) 20, (4) 30, (5) 40, (6) 60, (7) 80 and (8) 100.

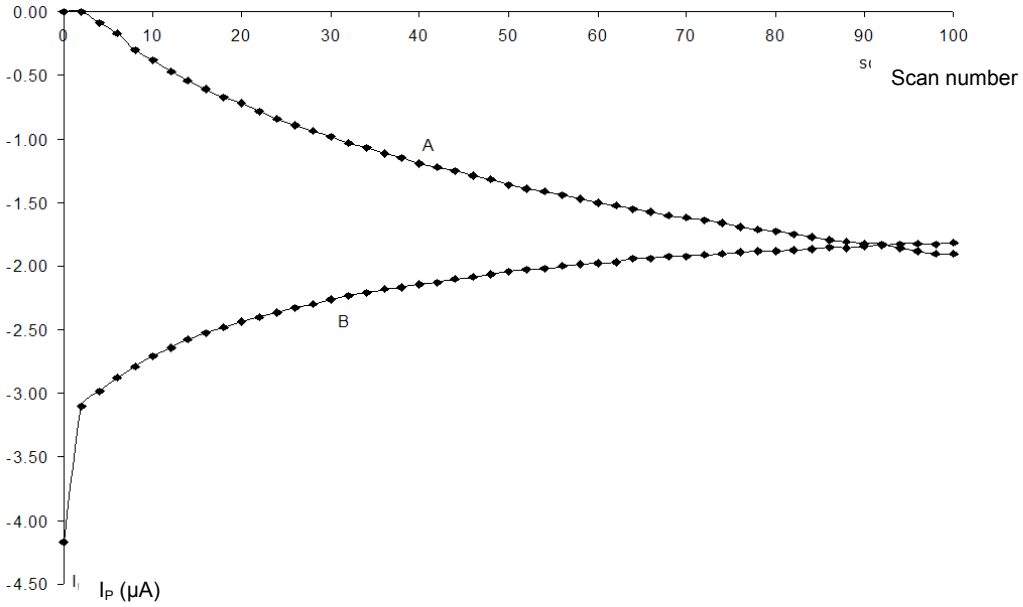

Fig. 7.2: Relationship between peak current of process X_c at -0.1 V vs. SCE (A) or I_c at 0.15V vs. SCE (B) in a pH 12 buffer solution containing 4.0 x 10^{-3} mol L^{-1} 3,4',4'',4'''-CuTSPc and voltammetric scan number.

7.2.2 Electrochemical proof of deposition

Based on the above results, a 3,4',4'',4'''-CuTSPc modified gold electrode is formed by recording successive cyclic voltammograms in a pH 12 buffer solution containing 3,4',4'',4'''-CuTSPc. The electrochemical proof of deposition could be obtained by bringing the modified electrode in a blank buffer solution and recording a set of cyclic voltammograms. Fig. 7.3 represents the voltammogram of a blank gold electrode (curve 1) and voltammetric scan 10 of a 3,4',4'',4'''-CuTSPc modified gold electrode (curve 2). The 3,4',4'',4'''-CuTSPc adsorption peaks appear at the same potentials as in a buffer solution containing 4.0 x 10^{-3} mol L^{-1} 3,4',4'',4'''-CuTSPc, ca. -0.1 and 0.05 V vs. SCE.

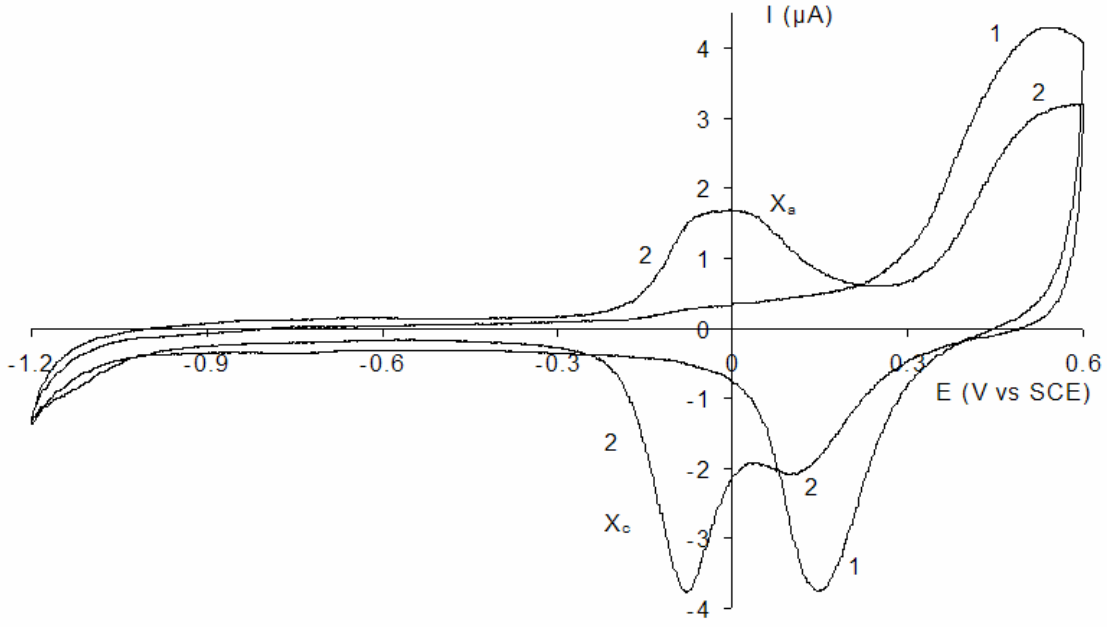

Fig. 7.3: Current-potential curve recorded at a blank gold electrode in a pH 12 buffer solution (1) and current-potential curve of a continuous voltammetric scanning experiment recorded at a gold electrode modified with 3,4',4'',4'''-CuTSPc in a pH 12 buffer solution (2).

A small redox system can be observed at ca. -1.1 V vs. SCE. In a buffer solution containing 4.0 x 10^{-3} mol L^{-1} 3,4',4'',4'''-CuTSPc (Fig. 7.1) a large reduction peak, explained as a ring reduction of 3,4',4'',4'''-CuTSPc, is seen at this potential. It is postulated that the small oxidation peak in the 3,4',4'',4'''-CuTSPc free buffer solution (Fig. 7.3) electrocatalyses the ring reduction of 3,4',4'',4'''-CuTSPc in solution.

The influence of the voltammetric scan rate on the peak current was investigated to confirm the adsorption electrochemically. A slope of the relationship between logarithm of the peak current (log I_p) and the logarithm of the voltammetric scan rate (log v) equals to 1 corresponds to oxidation and reduction of 3,4',4'',4'''-CuTSPc adsorbed at the gold electrode, while a slope of 0.5 rather indicates a rate determining diffusion of 3,4',4'',4'''-CuTSPc towards the electrode surface (see chapter 2, Eq. 2.2-2.5). Fig. 7.4 shows the relationship between log I_p and log v for peak X_a and X_c. The slope for the redox processes is respectively 0.911 and 1.0115, indicating the occurrence of redox processes of particles adsorbed on the electrode surface.

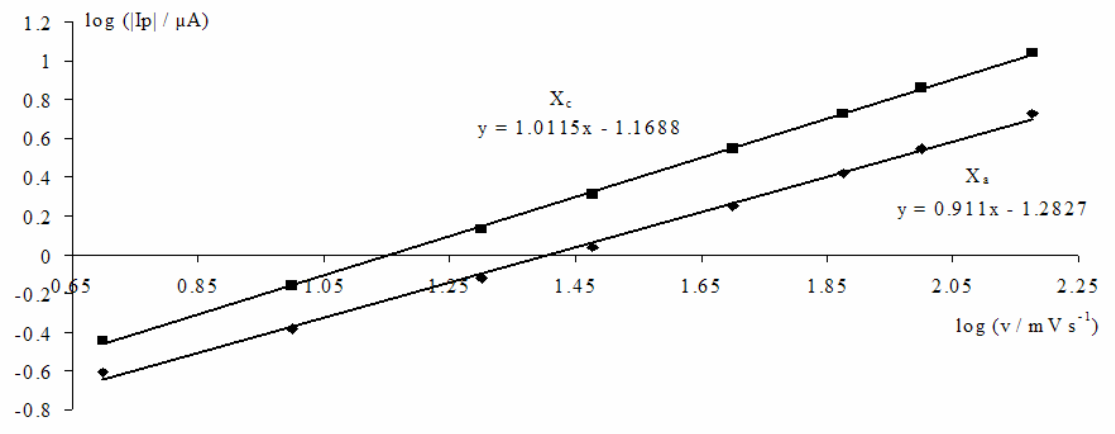

Fig. 7.4: Relationship between log of the peak current (I_p) and log of the voltammetric scan rate (v) for peak X_a and X_c. (same experimental conditions as in Fig. 7.3)

7.3 Comparison with r-CuTSPc

The difference in electrochemical behavior between r-CuTSPc and 3,4',4'',4'''-CuTSPc at a gold electrode is shown in Fig. 7.5. The electrodes were modified with r-CuTSPc (curve 2) (see chapter 4) or 3,4',4'',4'''-CuTSPc (curve 3) by recording successive cyclic voltammetric scans in a potential window from -1.2 to 0.6 V vs. SCE (50 mV s^{-1}) in a pH 12 buffer solution containing 4 x 10^{-3} mol L^{-1} CuTSPc. Voltammetric scan 20 is shown in Fig. 7.5. The background curve 1 is the tenth cyclic voltammogram measured in a pH 12 buffer solution. The oxidation and reduction peaks at -0.29 and -0.36 V vs. SCE (curve 2) are attributed to the r-Cu(II)$TSPc_{ads}$/r-Cu(I)$TSPc_{ads}$ redox system. A detailed explanation of the

electrochemical processes in curve 2 has been given in chapter 4. The data in Fig. 7.5 clearly demonstrates that 3,4',4'',4'''-CuTSPc shows a different electrochemical behavior. The redox processes in curve 2, however, are very analogous to the processes observed when modifying gold electrodes with other tetrasulphophthalocyanines such as iron tetrasulphophthalocyanine (FeTSPc) and alumina tetrasulphophthalocyanine (AlTSPc) (chapter 4, Fig. 4.5 and [DEWA-04]).

7.4 Comparison with CoTSPc

7.4.1 Comparison of the electrochemical behavior

The electrochemistry of 3,4',4'',4'''-CuTSPc is different as compared to the behavior of CoTSPc at a gold electrode especially in the potential range from -1.2 V to -0.6 V vs. SCE (see chapter 4). Characteristic for the voltammetric behavior of CoTSPc at gold is the occurrence of a breaking point at which a maximum coverage is reached. In the CoTSPc study, it was seen that the ring reactions of CoTSPc in solution (from -0.4 to -1.2 V vs. SCE) changed considerably after a maximum coverage was obtained. These changes were explained in the past as the reorganization of the deposited thin film to form, from a thermodynamic point of view, a more stable thin film consisting of columnar aggregates (see chapter 4). Fig. 7.1 shows that not any change or evolution of the ring processes is observed during the first 100 voltammetric scans cycling in a 3,4',4'',4'''-CuTSPc pH 12 buffer solution. The latter indicates that the deposition of 3,4',4'',4'''-CuTSPc is considered to be different as compared to the immobilization of CoTSPc. This means that as of voltammetric scan 1, the 3,4',4'',4'''-CuTSPc molecules are stacked in their definitive position resulting in a stable electrochemical signal.

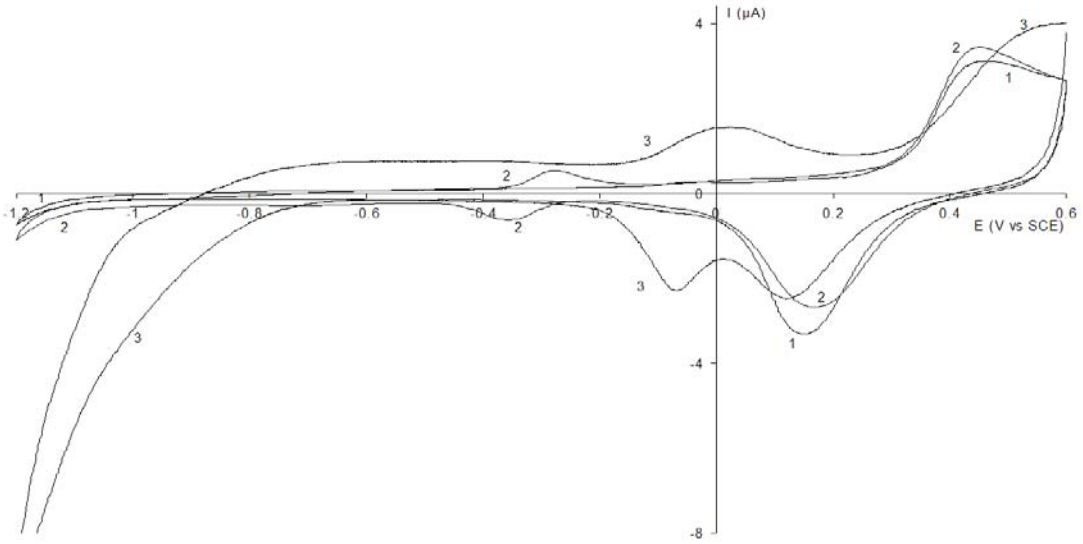

Fig. 7.5: Current-potential curves recorded at a gold electrode in a pH 12 buffer solution (voltammetric scan 10) (1) in a pH 12 buffer solution containing 4 x 10^{-3} mol L^{-1} r-CuTSPc (voltammetric scan 20) (see chapter 4) (2) or in a pH 12 buffer solution containing 4 x 10^{-3} mol L^{-1} 3,4',4'',4'''-CuTSPc (voltammetric scan 20) (3) at a voltammetric scan rate of 50 mV s^{-1} and a temperature of 298.0 K.

7.4.2 Determination of the monomer-dimer equilibrium of the phthalocyanine species in solution

The different electrochemical behavior of CoTSPc in comparison to that of 3,4',4'',4'''-CuTSPc during electrochemical modification can be explained by the fact that 3,4',4'',4'''-CuTSPc, when brought in solution, forms immediately stable dimer structures. The latter can be confirmed by the UV-Vis data of the two phthalocyanines which are shown in Fig. 7.6. The monomer peak for the phthalocyanine species in a pH 12 buffer solution is located at 661 nm, while the dimer peak is observed at 634 nm [THAM-02, CAMP-02]. The figure shows that even at very low concentrations (4 x 10^{-6} mol L^{-1}) 3,4',4'',4'''-CuTSPc (curve 1 in Fig. 7.6) forms a much higher amount of dimer species than CoTSPc (curve 2 in Fig. 7.6) which can be explained by the fact that six coordinate species, such as CoTSPc, generally do not aggregate principally because the species are kept apart by the axially bound ligands [LEZN-93]. Therefore, CoTSPc forms at low concentrations mainly monomers. At higher concentrations such as 4.0 x 10^{-3} mol L^{-1}, however, the concentration in which the electrodeposition occurs, there are dimers present next to the dominating amount of monomers. Given the fact that the monomer concentration

of CoTSPc in solution cannot be neglected, it can be postulated that at the beginning of the CoTSPc modification process there is a competition between the monomers and dimers (see chapter 5) and that in a further stage of the modification process mainly dimers adsorb.

In contrast for 3,4',4'',4'''-CuTSPc it is expected that mainly dimers are formed at low and high concentrations [ABRA-04]. As copper prefers a four-coordination, dimers are formed very easily. The monomer concentration is negligibly low in the case of 3,4',4'',4'''-CuTSP and it is seen that a stable 3,4',4'',4'''-CuTSPc thin film is formed from the first voltammetric scan on during electrodeposition. The latter indicates that the 3,4',4'',4'''-CuTSPc dimers, as well as the monomers are electrochemically active. So it can be concluded that the difference in equilibrium between monomers and dimers explains the difference in voltammetric behavior and the reorganization of the thin film.

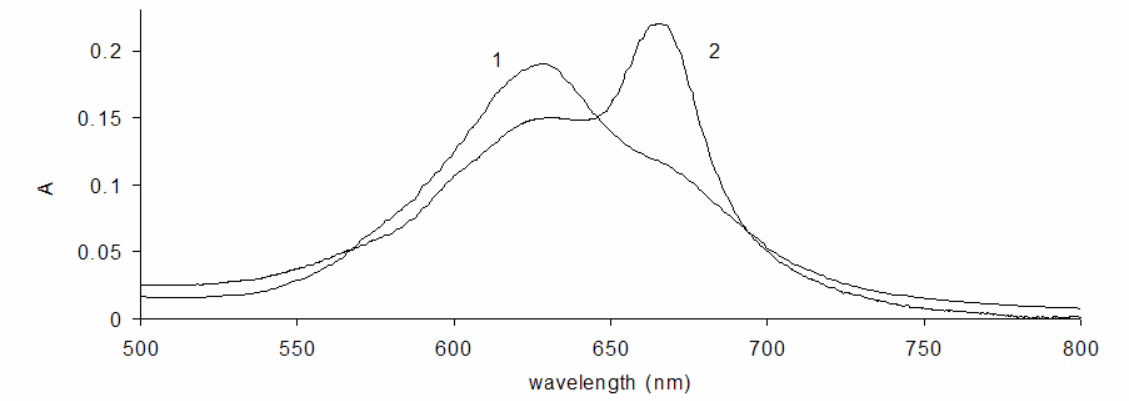

Fig. 7.6: Absorbance spectra of a pH 12 buffer solution containing 4 x 10^{-6} $molL^{-1}$ 3,4',4'',4'''-CuTSPc (1) or CoTSPc purchased from Rhodes University of Grahamstown (2).

7.5 Spectroscopic characterization of the adsorbed thin film

7.5.1 Spectroscopic proof of deposition

X-ray photoelectron spectroscopic analyses of the modified electrode were carried out and a coverage value of 67% could be calculated. Compared to the 18.3% coverage in the case of r-CuTSPc (see chapter 4), a significantly higher value is obtained for the well ordered 3,4',4'',4'''-CuTSPc. A potential explanation for this

difference is the fact that the well ordered 3,4',4'',4'''-CuTSPc is able to form stable columnar aggregates. Because of the conjugated π-systems of two CuTSPc molecules, in which the sulphonate groups take part, and the preference for four coordination, the ring structures can approach each other very closely resulting in strong π-π interactions. A dense packing of r-CuTSPc is more difficult because of the randomly oriented sulphonate groups.

Micro SR-XRF measurements were performed to provide further experimental evidence of the formation of the adsorbed 3,4',4'',4'''-CuTSPc thin film at the gold electrodes and to study the uniformity of the formed thin film in a quantitative manner. Fig. 7.7 shows a typical elemental map from a 600 x 600 μm^2 area and the corresponding intensity distribution of the detected Cu-K_α obtained by SR-XRF measurements after normalization with the gold M line. This figure provides not only direct evidence of the occurrence of adsorbed 3,4',4'',4'''-CuTSPc but also gives an estimate of the amount of adsorbed 3,4',4'',4'''-CuTSPc. The micro SR-XRF measurements were performed after different number of voltammetric scans cycling in a 4.0 x 10^{-3} mol L^{-1} 3,4',4'',4'''-CuTSPc buffer solution. Table 7.1 shows the copper surface concentrations derived from the XRF measurements as well as those derived from the electrochemical measurements. The average copper intensity, its relative standard deviation and the copper surface concentration of each SR-XRF measurement and the charge caused by the $Cu(II)_{ads}/Cu(I)_{ads}$ oxidation process and its calculated surface concentration are presented for different voltammetric scan numbers. Both techniques give similar results for the copper surface concentration indicating that 3,4',4'',4'''-CuTSPc monomers are electrochemical active as well as the dimers. The amount of adsorbed 3,4',4'',4'''-CuTSPc grows with voltammetric scan number. It is clear that the increase in surface concentration slows down at higher voltammetric scan number. Probably, further adsorption is slightly obstructed by the initially adsorbed molecules.

7.5.2 Comparison of different modification techniques

Based on the values in Table 7.1, it can be concluded that when cycling the gold electrode in a 3,4',4'',4'''-CuTSPc buffer solution during 100 voltammetric scans in a potential window from -1.2 to 0.6 V vs. SCE, the amount of adsorbed

3,4',4'',4'''-CuTSPc is much larger than is the case for the two other modification techniques (immersion and drop drying method). The first modification technique (immersion method) involved the immersion of a gold electrode in a $4x10^{-3}$ mol L^{-1} 3,4',4'',4'''-CuTSPc pH 12 buffer solution for two hours, the time equivalent of 100 voltammetric scans. After the modification, the electrode was scanned in a pH 12 buffer solution without 3,4',4'',4'''-CuTSPc in order to study the electrochemical behavior of the modified electrode and to obtain information about the amount of 3,4',4'',4'''-CuTSPc deposited on the gold surface. The $Cu(II)_{ads}/Cu(I)_{ads}$ redox processes do not appear. Based on the electrochemical results, one can assume that there is no adsorption. In contrast, the SR-XRF experiments show that there is a small amount of copper that is adsorbed on the surface. Based on these results, it can be stated that there must be an electrochemical activation before adsorption can occur. The small amounts that were detected with SR-XRF can be explained by the occurrence of at random adsorbed 3,4',4'',4'''-CuTSPc molecules. The same results were obtained with another non electrochemical modification technique. In the drop drying method, the gold electrode was modified by depositing a droplet of the $4x10^{-3}$ mol L^{-1} 3,4',4'',4'''-CuTSPc pH 12 buffer solution on its surface.

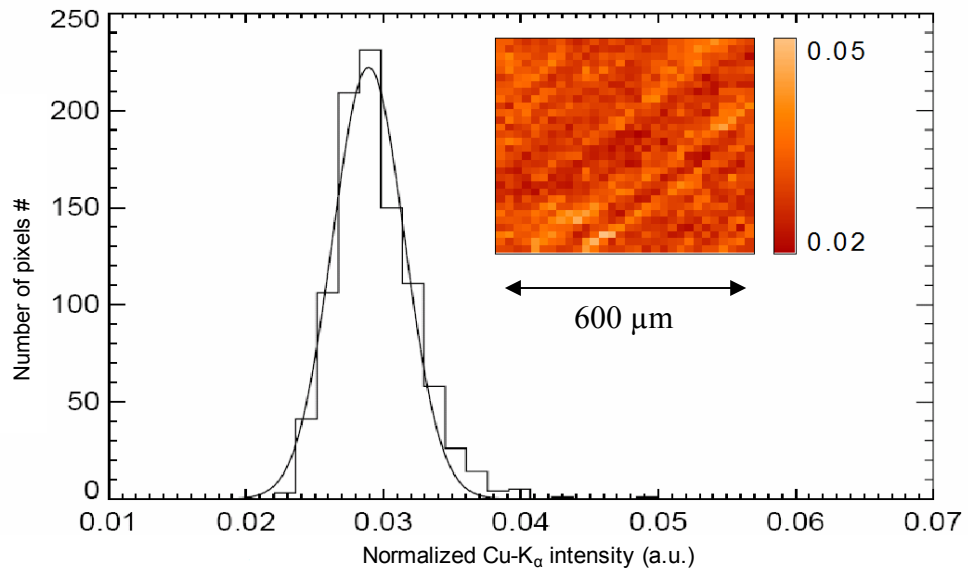

Fig. 7.7: Elemental map and intensity distribution of copper on a gold electrode electrochemically modified during 60 voltammetric scans in 6 x 10^{-3} molL^{-1} 3,4',4'',4'''-CuTSPc.

Table 7.1:SR-XRF and electrochemical data.[a]

Number of voltammetric scans	$\langle I_{Cu} \rangle$ (counts s^{-1})	$\delta_{Cu}/\bar{I}_{Cu}$ (%)	Surface concentration (µg cm^{-2}) determined by SR-XRF	Charge (µC)	Surface concentration (µg cm^{-2}) determined by voltammetry
5	75.8	25.3	0.045±0.010	1.1±0.2	0.034
10	92.4	27.4	0.064±0.015	1.6±0.2	0.053
17	121.8	25.9	0.072±0.017	1.9±0.2	0.061
30	132.3	21.5	0.076±0.016	2.8±0.3	0.093
60	152.1	19.1	0.103±0.022	3.9±0.3	0.128
100	228.4	23.7	0.142±0.032	3.8±0.2	0.124
immersion	63.4	19.2	0.038±0.005	0	0
drop drying	53.5	34.1	0.033±0.009	0	0

[a]*First column is the number of voltammetric scans. Next three columns show the SR-XRF data respectively the average copper intensity, its relative standard deviation and the copper surface concentration. The last columns show the electrochemical data respectively the charge due to the Cu(II)/Cu(I) oxidation peak and the calculated surface concentration.*

7.6. Conclusion

This chapter has discussed the electrochemical modification of gold electrodes with 3,4',4'',4'''-CuTSPc and has compared the electrochemical behavior with that of r-CuTSPc and CoTSPc. The voltammograms demonstrate that the position of the sulphonate groups on the phthalocyanine has an influence on its electrochemistry and thus on the characteristics of the modified electrode. It was shown that a better electrodeposition was obtained with 3,4',4'',4'''-CuTSPc as compared with r-CuTSPc. A study of the deposited CuTSPc thin film by XPS allowed us to derive the coverage value and showed that this was much higher for the 3,4',4'',4'''-CuTSPc (67%) in comparison with that of r-CuTSPc (18.3%). Compared to CoTSPc, both phthalocyanines have a different UV-Vis spectrum resulting in different monomer-dimer equilibrium which has its influence on the electrochemistry.

This paper also gives a brief study of the morphology and heterogeneity of the deposited phthalocyanine thin film onto a gold electrode using synchrotron micro X-ray fluorescence as a function of the applied modification method (immersion, drop-drying or electrodeposition) and as a function of the applied number of voltammetric scans during electrodeposition. It is seen that performing successive cyclic voltammetric scans leads to a more efficient deposition which results in a

uniformly adsorbed 3,4',4'',4'''-CuTSPc thin film. In addition, it can be postulated that the 3,4',4'',4'''-CuTSPc monomer species are electrochemical active as well as the dimer species which is in contrast with the CoTSPc monomer and dimer species (see chapter 5 and 6). The electrochemical activity of the monomer-dimer species is discussed in more detail in chapter 8.

7.7 References

[ABRA-04] Abramczyk H., Szymczyk I., Waliszewska G., Lebioda A., *J. Phys. Chem.* A, **2004**, 108 264-274.

[CAMP-02] Camp P.J., Jones A.C., Neely R.K., Speirs N.M., *J. Phys. Chem. A*, **2002**, 106, 10725-10732.

[DEWA-04] De Wael K., Westbroek P., Temmerman E., *J. Electroanal. Chem.*, **2004**, 567, 167-173.

[LEZN-93] Leznoff C. C., Lever A. B. P., *Phthalocyanines Properties and Applications*; VCH Publishers: Weinheim, **1993**, vol. 3.

[THAM-02] Thamae M., Nyokong T., *Polyhedron*, **2002**, 21, 133-140.

Chapter 8:
Quantitative heterogeneity study of CoTSPc and CuTSPc thin films electrochemically deposited on gold electrodes as a function of the phthalocyanine concentration in solution during modification

Previous chapters have described the modification study of gold electrodes with CoTSPc or CuTSPc as a function of the modification procedure (chapters 5 and 7) and as a function of the number of voltammetric scans during electrodeposition (chapters 6 and 7). In this chapter, the study of the electrodeposition of CoTSPc or CuTSPc as a function of the phthalocyanine concentration in solution is described. In addition, the quantification procedure and micro-heterogeneity determination of CoTSPc and CuTSPc thin films on the gold electrodes is discussed.

The experimental conditions of the measurements are briefly described in the first section of this chapter. The second section discusses the data reduction method applied for the determination of the heterogeneity of the CoTSPc and CuTSPc thin films and in the third section the derived CoTSPc and CuTSPc surface concentrations are shown. The comparison of the Co and Cu surface concentrations on gold electrodes obtained from the SR-XRF data and the electrochemical data are respectively discussed in sections three and four. The final section provides the conclusions of this chapter.

8.1 Experimental conditions

The gold electrodes were electrochemically modified with CoTSPc, purchased from the University of Grahamstown (South Africa), or 3,4',4'',4'''- CuTSPc, purchased from Sigma Aldrich (USA), according to the procedure described in chapter 2 and in a concentration range from 1 to 16 mmol L^{-1}. For CoTSPc, in the concentration range of 1 to 10 mmol L^{-1}, every modification was performed until the breaking point was reached (see chapter 4) in order to receive the same state of the immobilized layer. In the concentration range of 12 to 16 mmol L^{-1} the electrodeposition was performed until beyond the breaking point. The reason for this is that the number of voltammetric scans needed to reach the breaking point is lower than five for these CoTSPc concentrations, which has a negative influence on the reproducibility of the modification. For the electrodeposition with CuTSPc, 60 subsequent voltammetric scans were taken during the modification in a concentration range of 1 to 16 mmol L^{-1}.

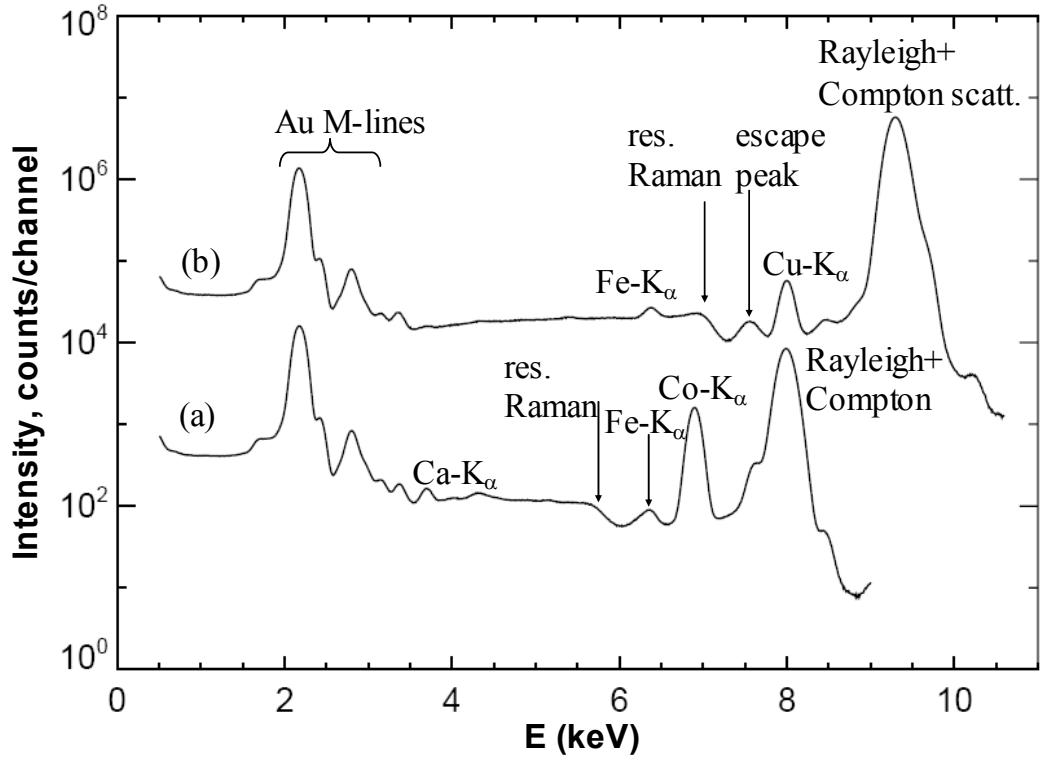

Fig. 8.1: SR-XRF spectrum of a gold electrode electrochemically modified with CoTSPc (a) or CuTSPc (b).

The heterogeneity of the modified gold electrodes was studied with SR-XRF having a similar experimental setup as described in the previous chapters. A Ni/C multilayer monochromater ($\Delta E/E \approx 10^{-2}$) was used and an example of the SR-XRF sum spectra obtained from a gold electrode with deposited CoTSPc (a) or CuTSPc(b) thin films is shown in Fig. 8.1.

8.2 Data reduction

The non linear least square fitting software AXIL [VEKE-94] was used to determine the net-peak intensities of the Co-K_α or Cu-K_α in the measured XRF spectra. The average deposited surface concentrations were calculated from the sum spectrum by the Fundamental Parameter (FP) method (see chapter 3) making use of pure thin Co (thickness 10 μm) and Cu (thickness 1 μm) foils as standards for the calibration (Goodfellow Inc). The data reduction described below aims the determination of the average surface concentration values and their relative variance $\delta_{sum,r}^2$ based on the sum spectra for the individual Co or Cu concentrations on the gold electrode. These values on the one hand are influenced by the relative variance of the experimental Co or Cu intensities originating from the deposited thin-films on the gold electrode. On the other hand, the uncertainty of the determined thin-film concentration also depends on the relative variance of the measured Co and Cu intensities from the applied standards used for calibration/normalization.

The concentrations of Co and Cu calculated by the FP method have been plotted as a function of Au-M line normalized Co-K_α or Cu-K_α intensities ($I_{Co\text{-}K\alpha}/I_{Au\text{-}M}$ or $I_{Cu\text{-}K\alpha} / I_{Au\text{-}M}$) derived from the sum spectra (Fig. 8.2). In this way, a calibration curve for Co and Cu could be obtained.

During one set of experiments (see further), this calibration curve has been used to quantify the data which simplifies the quantification procedure considerably by using the gold M-lines as internal reference, without the need of using external standards. Instead of the direct application of the fundamental parameter method, the calibration curves shown in Fig. 8.2 were used to derive the surface concentrations of the Co or the Cu on the gold electrodes from the sum spectra. This results in an increase of $\delta_{sum,r}^2$ for Co and a decrease of $\delta_{sum,r}^2$ for Cu. Since the energy of the incoming beam was shifted to more positive values (ca. 260 eV for Co and 390 eV for

Cu) for this set of experiments compared to those from which the calibration curves were derived, a sensitivity correction term has been applied. The sensitivity correction term for these shifts has been determined by using the corresponding mass attenuation coefficients derived from the McMaster tabulation [MCMA-68].

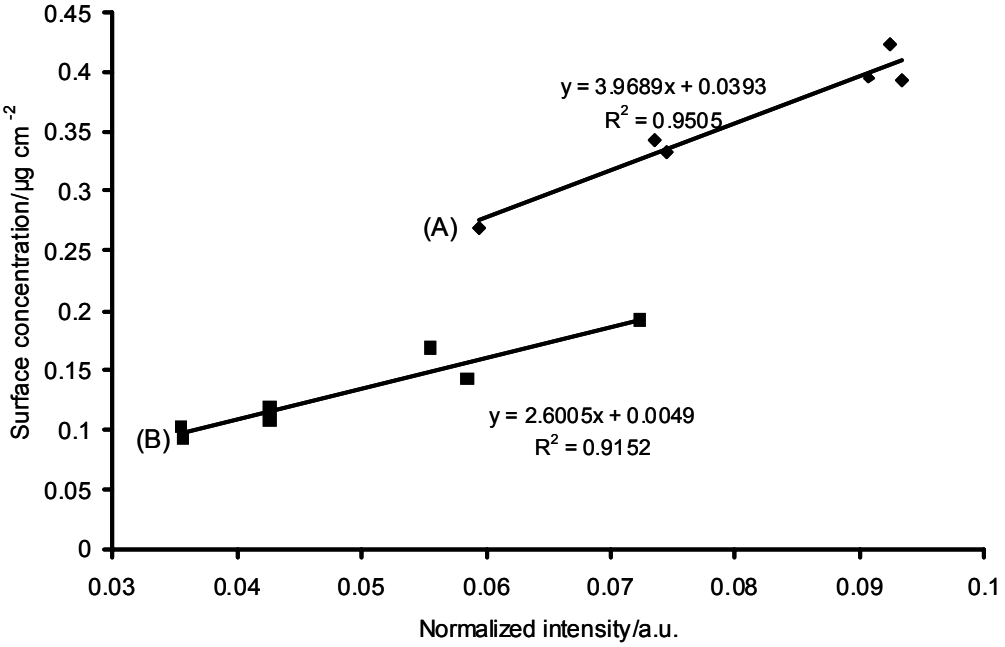

Fig. 8.2: Calibration curve of cobalt (A) and copper (B) concentrations on the gold electrode surface as a function of the total Co or Cu intensity derived from the sum spectrum after normalization with the gold M lines.

The Co or Cu surface concentrations on the pixel-level were also derived form the 961 individual spectra (representing a 31 x 31 SR-XRF map), each of which corresponds to concentration values from microscopic regions on the 20 µm scale. Within the 31 × 31 elemental maps, the individual pixel intensities represent the Co K_α or Cu K_α line-intensities normalized by the Au M lines (after integration between 1.862 keV and 2.362 keV). From these normalized SR-XRF maps, corresponding histograms of the detected Co and Cu signals were derived. By fitting Gaussian curves on these histograms the mean value and the full-width-at-half-maximum (FWHM) of the measured intensity distributions have been obtained. According to Kempenaers et al. [KEMP-00, KEMP-01, KEMP-02], the relative total variance $\delta_{tot,r}^2$ calculated on these 961 pixels can be split up in the relative statistical variance $\delta_{stat,r}^2$, the relative instrumental variance $\delta_{instr,r}^2$ and the relative heterogeneity $\delta_{het,r}^2$ terms, according to the equation $\delta_{tot,r}^2 = \delta_{stat,r}^2 + \delta_{instr,r}^2 + \delta_{het,r}^2$.

Using the mean values of these histograms and the calibration curve from the sum spectra, the mean Co and Cu concentrations were obtained on the individual pixel level. Using the FWHM of the derived histograms, the total variance $\delta_{tot,r}^2$ can be calculated which can be split in contributions of statistical, instrumental and heterogeneity variance terms (respectively, $\delta_{stat,r}^2$, $\delta_{instr,r}^2$ and $\delta_{het,r}^2$) of the sample according to Kempenaers et al [KEMP-02]. The instrumental term $\delta_{inst,r}^2$ is considered to be negligible here since it is smaller than 1% in case of the given experimental setup [KEMP-00]. The statistical term, $\delta_{stat,r}^2$ can be derived from the effective counts according to the Co or Cu signal of the sum spectrum, assuming Poisson statistics. With these assumptions, the heterogeneity term of interest $\delta_{het,r}^2$ can be derived as the difference of the measured total variance term $\delta_{tot,r}^2$ and that of the statistical variance term $\delta_{stat,r}^2$.

8.3 Determination of CoTSPc or CuTSPc surface concentrations deposited on a gold electrode

Table 8.1 lists the parameters of the modification procedure used in this study together with the obtained electrochemical data and the derived surface concentrations for the modification with CoTSPc as well as with CuTSPc. The voltammetric scan numbers labelled with an asterix (*) symbol in Table 8.1 indicates that the modification occurred until the breaking point for this CoTSPc concentration in solution. From Table 8.1 it can be seen that the calculated Co surface concentration is independent from the CoTSPc concentration during the modification process at the breaking point (measurements 1-6) and after the breaking point (measurements 7-9) in the studied concentration range. It can also be seen that the deposited Cu surface concentration is more or less independent from the initial CuTSPc concentration in solution in the concentration range of 1-16 mmol L^{-1} during the modification procedure after 60 subsequent voltammetric scans.

The SR-XRF based surface concentration values of CoTSPc or CuTSPc were derived from the sum spectra (yielding the average concentration) as well as from the 961 individual spectra (yielding the concentration on the microscopic level). From the sum spectra a calibration curve has been plotted (Fig. 8.2) showing that the $I_{Cu\text{-}K\alpha}$ / $I_{Au\text{-}M}$ ratio, shown in the X-axis of the calibration curve, is higher than

$I_{Co\text{-}K\alpha}$ / $I_{Au\text{-}M}$ ratio because of the higher excitation energy used during the Cu detection. The higher excitation energy reduces considerably the gold M line intensity (used as internal reference) during Cu detection, which results in a higher normalized Cu/Au-M signal for the same Cu or Co surface concentration. The standard deviations of the measured Co and Cu concentrations in the calibration curve are respectively 0.0139 μg cm^{-2} and 0.0118 μg cm^{-2}.

Table 8.1: Overview of the electrochemical data, including from left to right the number of the measurement, the number of subsequent scans in a pH 12 buffer solution containing either CoTSPc or CuTSPc (the asterix (*) symbol indicates that this number of scans is the breaking point for the given concentration), the concentration CoTSPc or CuTSPc in the solution during the modification, the charge due to the Co(III)/Co(II) or Cu(II)/Cu(I) adsorption peak and the Co or Cu surface concentration.

	Number of scans	**Phthalocyanine concentration (mmol L^{-1})**	**Charge (μC)**	**Surface concentration (μg cm^{-2})**
CoTSPc				
1	27*	1.0	4.7	0.143
2	25*	2.0	4.5	0.137
3	21*	4.0	4.7	0.143
4	17*	6.0	4.9	0.148
5	13*	8.0	5.4	0.163
6	9*	10.0	4.5	0.136
7	9	12.0	3.2	0.097
8	9	14.0	6.3	0.191
9	9	16.0	5.0	0.151
CuTSPc				
10	60	1.0	2.8	0.094
11	60	2.0	2.1	0.099
12	60	4.0	3.9	0.144
13	60	6.0	3.8	0.179
14	60	8.0	4.3	0.141
15	60	10.0	5.5	0.123
16	60	12.0	4.4	0.128
17	60	14.0	3.0	0.069
18	60	16.0	2.9	0.091

The normalized elemental maps of the deposited Co thin-films and the corresponding histograms of the normalized Co-K_α intensities for different CoTSPc concentrations in the solution are shown in Fig. 8.3. The equivalent XRF maps and histograms for Cu are shown in Fig. 8.4, corresponding to a modification of 60 voltammetric scans as a function of CuTSPc concentration. The histograms shown in these figures have been used to derive the surface concentration values and their variances listed in Table 8.2, which provides an overview of the results obtained from the SR-XRF experiments. The table shows the total Co or Cu intensities, the normalized Co or Cu intensities, the surface concentration values $\delta_{sum,r}$ derived from the sum spectrum. Also indicated are the (microscopic) mean surface concentrations obtained from the mean of the histograms, as well as the quantities $\delta_{tot,r}$, $\delta_{stat,r}$, and δ_{het}, defined earlier. The numbering of the experiments is the same as the numbering used in Table 8.1. Comparison of the average Co/Cu surface concentrations and the Co/Cu concentration on the microscopic level shows that the Co/Cu concentration on the microscopic level is slightly smaller. This can be explained by the detected heterogeneities on the deposited layer having high-concentrations, which can be seen as small bright areas on the recorded elemental-maps. These areas correspond to the high-intensity tails on the right-hand side of the calculated histograms, representing in some cases considerable deviations from the ideal Gaussian distribution. It is also seen in Table 8.2 that $\delta_{sum,r}$ is about 40 times higher for Cu than for Co. This can be explained by the considerably higher waviness of the thinner (1μm) copper foil used as standard compared to the Co reference foil (10 μm), resulting in higher uncertainties of the illuminated excitation volume (and detected reference intensity) for Cu.

Fig. 8.5 shows the elemental maps of Co or Cu deposited using different CoTSPc (9 voltammetric scans) or CuTSPc (60 voltammetric scans) concentrations in solution and the corresponding histograms of the normalized Co-K_α or Cu-K_α intensities derived from another set of experiments. For the determination of the surface concentrations from these SR-XRF measurements, the calibration curve shown in Fig. 8.2 has been used. In this case the surface concentrations could be derived directly from the $I_{Co\text{-}K\alpha}$ /$I_{Au\text{-}M}$ or $I_{Cu\text{-}K\alpha}$ / $I_{Au\text{-}M}$ ratios without the use of an external standard. It can be seen in Table 8.2 (measurements 7,8,9,17 and 18) that the use of internal reference results in increased $\delta_{sum,r}$ values for Co, while $\delta_{sum,r}$ reduces for Cu when compared to the FP quantification using an external reference. This can

Table 8.2: Overview of the SR-XRF data, including the number of the measurement, the data derived from the sum spectrum (resp. total Co or Cu intensity, the normalized intensity and the surface concentration) and the data calculated from the histograms (resp. mean of the histogram, the Co or Cu surface concentration, $\delta_{tot,r}$, $\delta_{stat,r}$ and $\delta_{het,r}$).

	Total Co/Cu intensity (counts s^{-1})	Normalized intensity	Surface concentration ($\mu g\ cm^{-2}$)	$\delta_{sum,r}$ (%)	Mean (histogram)	Surface concentration ($\mu g\ cm^{-2}$)	$\delta_{tot,r}$ (%)	$\delta_{stat,r}$ (%)	$\delta_{het,r}$ (%)
CoTSPc									
1	663	0.0744	0.333	0.37	0.068	0.31	11.8	1.3	11.8
2	772	0.0923	0.423	0.36	0.085	0.38	6.5	1.2	6.4
3	727	0.0907	0.395	0.37	0.085	0.38	7.8	1.2	7.7
4	678	0.0933	0.393	0.35	0.083	0.37	10.8	1.3	10.7
5	658	0.0735	0.342	0.37	0.068	0.31	14.0	1.3	14.0
6	499	0.0594	0.279	0.37	0.055	0.26	7.5	1.5	7.3
7	1602	0.1204	0.558	2.48	0.112	0.52	9.9	0.8	9.9
8	1177	0.0904	0.429	3.24	0.096	0.46	16.7	0.9	16.7
9	2316	0.1343	0.618	2.24	0.113	0.53	24.5	0.8	24.5
CuTSPc									
10	145	0.0366	0.092	12.4	0.031	0.09	10.2	2.8	9.8
11	181	0.0427	0.108	12.4	0.036	0.10	10.4	2.5	10.0
12	123	0.0355	0.103	12.4	0.029	0.08	9.0	3.2	8.4
13	157	0.0427	0.119	12.4	0.034	0.09	19.0	2.8	18.8
14	174	0.0585	0.143	12.4	0.048	0.13	22.7	2.6	22.6
15	120	0.0723	0.192	12.4	0.063	0.17	12.6	3.1	12.1
16	117	0.0555	0.168	12.4	0.041	0.11	15.6	3.4	15.3
17	90	0.0375	0.114	10.4	0.021	0.07	16.3	4.5	15.7
18	126	0.0415	0.125	9.6	0.024	0.08	21.9	3.7	21.5

be explained by the relatively high $\delta_{sum,r}$ values for Cu in case of the external standard based quantification as a result of waviness of the thin Cu reference foil (1µm). In case of the quantification of Co, the standard deviation on the calibration curve dominates when compared to the negligible standard deviation measured from the external standard foil (10 µm). In this case switching from external reference to the calibration curve based quantification increases $\delta_{sum,r}$.

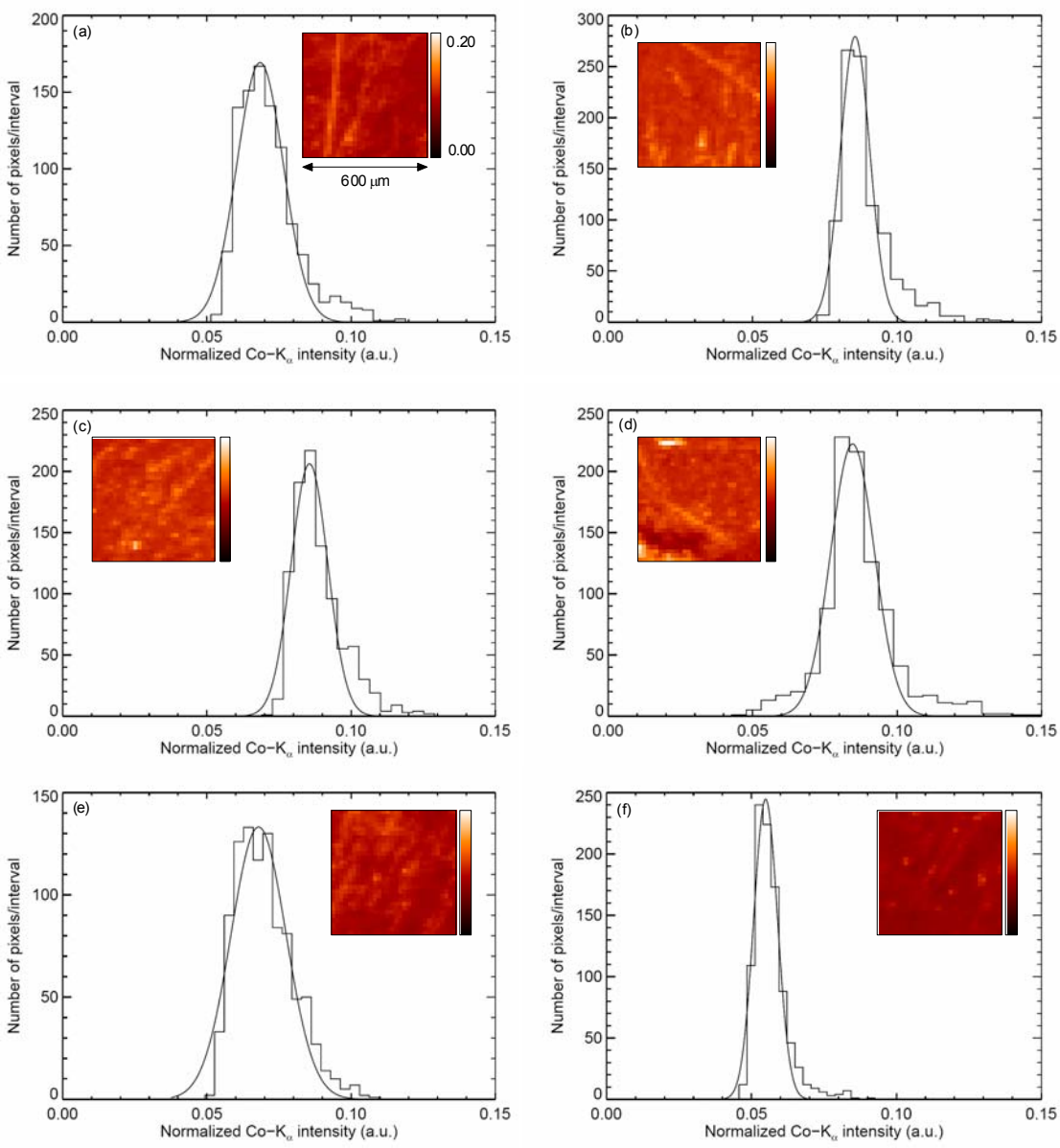

Fig. 8.3: Elemental maps of deposited Co and the corresponding histogram of the detected Co K_α line obtained from a modified gold electrode at the breaking point as a function of the concentration of CoTSPc in solution: (a) 1, (b) 2, (c) 4, (d) 6, (e) 8 and (f) 10 mmol L^{-1}. The XRF maps consists of a 31 × 31 raster using 20 µm step size in both X and Y direction and the scale bar is for all the maps the same indicating a normalized Co-K_α intensity between 0 and 0.2.

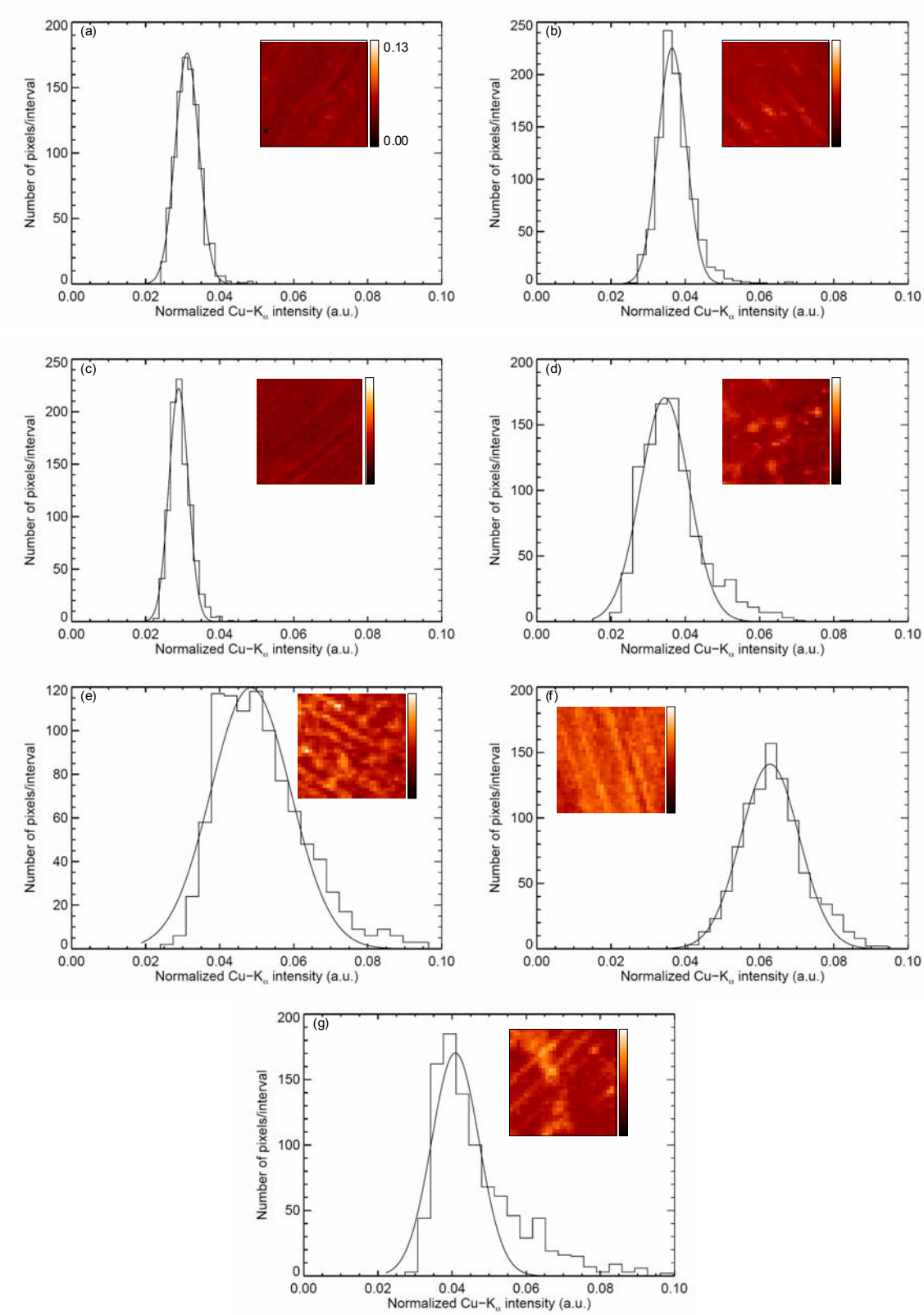

Fig. 8.4: Elemental maps of deposited Cu and the corresponding histogram of the detected Cu-K_α line obtained from a modified gold electrode at the breaking point as a function of the concentration of CoTSPc in solution: (a) 1, (b) 2, (c) 4, (d) 6, (e) 8, (f) 10 and (g) 12 mmol L^{-1}. The XRF maps consists of a 31 × 31 raster using 20 µm step size in both X and Y direction and the scale bar is for all the maps the same indicating a normalized Cu-K_α intensity between 0 and 0.13.

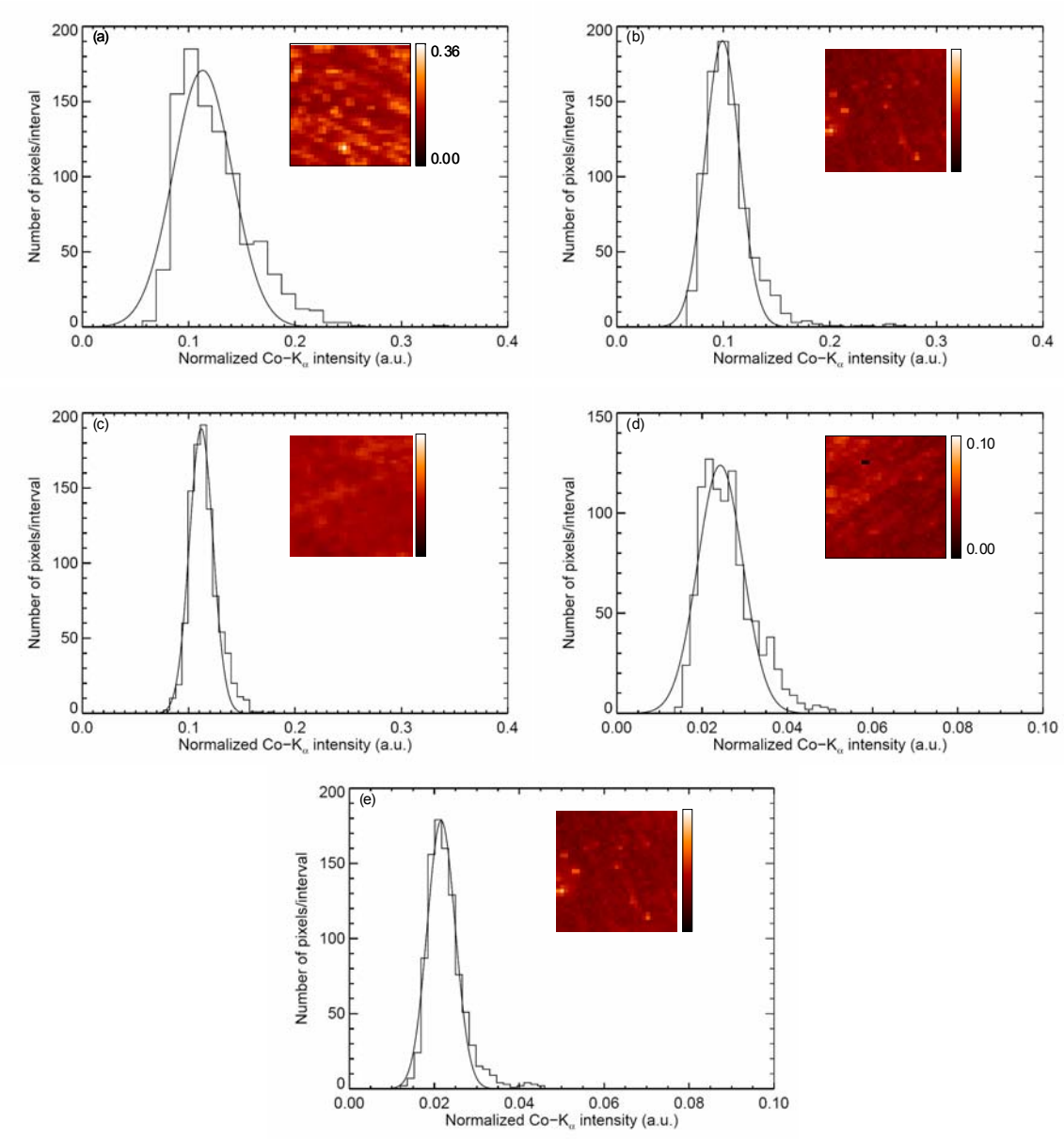

Fig. 8.5: Elemental maps of Co or Cu deposited with different CoTSPc (9 scans) or CuTSPc (60 scans) concentrations in solution and the corresponding histograms of the normalized Co-K_α or Cu-K_α intensities derived from this set of experiments: (a) 16 mmol l^{-1} CoTSPc, (b) 14 mmol L^{-1} CoTSPc, (c) 12 mmol L^{-1} CoTSPc, (d) 16 mmol L^{-1} CuTSPc, (e) 14 mmol L^{-1} CuTSPc. The XRF maps consists of a 31 × 31 raster using 20 µm step size in both X and Y direction. The scale bar is for all the Co maps (indicated in (a)) the same and another scale bar is valid for all the Cu maps (indicated in (d)).

In the rest of this chapter, the surface concentrations derived from the electrochemical data (Table 8.1) are compared with the surface concentrations derived from the SR-XRF data (Table 8.2). This comparison gives detailed information about the layer buildup of the CoTSPc or CuTSPc thin layer which is discussed in the next sections.

8.4 Comparison of the Co surface concentrations on gold electrodes derived from SR-XRF and electrochemical data

Figure 8.6 shows the Co surface concentrations calculated using the electrochemical data, the SR-XRF sum spectra and using the mean of the histogram as a function of the CoTSPc concentration (1 – 10 mmol L^{-1}). The number of voltammetric scans during the modification is each time indicated between brackets. It is observed that the surface concentrations derived from the electrochemical data as well as from the SR-XRF data are reasonably constant across the concentration range studied. Moreover, it is seen that the Co surface concentration derived from the electrochemical data is significantly lower than those obtained from the SR-XRF data. This constant difference between the electrochemical and SR-XRF surface concentrations means that there is a constant ratio between the electro active (electrochemical data) and electro inactive species on the surface at the breaking point. Note, that the SR-XRF data show both electrochemically active as well as the electrochemically inactive species.

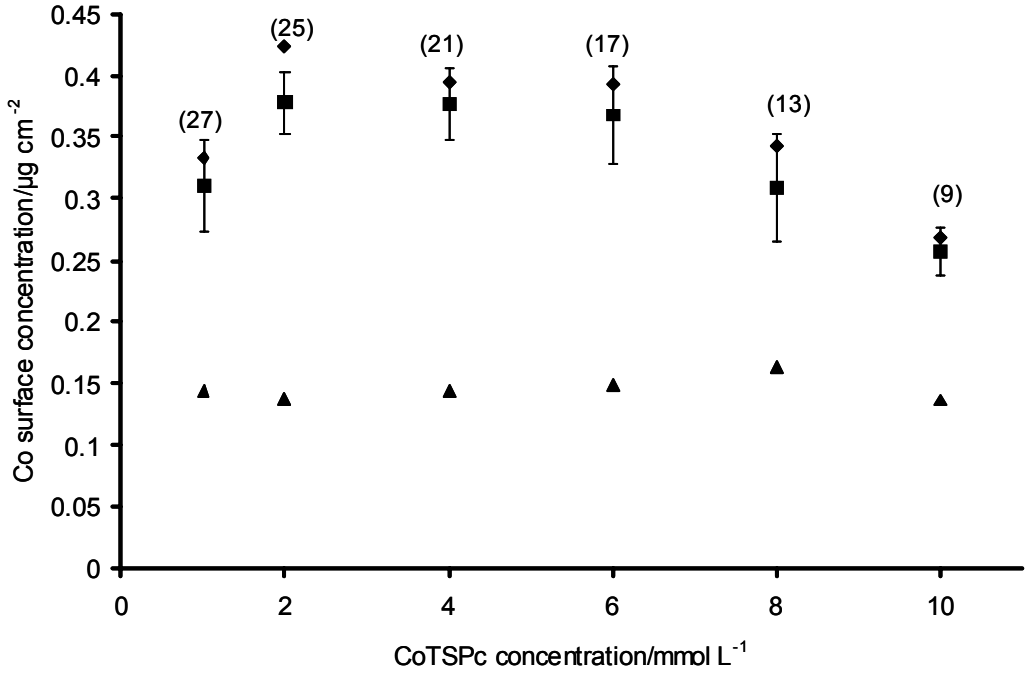

Fig. 8.6: Relationship between the Co surface concentrations calculated using the electrochemical data (▲), the sum spectra (♦) and using the mean of the histogram (■) (δ_{tot} is shown as error bar) as a function of the CoTSPc concentration during the modification at the breaking point. The value between brackets above each data point indicates the number of successive voltammetric scans.

Figure 8.7 shows the surface concentrations of cobalt on a gold electrode derived from the electrochemical and SR-XRF data after a modification using nine voltammetric scans with the CoTSPc concentration varying between 10 and 16 mmol L^{-1} in the solution. Here, the micro-heterogeneity term (δ_{het}) is represented by the error bars on the concentrations derived from the mean of the histograms. For the CoTSPc concentrations of 12, 14 and 16 mmol L^{-1}, nine voltammetric scans are beyond the breaking point; for the CoTSPc concentration of 10 mmol L^{-1}, on the other hand, this is just at the breaking point. Based on earlier chapters, it is expected that the cobalt concentration obtained via the electrochemical data is constant after the breaking point, which is indeed the case here. In contrast, the Co concentration calculated from the SR-XRF data, increases for the three latter concentrations. An explanation could be that at these concentrations the modification procedure takes 9 voltammetric scans. It has been shown in chapter 6 that at the beginning of the modification (5 subsequent voltammetric scans in 6 mmol L^{-1} CoTSPc) there is a fast growth of electro active species (monomer) on the surface in comparison with the electro inactive species (dimers). This indicates that on the bare gold electrode, primarily monomers are adsorbed. According to this behaviour, it can be postulated that at the breaking point there is a concentration independent equilibrium between the constant amount of monomers and dimers. The surface area is the limiting factor according to the amount of monomer adsorbed on the surface and there is a maximum amount of dimers adsorbed on the monomer layer. The continuous potential cycling after the breaking point causes further aggregation between the electro active species. This means that there is a stabilization of the layer and that it is better defined. On this well defined layer, however, there is an increasing amount of dimers adsorbed after the breaking point. It is also noticed that δ_{het} on the Co concentration after the breaking point increases with increasing concentration indicating an increase in heterogeneity. This can be explained by electro inactivity of the dimers which makes that they are much less affected by the potential cycling.

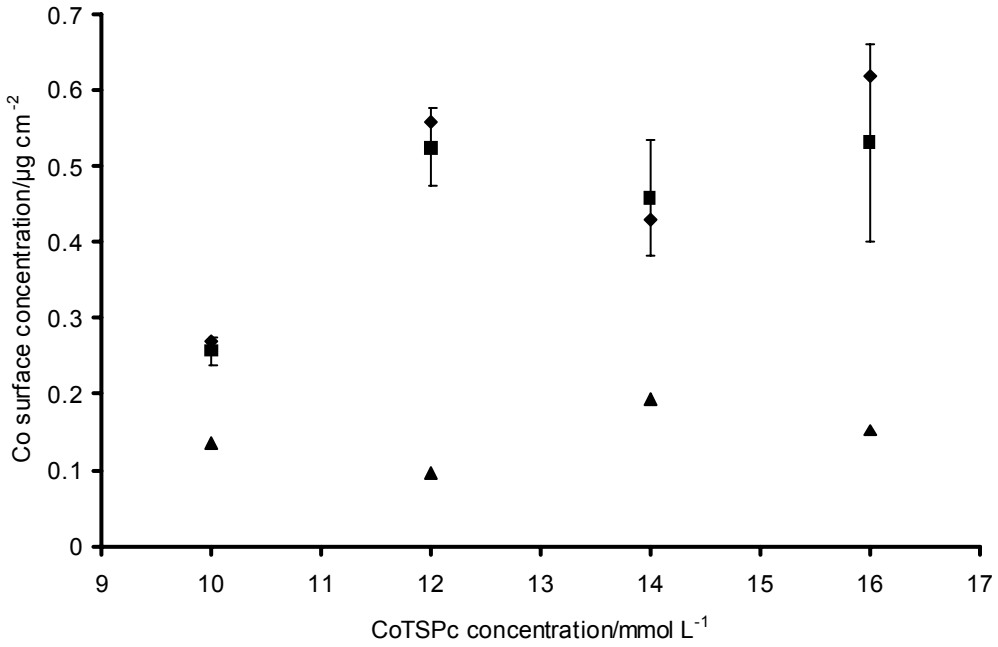

Fig.8.7: Relationship between the Co surface concentrations calculated using the electrochemical data (▲), the sum spectra (♦) and using the mean of the histogram (■) (δ_{het} is shown as error bar) as a function of the CoTSPc concentration after 9 successive voltammetric scans.

8.5 Comparison of the Cu surface concentrations on gold electrodes derived from SR-XRF and electrochemical data

A similar experiment was performed using CuTSPc. Electrochemical and SR-XRF analysis of modified gold electrodes during 60 subsequent voltammetric scans as a function of the CuTSPc concentration in solution (between 1 and 16 mmol L^{-1}) were performed. Fig. 8.8 shows the plot of the deposited copper surface concentrations calculated using the three methods described above as a function of the CuTSPc concentration during modification. It is seen that these surface concentrations determined are more or less independent of the CuTSPc concentration in the studied range. In contrast with CoTSPc, the same copper surface concentrations are calculated from the electrochemical as well as the SR-XRF data. One can also observe that the surface concentrations calculated from the mean of the histogram and the sum spectrum are different from each other for the CuTSPc concentrations in solutions of 4, 12, 14 and 16 mmol L^{-1}. For 4 and 12 mmol L^{-1} CuTSPc concentration in solution, this can be explained by the distortion of the histogram from the fitted Gaussian (see

Fig. 8.4). These histograms, indeed, show a relatively large number of high concentration pixels which can be caused by surface artefacts.

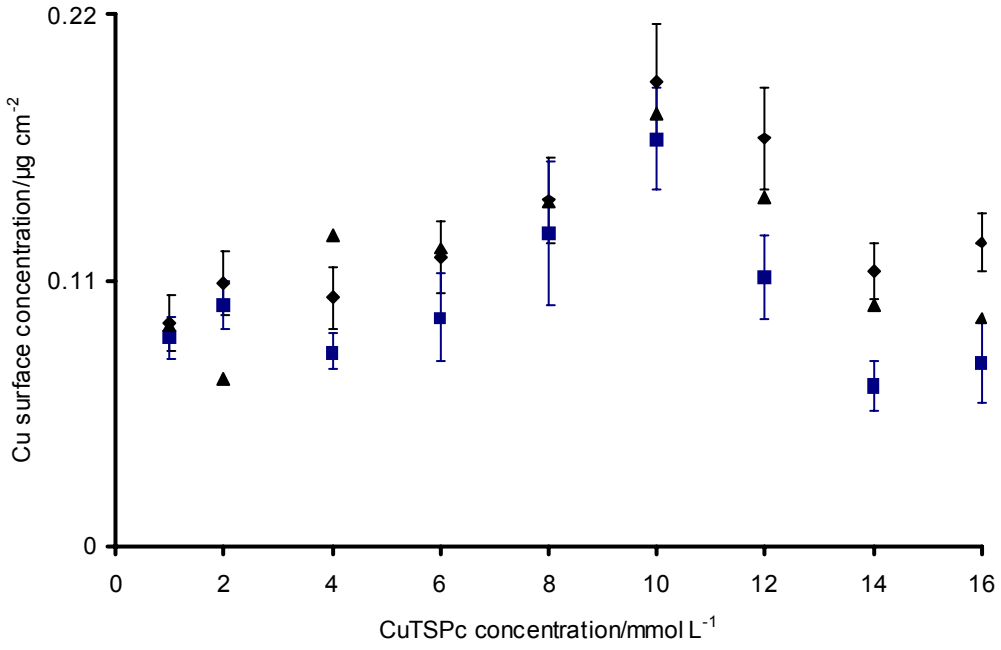

Fig. 8.8: Relationship between the Cu surface concentrations calculated using the electrochemical data (▲),the sum spectra (δ_{sum} is shown as error bar) (♦) and using the mean of the histogram (■, blue) (δ_{tot} is shown as error bar, blue) as a function of the CuTSPc concentration during the modification after 60 subsequent scans.

For the 14 and 16 mmol L^{-1} CuTSPc concentrations in solution, the difference in surface concentration can be explained by the energy shift of the incoming beam over 390 eV. As a result of this energy shift, the escape peak from the Si detector of the Rayleigh and Compton scatter interferes with the detected Cu-K_α which has in this case a similar intensity. This has a much higher influence on the (statistically more uncertain) individual pixel intensities than on the sum spectrum which causes the mean to be underestimated together with the corresponding Cu surface concentration.

In contrast with CoTSPc, there is no breaking point observed electrochemically for CuTSPc and the surface concentrations calculated from the electrochemical data closely match those derived from the SR-XRF data. These differences in electrochemical behaviour can be explained by the difference in structure of the immobilized layer caused by the four coordination of the CuTSPc in comparison with the six coordination of the CoTSPc. The four coordination of the CuTSPc causes the molecules to approach very easily without the formation of

bridged systems (e.g. with oxygen or hydroxyl particles) as is the case with CoTSPc. This makes that the formed dimers (containing a Cu-Cu bond), which are much higher in concentration than for the CoTSPc, are electrochemical active. This means that during the modification process the monomers as well as the dimers are electrochemically deposited and active on the gold electrode. As a result, the electrochemical deposition causes the formation of a compact layer consisting of dimers as well as monomers which makes electron tunnelling throughout the stacked aggregates possible. This also may explain the absence of the breaking point during the electrodeposition of the CuTSPc on the gold electrode since there is no interference of an electro inactive species during the modification which makes the stacking of the phthalocyanine aggregates possible.

8.6 Conclusions

This chapter has discussed the determination of the surface concentration and the (micro)-heterogeneity of thin layers of CoTSPc and CuTSPc on gold electrodes by means of synchrotron radiation X-ray micro fluorescence on 20 and 600 μm scales. CoTSPc or CuTSPc were deposited electrochemically on a gold electrode by recording successive cyclic voltammetric scans. The properties of the CoTSPc or CuTSPc layers were studied after modification using different phthalocyanine concentrations during the modification procedure.

It can be postulated that for the modification of a gold electrode with CoTSPc, an equilibrium exists between the constant amounts of electro active species (monomer) and the electro inactive species (dimers) at the breaking point. The surface area is the limiting factor according to the amount of monomer adsorbed on the surface and there is a maximum constant amount of dimers adsorbed on the monomer layer. After the breaking point, the monomer layer stabilizes increasing the free spaces for the dimers to adsorb.

For the modification of a gold electrode with CuTSPc it can be assumed that the monomers as well as the dimers are electrochemically active because of the absence of bridged dimers. This changes the modification in such a way that during the modification procedure stacked phthalocyanine structure can be formed immediately and that there is no stabilization of the layer needed.

8.7 References

[KEMP-00] Kempenaers L., Vincze L., Janssens K., *Spectrochim. Acta B*, **2000**, 55, 651-669.

[KEMP-01] Kempenaers L., De Koster C.,Van Borm W., Janssens K., *Fresenius J. Anal. Chem.*, **2001**, 369, 733-737.

[KEMP-02] Kempenaers L., Janssens K., Vincze L., Vekemans B., Somogyi A., Drakopoulos M., Simionovici A., Adams F., *Anal. Chem.*, **2002**, 74, 5017-5026.

[MCMA-68] McMaster W.H., Delgrande N.K., Mallet J.H., Hubbel J.H., Lawrence Radiation Laboratory report UCLR-50174, Sec. II, Ref. 1; University of California, Berkely, CA, **1968**.

[VEKE-94] Vekemans B., Janssens K., Vincze L., Adams F., Vanespen P., *X-ray Spectrom*., **1994**, 23, 278-285.

Chapter 9:
The investigation of X-ray Raman scattering effects on the detection of CuTSPc thin films deposited on gold electrodes

In the previous chapters, the SR-XRF study of gold electrodes modified with cobalt tetrasulphophthalocyanine and copper tetrasulphophthalocyanine were described extensively. We emphasized the experimental difficulty of the thin film uniformity studies as a result needing to determine low amounts of Co or Cu in the presence of partially overlapping Compton and Au X-ray resonant Raman scattering (XRRS) peaks. This chapter investigates the influence of the choice of excitation energy on the detection limit (DL) and on the peak to background ratio of copper on the spectroscopically infinitely thick gold substrate.

The experimental conditions for the electrochemical modification as well as for the SR-XRF measurements to perform this study are briefly described in the first section of this chapter. In addition, the data reduction method used to quantify the SR-XRF data and to derive the DL is described. In the second section, the influence of the XRRS process of a gold substrate on the Cu detection is studied by varying the exciting photon energy between 9 and 12 keV and in the final section the conclusions are provided.

9.1 Experimental conditions

During this study, the gold electrodes were modified by recording 60 successive cyclic voltammetric scans in a potential window from -1.2 to 0.6 V in a pH 12 buffer solution containing 4×10^{-3} mol L^{-1} 3,4',4'',4'''- copper tetrasulphophthalocyanine (CuTSPc).

During the SR-XRF measurements, the beam was monochromatized by a Si(111) fixed exit monochromator ($\Delta E/E \approx 10^{-4}$) and the excitation energies were varied form 9.2 keV- 11.7 keV and a data collection time of 300 s was used.

The quantification of the Cu surface concentration C_{Cu} at 9.3 keV occurred by the calibration curve given in Fig. 8.2 and the DL values for Cu have been calculated according to the well-known relationship:

$$DL_{Cu} = \frac{3\sqrt{B_{Cu-K\alpha}}}{I_{Cu-K\alpha}} C_{Cu} \qquad \text{(Eq. 9.1)}$$

where $I_{Cu\text{-}K\alpha}$ and $B_{Cu\text{-}K\alpha}$ are the net-peak intensity and background of the $Cu\text{-}K_\alpha$ line, respectively, measured at the known surface concentration level of C_{Cu}.

9.2 Study of the detection limit and peak to background ratio as a function of excitation energy

In our earlier scanning SR-XRF studies on CuTSPc thin films on gold substrates, surface-concentration detection limits (DL) in the range of 1-2 ng cm^{-2} have been determined assuming a live time of 300 s for data collection. These CuTSPc thin film DL values are strongly influenced by the elemental yield of the analyte element (Cu) and by the detected background which mainly arises as a result of various types of photon-matter interactions within the spectroscopically infinitely thick gold substrate. These interactions which determine the observed background include continuum radiation corresponding to photo-electron bremsstrahlung, the low-energy tail of the (multiple) Compton scattering peak just below the excitation energy and X-ray Raman scattering peaks/bands whose intensity is strongly influenced by the energy chosen for the monochromatic exciting beam. Similarly to analytical difficulties observed in case of TXRF detection of Al impurities on Si-wafers [BAUR-00], X-ray resonant Raman scattering (XRRS) can also cause a considerable deterioration of DLs in case XRF analysis of transition-metal thin films deposited on metallic substrates, such as gold electrodes. In our specific example, the efficient excitation of Cu thin films on Au-substrates requires the selection of excitation energy above the Cu-K absorption edge (8.979 keV), while remaining below the Au L3-edge

(11.918 keV) in order to achieve efficient excitation conditions for Cu K-lines and, at the same time, avoid detector overload by the orders of magnitude more intense Au L-lines. Fig.9.1. shows a series of experimental XRF-spectra obtained from CuTSPc thin films electrochemically deposited on a gold electrode, corresponding to excitation energies in the energy range of 9.2-11.7 keV. While at lower energies ($E_0 \leq 10$ keV) the XRRS contribution appears as a relatively small step-like discontinuity (below the Cu-peaks) on the detected spectra, it becomes an overwhelming and partially coinciding spectral feature when the excitation energy (E_0) approaches the Au L_3-edge.

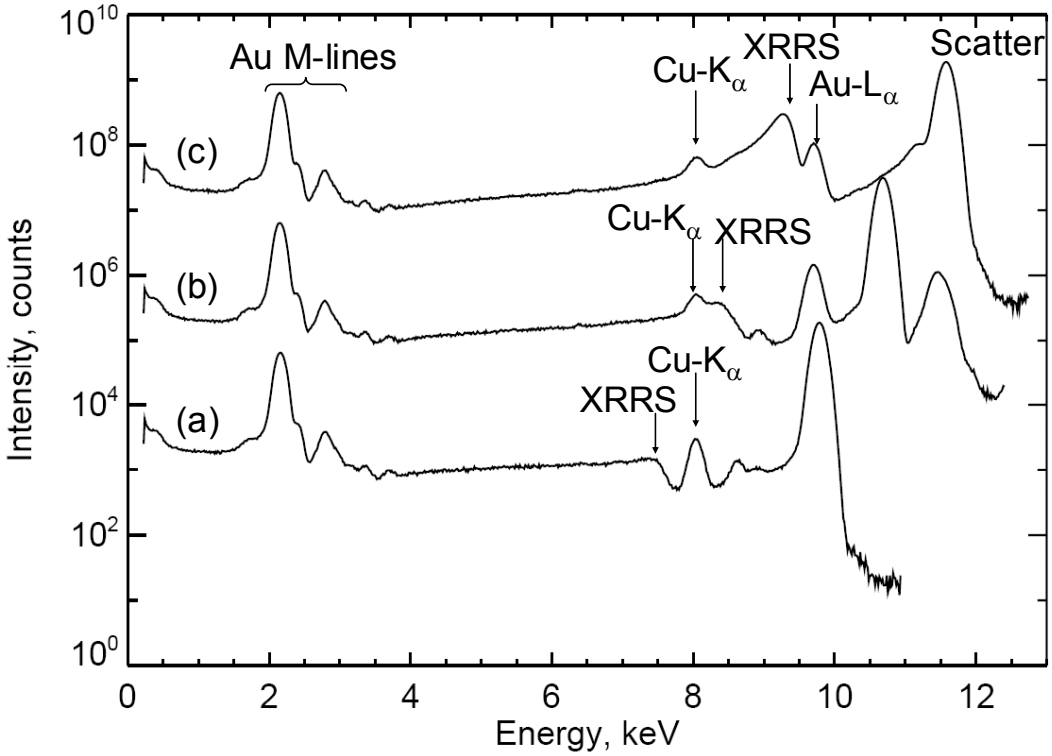

Fig. 9.1: Experimental XRF-spectra of the Au-substrate/CuTSPc thin-film system, illustrating the evolution of the XRRS-peak as the excitation energy varies from 9.8 (a) over 10.7 (b) to 11.6 keV (c). The reduction of peak-to-background ratios at Cu-Kα towards higher energies can be easily observed. The top two XRF-spectra were multiplied by a factor 10^2 and 10^4 respectively for clarity. Note the presence of Au-Lα as a result of excitation by the Si(111) 3^{rd} harmonic, which could only be partially suppressed by monochromator mistuning.

Next to simply increasing DLs (or reducing effective sensitivities) this XRRS interference can in special cases cause the detection of Cu virtually impossible, due to the complete overlap of strong XRRS-peaks with the Cu K-lines. Such condition of

severe Cu-K_α and XRRS interference is shown in Fig.9.2, in which case the excitation energy is chosen to be at the following energy:

$$E_0 \approx E\ (Cu\text{-}K_\alpha) + E\ (Au\text{-}M_V) \qquad \text{(Eq. 9.2)}$$

where $E\ (Cu\text{-}K_\alpha)=8.04$ keV is the Cu-K_α line energy, $E(Au\text{-}M_V)=2.21\ keV$ the Au-M_V absorption edge energy, respectively.

At excitation energies above this region, the detection of Cu becomes reliable again due to the shift of the XRRS peaks towards higher energies, however, detection limits are progressively increased by the rapid increase of XRRS-tailing, and the reduction of Cu excitation efficiency as E_0 becomes considerably higher than the Cu K-edge.

The variation of detection limits is shown in Fig. 9.3a as a function of excitation energy in the studied energy interval. These DL values approximately increase by a factor 4, from 1.0 ng cm^{-2} (A in Fig. 9.3a) to approximately 4.2 ng cm^{-2} (B in Fig. 9.3b), when the excitation energy is increased gradually in the energy range of 9.2 – 11.4 keV. This is mainly attributed to the considerable increase of overlapping spectral components as a result of XRRS, resulting in approximately a 9-fold increase of the detected background level at 11.7 keV compared to 9.2 keV. This effect is coupled with the decreasing excitation efficiency for Cu towards higher E_0 values, resulting in an overall reduction of peak-to-background ratios as a function of increasing excitation energy, as shown in Fig. 9.3b. In the energy region of 9.2 – 11.7 keV, the peak-to-background ratio changes from 2.76 (A in Fig. 9.3b) to 0.30 (B in Fig. 9.4b) which indicates a dramatic reduction of effective elemental yield for Cu.

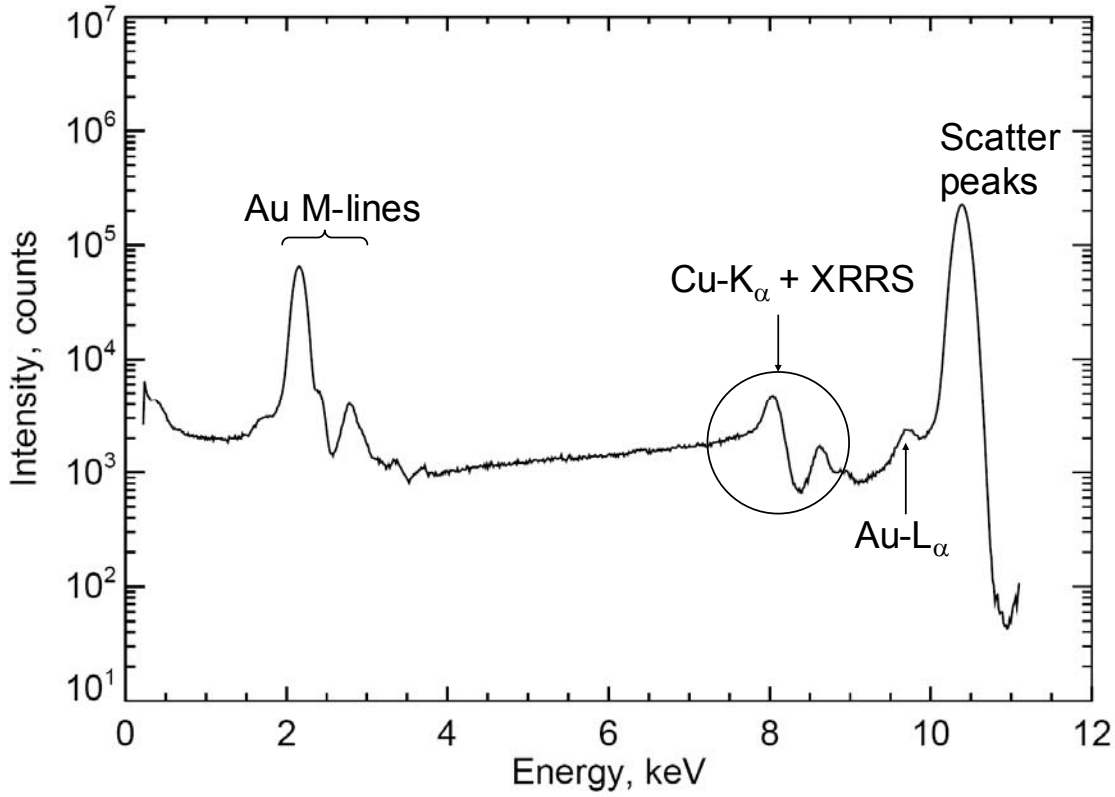

Fig. 9.2: Experimental XRF-spectrum showing the coinciding analyte-line (Cu-Kα) and the resonant Raman band at an excitation energy of 10.40 keV. At this excitation energy, the separation of Cu-Kα and XRRS becomes virtually impossible.

9.3. Conclusions

This chapter has discussed the effects of X-ray Resonant Raman Scattering (XRRS) in the context of its analytical influence on the outcome of monochromatic SR-XRF measurements on CuTSPc thin film detection on gold substrates. In the specific case of the detection of Cu deposited on spectroscopically infinitely thick gold electrodes, the choice of excitation energy in the relatively narrow energy band of 9.2 – 11.7 keV has shown to have a great influence on the expected DL values and peak-to-background ratios which can be observed during the XRF-measurements. DL values range from 1.0 to 4.2 ng cm^{-2} as the excitation energy is varied between 9.2 to 11.4 keV, while peak-to-background ratios worsen by a factor of 9 (from 2.76 to 0.30), indicating the strong interference effects of XRRS with respect to the detection of the CuTSPc thin film. This study has represented a new example of the often unexpected contribution of XRRS on the outcome SR-XRF measurements using

monochromatic X-rays for specific analyte/sample substrate combinations, such as transition-metal thin film detection on gold electrodes.

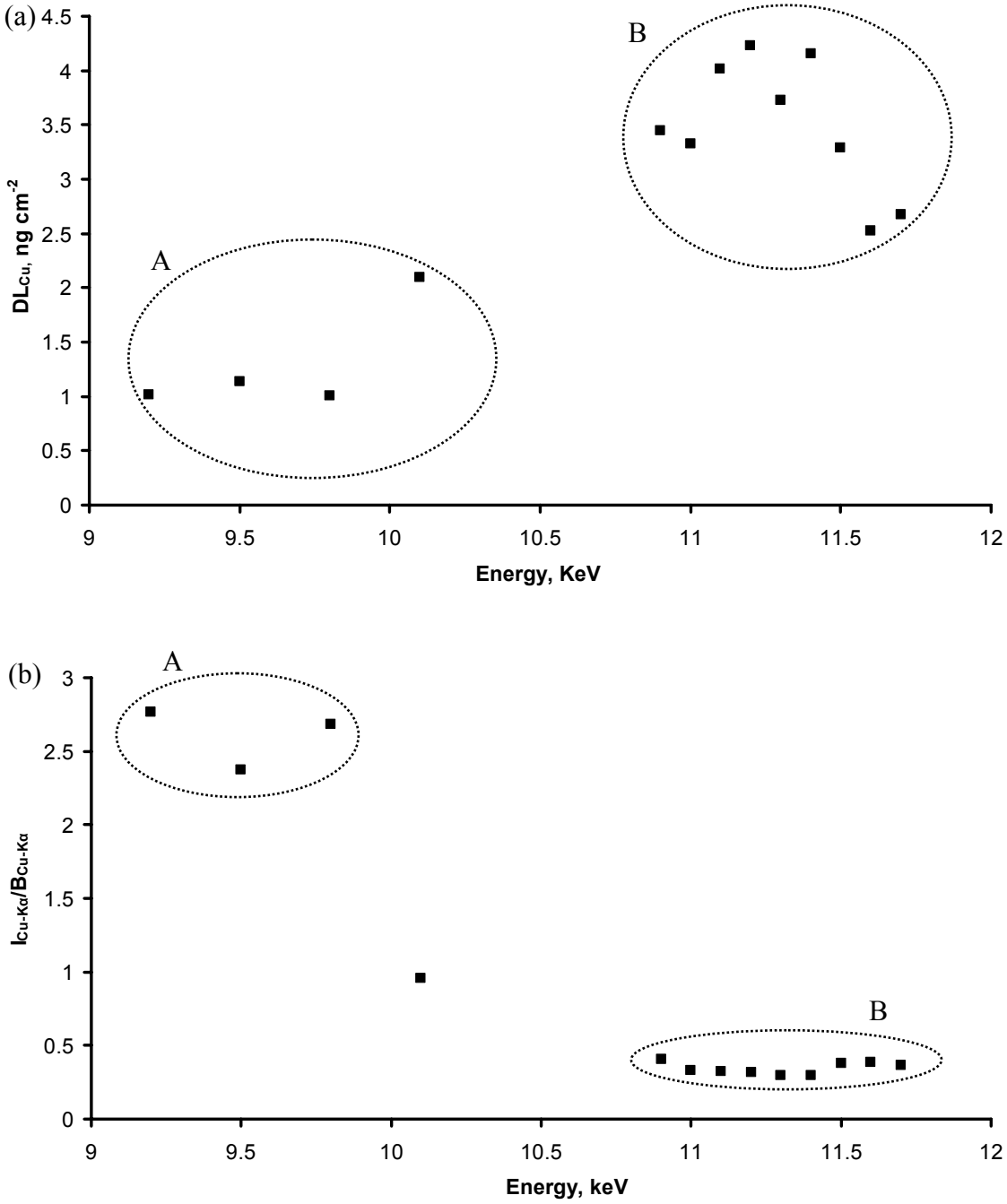

Fig. 9.3: Detection limits (a) and peak-to-back-ground ratios (b) of Cu thin films on a infinite thick gold substrate as a function of the excitation energy. The excitation energies with low DL and high peak-to-back-ground ratios (A) and with high DL and low peak-to-back-ground ratios (B) are grouped.

9.4 References

[BAUR-00] Baur K., Kerner J., Brennan S., Singh A., Pianetta P., *J. Appl. Phys*, **2000**, 88, 4642-4647.

Chapter 10:
Comparison of the oxidation of 4-chlorophenol on a bare gold electrode with that on gold electrodes modified with CoTSPc or CuTSPc in alkaline solution

The previous chapters encompassed the description and discussion of the thin film buildup of CoTSPC and CuTSPc on gold electrodes in a pH 12 buffer solution. In this chapter, the oxidation of the target molecule, 4-chlorophenol (4-Cp) on a bare gold electrode is compared to that with the oxidation on a gold electrode electrochemically modified with CoTSPc or CuTSPc.

The first section of this chapter describes the experimental details concerning the modification and the data reduction method concerning the oxidation of 4-Cp. In the second section of this chapter, the oxidation potentials of 4-Cp at the modified and on the bare gold electrodes are discussed. A discussion is provided on the fouling of the electrode material in the third section and in the fourth section; the calibration curves obtained at the different electrode materials are discussed. The fifth section link the oxidation characteristics of the modified electrodes with the molecular structure of the phthalocyanine thin films on the gold surface and the results are discussed in terms of the coordinating properties of the phthalocyanines which make the postulation of the more general preferred phthalocyanine characteristics in the conclusions possible.

10.1 Experimental details and data reduction method

The electrochemical modification was performed as described in chapter 2 with CoTSPc purchased from the Rhodes University of Grahamstown (South-Africa) and CuTSPc purchased from Sigma Aldrich (USA). Important for the study described in this chapter, is that the modification was performed prior to the breaking point (10

voltammetric scans, 6 mmol L^{-1} CoTSPc), at the breaking point (respectively 17, 21 and 25 voltammetric scans for 6, 4 and 2 mmol L^{-1} CoTSPc) and after the breaking point (100 voltammetric scans in 6 mmol L^{-1} CoTSPc) for the modification with CoTSPc and during 10, 60 and 100 voltammetric scans for the modification with CuTSPc. After this modification step, the modified electrode was scanned during 20 voltammetric scans in a blank buffer solution followed by adding different concentrations of freshly made 4-Cp solution. For each concentration, a freshly modified electrode was used and the net peak current (I) of the first voltammetric scan in a pH 12 buffer 4-Cp solution was measured at the oxidation peak potential of 4-Cp. This value was plotted as function of the concentration (C_{Cp}) to obtain calibration curves in a concentration range from 0.05 to 1 mmol L^{-1}. Linear regression by the least squares method was applied using the model: $I = b_0 + b_1 \times C_{Cp} + e$ where e is the residual. The uncertainty of these values (s_{b0} and s_{b1}) next to the pure (experimental) error (s_y) was calculated. The pure (experimental) errors were statistically compared on the 95% confidence level using the F-test for the precision. The calibration curves have been statistically compared with each other on the 95% confidence level with the two tailed t-test using the Bonferroni adjustment. This adjustment had to be used since more than two means had to be compared which makes that the same mean is used several times and consequently the t-tests are not independent of each other. As a result, when all population means are equal, the probability that at least one comparison will be found to be significant different increases [MASS-97].

10.2 Oxidation potential of 4-Cp

Fig. 10.1 shows the first cyclic voltammetric scan of 1.0 mmol L^{-1} 4-Cp in a pH 12 buffer solution on a bare gold electrode (a, curve 1), on a gold electrode modified with CoTSPc until the breaking point (b, curve 1) and on a gold electrode modified with CuTSPc during 60 subsequent voltammetric scans (c, curve 1). Also the current potential curves recorded under the same conditions of the respective electrodes (resp. a, b and c, curve 2) in a 4-Cp free pH 12 buffer solution are shown. Results show that oxidation of 4-Cp occurs at the bare gold electrode, as well as at the modified electrodes around 0.5 V vs. SCE.

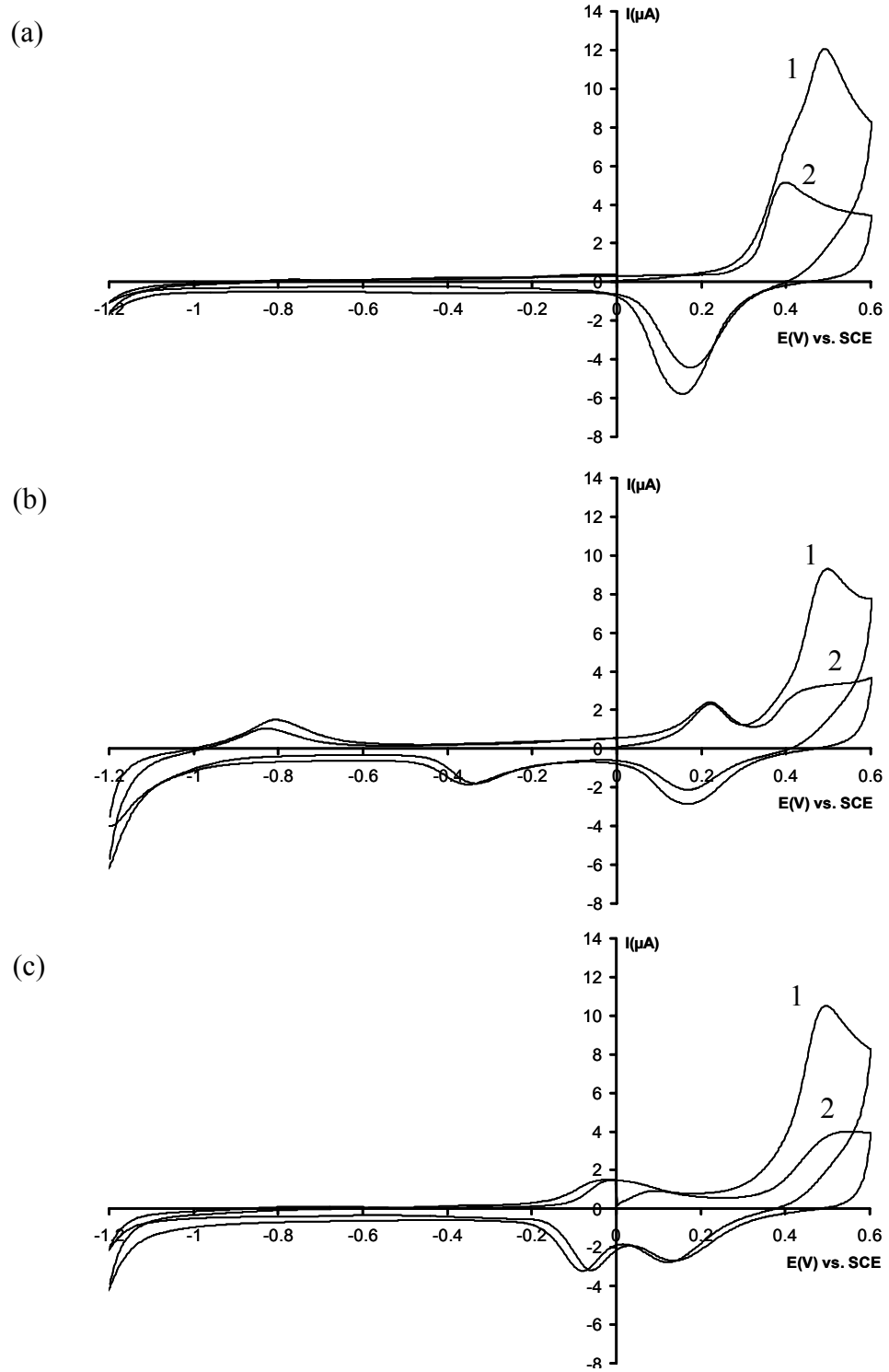

Fig. 10.1: Current potential curves recorded with a voltammetric scan rate of 50 mV s^{-1} between 0.6 V and -1.2 V vs. SCE in a 1.0 mmol L^{-1} 4-Cp pH 12 buffer solution at a bare gold electrode (a, curve 1), at a gold electrode modified in 6 mmol L^{-1} CoTSPc till the breaking point (b, curve 1) and at a gold electrode modified during 60 voltammetric scans in 4 mmol L^{-1} CuTSPc (c, curve 1) at 298 K. Also the current potential curves recorded under the same conditions of the respective electrodes (resp. a,b and c, curve 2) in a 4-Cp free pH 12 buffer solution are shown.

In Fig. 10.2, the oxidation of 1.0 and 0.4 mmol L^{-1} 4-Cp at a bare gold (resp. a and d) and at modified electrodes (resp. b and e for CuTSPc and c and f for CoTSPc) are shown in more detail. The peak potential of the oxidation of 4-Cp at a bare gold electrode shifts over 30 mV to higher potentials when the 4-Cp concentration is changed from 1.0 to 0.4 mmol L^{-1}. Moreover, it is noticed that the 4-Cp oxidation peak interferes with the gold oxidation peak (see chapter 4). The peak potentials of the oxidation of 4-Cp at modified electrodes, however; show only a minor change when the 4-Cp concentration is changed.

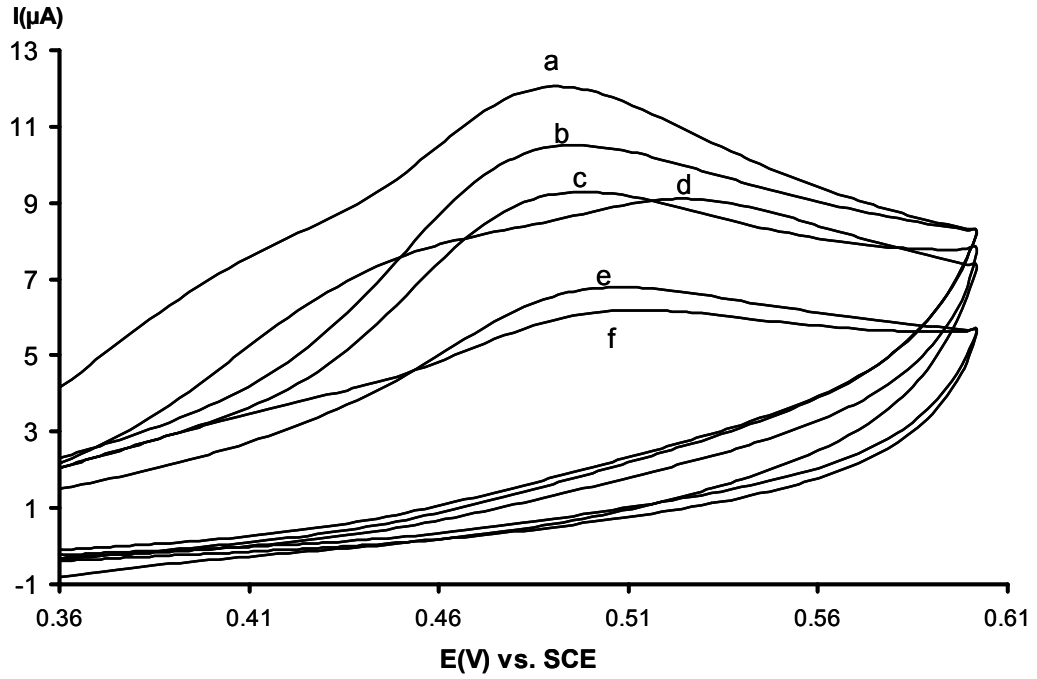

Fig. 10.2: Current potential curves recorded with a voltammetric scan rate of 50 mV s^{-1} between 0.6 V and -1.2 V vs. SCE in a pH 12 buffer solution at a bare gold electrode containing 1.0 (a) or 0.4 mmol L^{-1} (d) 4-Cp, at a gold electrode modified with CoTSPc till the breaking point containing 1.0 (c) or 0.4 mmol L^{-1} (f) 4-Cp and at a gold electrode modified during 60 voltammetric scans in 4 mmol L^{-1} CuTSPc containing 1.0 (b) or 0.4 mmol L^{-1} (e) 4-Cp.

10.3 Fouling of the electrode materials

Fig. 10.3 shows a detail of the oxidation of 0.6 mmol L^{-1} 4-Cp at a gold electrode modified with CoTSPc till the breaking point (a-e) and during 60 voltammetric scans with CuTSPc (f-j) as a function of time (voltammetric scan number). It is seen that the current decreases with growing voltammetric scan number indicating the fouling of the electrode. This can be explained by the formation of

phenoxy radicals which can react through two pathways. One pathway yields species with a quinonic structure; the other one is the formation of insoluble polymers that passivate the electrode surface (see chapter 1). In this study, it is observed that the net current decreases with 10% during 10 subsequent voltammetric scans in 0.6 mmol L^{-1} 4-Cp for a gold electrode modified with CoTSPc. For the CuTSPc modified gold electrode and the bare gold electrode, the current however decreases respectively with 22% and 26% indicating that the fouling of the electrode occurs slower on the gold electrode modified with CoTSPc. An explanation for this difference will be given further in this discussion.

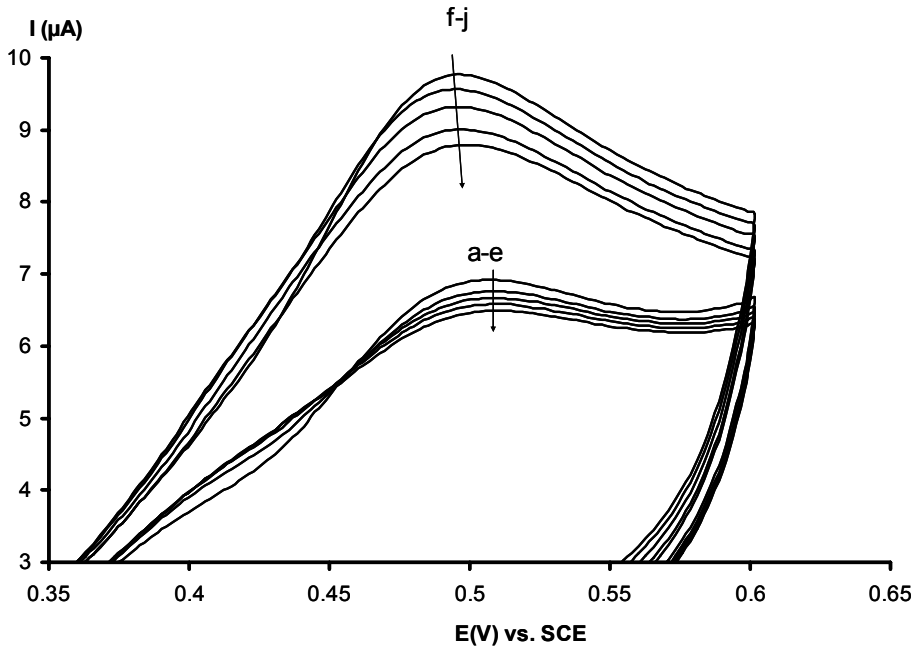

Fig. 10.3: Current potential curves recorded between 0.6 V and -1.2 V vs. SCE in a pH 12 buffer solution with a voltammetric scan rate of 50 mV s^{-1} at a gold electrode modified with CoTSPc at the breaking point in a 0.6 mmol L^{-1} 4-Cp solution with the successive voltammetric scan numbers (a) 2, (b) 4, (c) 6, (d) 8 and (e) 10 and at a gold electrode modified with CuTSPc during 60 scans in a 0.6 mmol L^{-1} 4-Cp solution with the successive voltammetric scan numbers (f) 2, (g) 4, (h) 6, (i) 8, (j) 10.

10.4 Comparison of calibration curves of 4-Cp

Because of the fouling of the electrode, a fresh electrode is needed for each experiment. In addition only the first cyclic voltammeric scan of the electrode under investigation in the 4-Cp solution is taken into account to plot a calibration curve. Fig. 10.4 compares the calibration curves of 4-Cp for a gold electrode modified with

CoTSPc till the breaking point (curve 1) and for a gold electrode modified with CuTSPc during 100 voltammetric scans (curve 2). The calibration curve obtained on a bare gold electrode is also shown (curve 3). In Table 10.1, the slope of the calibration curves (b_1), the intercept with the Y axis (b_0) and their respective uncertainties (s_{b0} and s_{b1}) are shown together with the pure (experimental) error (σ_y) of the detection of 4-Cp on gold electrodes modified with CoTSPc before the breaking point, at the breaking point and after the breaking point. Analogue results for different CuTSPc modified electrodes (during 17, 60 and 100 voltammetric scans) and for a bare gold electrode are also presented in Table 10.1.

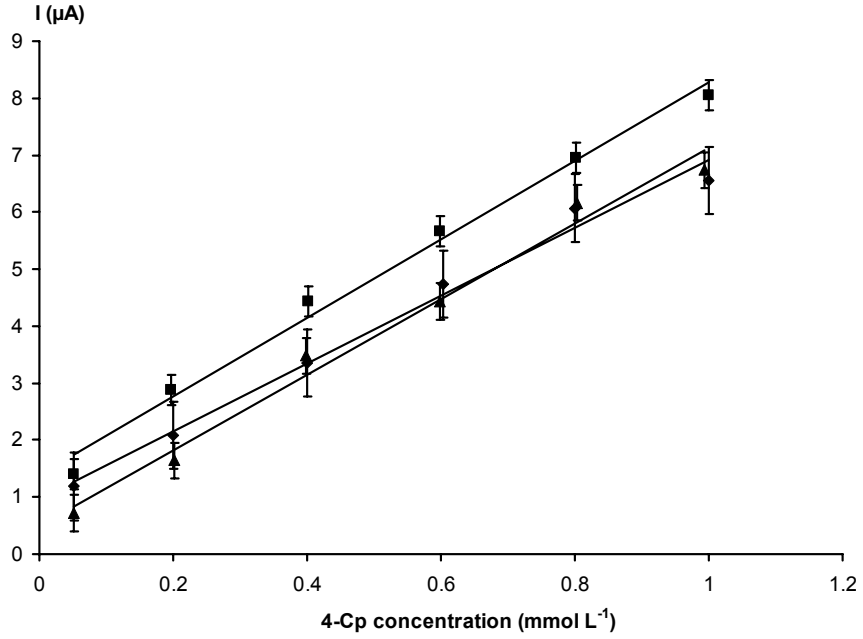

Fig. 10.4: Calibration curves of 4-Cp oxidation obtained at a bare gold electrode (3,■), at a gold electrode modified with CoTSPc at the breaking point (1,♦) and at a gold electrode modified with CuTSPc during 100 voltammetric scans (2,▲) in a pH 12 buffer solution, with a voltammetric scan rate of 50 mV s^{-1} at 298 K. The error bars shown are σ_y.

The results show that the uncertainty on the detection of 4-Cp is significantly smaller before the breaking point (CoTSPc), on the breaking point (CoTSPc) and on a bare gold electrode than after the breaking point (CoTSPc). This indicates that the precision decreases with the modification time (increasing voltammetric scan number). Moreover, it is seen that the sensitivity of the 4-Cp detection is significantly lower at the breaking point than before the breaking point and at the bare gold electrode. For the detection of 4-Cp on a gold electrode modified with CuTSPc, it is noticed that the precision and the sensitivity are independent from the number of

voltammetric scans during the modification process. No significant difference between the detection of 4-Cp at a bare gold electrode and a gold electrode modified with CuTSPc is detected.

Table 10.1: Overview of the data related to the calibration curves obtained from the electrochemical oxidation of 4-Cp at a bare gold electrode and at gold electrodes electrochemically modified with CoTSPc or CuTSPc in a concentration range of 0.05 to 1 mmol L^{-1} with respectively the electrode condition, b_1,s_{b1}, b_0, s_{b0}, s_y and the number of data points shown.

	b_1 (µA mol^{-1} L)	s_{b1} (µA mol^{-1} L)	b_0 (µA)	s_{b0} (µA)	s_y (µA)	Data points
CoTSPc						
Before the breaking point	6412	335	0.440	0.203	0.382	12
At the breaking point	5960	347	0.965	0.257	0.593	18
After the breaking point	6021	738	0.759	0.548	1.157	17
CuTSPc						
17 scans	6529	288	0.640	0.174	0.232	6
60 scans	6438	107	0.5979	0.065	0.086	6
100 scans	6633	397	0.495	0.240	0.319	6
Au	6897	330	1.3925	0.200	0.267	6

10.5 Relationship between CoTSPc and CuTSPc thin film buildup and the 4-Cp oxidation properties

The similarity of the detection of 4-Cp at a bare gold electrode and at an electrode modified with CuTSPc can be explained by the thin film buildup as described in chapters 5-8. We were able to show that for the CuTSPc modified gold electrodes from the first voltammetric scan on, a stable CuTSPc thin film is formed with nicely stacked columnar aggregates. During further modification, the thin film keeps on growing steadily, increasing the number of electrochemically active CuTSPc molecules. The CuTSPc aggregates on the electrode make electron transfer through

the thin film possible and have only a minor influence on the electrode sensitivity explaining the independency of the 4-Cp detection from the number of voltammetric scans during modification and from the modification of the electrode. Moreover, above results show that the rate of fouling of both the bare gold electrode and the CuTSPc modified electrode is the same, indicating that the oxidation process at both electrodes is comparable and that the modification of the gold electrode with CuTSPc is not an improvement for the detection of 4-Cp.

For CoTSPc another effect concerning the relationship between the thin film buildup and the detection of 4-Cp is observed. In this case, the change in sensitivity and selectivity for the detection of 4-Cp with a gold electrode modified with CoTSPc before, at and after the breaking point, can also be explained by the change of the thin film buildup during the modification procedure as described in chapter 4. As already mentioned in previous chapters, in the beginning of the modification procedure only electrochemical active monomer species are adsorbed on the gold electrode. On this CoTSPc monomer thin film, monomers as well as dimers are adsorbed. At the breaking point, there is an equilibrium between the monomer and the dimer species. Only adsorption of the electrochemically inactive dimer species on the formed thin film is observed after the breaking point. The similarity in sensitivity for the 4-Cp detection for a gold electrode modified with CoTSPc before the breaking point and for a bare gold electrode can be explained, as for CuTSPc, by the availability of electrochemical active CoTSPc species for the oxidation of 4-Cp. During continuous modification however, the number of dimers, adsorbing on the CoTSPc thin film starts to increase. At the breaking point, the high amount of electrochemical inactive dimer species results in a decrease of the sensitivity of the modified electrode. During further modification, the amount of dimers on the electrode surface keeps increasing which has a negative influence on the reproducibility of the 4-Cp detection. The presence of the CoTSPc dimers on the surface however, appear to have a positive influence on the fouling of the electrode. This can be explained by the more chaotic thin film buildup resulting in a more difficult adsorption of the phenoxy polymer on the surface. It is also possible that the formed phenoxy polymer adsorbs on a CoTSPc dimer site which is not electrochemically active.

10.6 Conclusions

In this chapter the oxidation of 4-Cp in a pH 12 buffer solution at a bare gold electrode is compared with its oxidation at a gold electrode modified with CoTSPc or CuTSPc. The modification of the electrode was performed by successive cyclic voltammetric scans in CoTSPc or CuTSPc solutions. It is noticed that the gold electrodes modified with CoTSPc or CuTSPc show no electrocatalytic behavior concerning the oxidation of 4-Cp. It is, however, seen that the buildup of the CoTSPc or CuTSPc thin film on the gold electrode has a major influence on the sensitivity and the reproducibility of the electrode. High amounts of electrochemical inactive species on the electrode surface have to be avoided. Therefore, four coordinating metal phthalocyanines are preferred and six coordinating metal phthalocyanines (see chapter 5 to 8) have to be avoided as electron transfer mediator. On the other hand, it is noticed that the more chaotic thin film buildup and the presence of electro inactive six coordinating CoTSPc species have a positive effect on the fouling of the electrode surface.

10.7 References

[MASS-97] D.L. Massart, B.G.M. Vandeginste, L.M.C. Buyens, S. De Jong, P.J. Lewi, J. Smeyers-Verbeke, *Handbook in Chemometrics and Qualimetrics: Part A*, Elsevier, Amsterdam, **1997**.

Summary and conclusions

Summary and conclusions

This work aimed at studying the the modification of gold electrodes with cobalt(II) tetrasulphophthalocyanine (CoTSPc) and 3,4',4'',4''' copper(II) tetrasulphophthalocyanine (CuTSPc) in a pH 12 buffer solution. A better understanding of the characteristics of this phthalocyanine thin film makes it possible to optimize the modification procedure resulting in the use of the phthalocyanine thin film as electron transfer mediator. The latter is extremely useful in the development of electrochemical sensors.

Different surface modification techniques (drop-drying, immersion and electrodeposition) were used and compared. In addition the phthalocyanine concentration and the number of cyclic voltammetric scans during electrodeposition were varied. In comparison to earlier studies concerning the modification of gold electrodes with CoTSPc and CuTSPc, the emphasis was not only on the electrochemical properties of the modified electrodes. Also the heterogeneity and the morphology of the CoTSPc and CuTSPc thin films on the gold electrodes were studied. The latter was done using scanning synchrotron micro X-ray fluorescence (SR-XRF) on the 20 μm scale. Furthermore, the coverage of CoTSPc and CuTSPc on the gold electrodes was determined by X-ray photoelectron spectroscopy and the monomer-dimer equilibrium of the phthalocyanine species in solution was studied with UV-Vis spectroscopy. The combination of these electrochemical and spectroscopic techniques provided a better understanding with regard to the thin film buildup and was useful in the optimization of the modification procedure.

In a second stage the modified electrodes were used as an electron transfer mediator for the electrochemical oxidation of 4-chlorophenol (4-Cp) and the oxidation characteristics were linked with the CoTSPc or CuTSPc thin film structure.

In what follows the major results and conclusions will be elaborated.

A comparison of the different surface modification techniques such as drop-drying, immersion and electrodeposition showed that the latter leads to a more efficient deposition and that a uniformly adsorbed CoTSPc or CuTSPc thin film is formed. As a result the electrodeposition was studied in more detail.

In previous studies and in fact also during this study, it was noticed that the oxidation and reduction currents of the adsorbed cobalt ions first increase with scan number during the electrodeposition with CoTSPc. After a concentration dependent number of cyclic voltammetric scans, however, a breaking point is reached and not any further increase of the current could be noticed. For the electrodeposition of CuTSPc on gold electrodes, on the other hand, there was no breaking point to be observed. Instead it was seen that the oxidation and reduction peak currents of the adsorbed copper ions keep increasing with scan number. Moreover, by comparing the electrodeposition described in this work with literature data, it was noticed that the position of the sulphonate groups on the phthalocyanine ring has a major influence on its electrochemical behavior and thus on the characteristics of the modified electrode.

In order to obtain a better understanding of the modification process and the thin film buildup a heterogeneity and morphology study of the CoTSPc or CuTSPc thin films was performed with SR-XRF. Experimental difficulty of the CoTSPc or CuTSPc thin film uniformity studies included the determination of low amounts of Co or Cu in the presence of partially overlapping Compton and Au X-ray resonant Raman peaks. The X-ray resonant Raman phenomenon was studied on a gold electrode modified with CuTSPc. The detection limits of the Cu surface concentrations on the electrode were calculated as a function of the excitation energy which made the optimization of the experimental parameters possible. The optimized absolute detection limits received for Co and Cu are respectively 7-8 ng cm^{-2} and 5-6 ng cm^{-2} using a measuring time of 20 s and an excitation energy for Co of 7.7 ± 0.1 keV and of 9.0 ± 0.1 keV for Cu. The low detection limits, together with the rapid detection and the small beam size makes this technique very useful for this type of application.

Comparison of the Co surface concentrations of electrochemically modified electrodes derived from the electrochemical and SR-XRF data showed that these of the electrochemical data are significantly lower. This indicated that apart from electrochemical active phthalocyanine species also electrochemically inactive species

are to be present on the electrode surface. Moreover, it was seen that at the beginning of the modification procedure the difference between the concentrations derived from the two techniques is very small and increases with scan number.

According to the SR-XRF data, the cobalt surface concentration is independent from the CoTSPc concentration in solution at the breaking point, while after the breaking point the cobalt surface concentration keeps increasing. Based on the UV-Vis data it was seen that monomer as well as dimer species are present in the CoTSPc solution during the modification process. Moreover, comparison of the modification of gold electrodes with CoTSPc purchased from different suppliers showed that the monomer-dimer equilibrium highly influences the modification process. A high monomer concentration in solution has a positive effect on the modification of the electrode material. Based on these results and on information from the literature stating the preference of CoTSPc for six coordination, it was postulated that the CoTSPc monomers are electrochemical active and the dimers electrochemical inactive. Furthermore, it was postulated that at the beginning of the modification procedure, there is a fast growth of electrochemical active species (monomers) on the surface in comparison with the electrochemical inactive species. This indicates that on the bare gold electrode, primarily monomers are adsorbed. As soon as a thin electrochemical active CoTSPc monomer thin film is formed, electrochemical inactive dimer species start to adsorb. At the breaking point, there is a concentration independent equilibrium between the constant amount of monomers and dimers. The surface area is the limiting factor according to the amount of monomer adsorbed on the surface and there is a maximum amount of dimers adsorbed on the monomer thin film. The continuous potential cycling after the breaking point causes further aggregation between the electro active species. This means that there is a stabilization of the thin film and that it is better defined. On this well defined thin film there is an increasing amount of dimers adsorbed after the breaking point which show a decrease in heterogeneity.

Similar experiments for the modification of gold electrodes with CuTSPc show that the calculated copper surface concentrations based on the electrochemical and the SR-XRF data are the same indicating that only electrochemical active species are adsorbed on the gold surface. As already mentioned, it was seen that the

Cu surface concentration steadily increases with growing scan number and that there is no breaking point to be reached. It was also noticed that the Cu surface concentration is more or less independent of the CuTSPc concentration in solution in the studied concentration range (1-16 mmol L^{-1}). UV-Vis data showed that mainly dimers are present in the phthalocyanine solution. These differences in behavior in comparison to the CoTSPc are explained by the preference of four coordination of CuTSPc. It was postulated that the four coordination of the CuTSPc causes the molecules to approach very easily, without the formation of bridged systems as is the case with CoTSPc. This makes that the formation of CuTSPc dimers occurs much easier than for CoTSPc, explaining the high dimer concentration and their electrochemical activity. This means that during the modification process, the monomers as well as the dimers are electrochemically deposited and active on the gold electrode. As a result, the electrochemical deposition causes the formation of a compact thin film consisting of dimers as well as monomers which makes electron transfer throughout the stacked aggregates possible. This also may explain the absence of the breaking point during the electrodeposition of the CuTSPc on the gold electrode since there is no interference of an electro inactive species during the modification which makes the stacking of the phthalocyanine aggregates from scan 1 possible. In view of this, also the influence of the position of the sulphonate groups on the phthalocyanine ring on the modification is explained. It was indeed postulated that the sulphonate groups take part in the π-π stabilization interactions during the CuTSPc thin film formation which is in favor of the 3,4',4'',4''' CuTSPc.

In the final part of this work, the electrochemically modified electrodes were used for the oxidation of 4-Cp in a pH 12 buffer solution and compared with its oxidation at a bare gold electrode. It is seen that the gold electrodes modified with CoTSPc or CuTSPc show no electrocatalytic behavior concerning the oxidation of 4-Cp. It was, however, seen that the oxidation potential of 4-Cp at a bare gold electrode is highly concentration dependent in comparison with the oxidation potential at a modified electrode. Moreover, it was seen that the thin film buildup of the CoTSPc or CuTSPc thin film has a major influence on the sensitivity and the reproducibility of the electrode. High amounts of electrochemical inactive species have to be avoided. Therefore, four coordinating metal phthalocyanines are preferred

and six coordinating metal phthalocyanines have to be avoided as electron transfer mediator.

In the future, this work can be extended to other electrode materials (e.g. Pt) and other phthalocyanine species (containing e.g. Fe, Ni, Zn as central ion) to refine and generalize the theory about the thin film buildup of the phthalocyanine species electrochemically adsorbed on the gold electrode. The study can also be extended to X-ray absorption spectroscopy which allows the determination of the ionization stage and the nearest neighbor atom in the phthalocyanine thin film. Furthermore, in this study only the start of research towards the detection of a target molecule with electrochemically modified electrodes is given. The number of target molecules that can be tested in the future is as good as inexhaustible.

Concerning the use of SR-XRF to study the heterogeneity and morphology of thin films on electrode materials it can be stated that not only electrodeposited phthalocyanine species can be investigated. Also phthalocyanine species e.g. covalently bonded on the electrode surface or other species as for example electrochemical active enzymes containing a transition metal can be studied. The properties of this technique, indeed, makes the heterogeneity and morphology study of numerous thin films on different electrode materials possible.

Samenvatting en conclusies

Het doel van dit werk was de studie van de modificatie van goudelektroden met kobalt(II)tetrasulfoftalocyanine (CoTSPc) en 3,4',4'',4''' koper(II)-tetrasulfoftalocyanine in een pH 12 bufferoplossing. Een beter begrip van de karakteristieken van de ftalocyaninelagen op de elektrode maakt immers de optimalisatie van de modificatieprocedure mogelijk wat op zijn beurt het gebruik van de ftalocyanine laag als elektrontransfermediator mogelijk maakt. Deze laatste vinden hun nut bij de ontwikkeling van elektrochemische sensoren.

Verschillende modificatietechnieken ('drop-drying', onderdompelen en elektrodepositie) werden bestudeerd en vergeleken. Bovendien werd de ftalocyanineconcentratie in oplossing tijdens de modificatie en het aantal cyclisch voltametrische scans tijdens de elektrochemische modificatie gevarieerd. In tegenstelling tot vroegere studies omtrent de modificatie van goudelektroden met CoTSPc of CuTSPc, werd de nadruk in deze studie niet enkel op de elektrochemische eigenschappen van de gemodificeerde elektroden gelegd. Ook de heterogeniteit en de morfologie van de CoTSPc en CuTSPc dunne lagen op de goudelektroden werden bestudeerd. Hiervoor werd gebruik gemaakt van raster micro synchrotron radiatie X-straal fluorescentie (SR-XRF). Het monomeer-dimeer evenwicht van de ftalocyanines in oplossing werden bestudeerd met UV-Vis spectroscopie. De combinatie van deze elektrochemische en spectroscopische technieken gaf een beter begrip van de laagopbouw en hielp bij de optimalisatie van de modificatieprocedure.

In een tweede deel van het onderzoek werden de gemodificeerde elektroden gebruikt als elektrontransfermediator voor de detectie van 4-chloorfenol (4-Cp) en werden de oxidatiekarakteristieken in verband gebracht met de CoTSPc of CuTSPc dunne laag structuur.

In wat volgt worden de belangrijkste resultaten en conclusies van het onderzoek uiteengezet.

Onderlinge vergelijking van de verschillende modificatietechnieken zoals ‘drop-drying’, onderdompeling en elektrodepositie heeft aangetoond dat deze laatste tot een meer efficiënte depositie leidt en dat er een uniforme geadsorbeerde CoTSPc of CuTSPc laag gevormd wordt. Daarom werd de elektrodepositie meer in detail bestudeerd.

In voorgaande studies en ook gedurende deze studie, werd opgemerkt dat de stroom afkomstig van de oxidatie en reductie van de geadsorbeerde kobaltionen tijdens de elektrochemische modificatie initieel stijgt met het scannummer. Na een concentratieafhankelijk aantal cyclisch voltametrische scans wordt een breekpunt bereikt en wordt er geen toename van de stroom meer waargenomen. Bij de elektrodepositie van CuTSPc op goudelektroden daarentegen, werd geen breekpunt vastgesteld. Hier blijft de oxidatie en reductiepiek van de geadsorbeerde koper ionen toenemen. Een vergelijking van de bekomen gegevens met deze in de literatuur toonde aan dat de positie van de sulfonzure groepen op de ftalocyanine-ring een grote invloed heeft op de elektrochemische eigenschapen. Dit heeft dan ook zijn weerslag op de eigenschappen van de gemodificeerde elektrode.

Om het modificatieproces en de laagopbouw beter te begrijpen, met als doel de de modificatieprocedure te optimaliseren, werd de heterogeniteit en de morfologie van de CoTSPc en CuTSPc dunne lagen bestudeerd met behulp van SR-XRF. De experimentele moeilijkheid bij de uniformiteitstudie van de lage CoTSPc en CuTSPc concentraties in de dunne lagen, was de aanwezigheid van de overlappende Compton en goud X-straal resonant Raman (XRRS) pieken. Het X-straal resonant Raman fenomeen werd bestudeerd op een goudelektrode gemodificeerd met CuTSPc. De detectielimieten van de koperoppervlakconcentraties werden berekend in functie van de excitatie-energie wat de optimalisatie van de experimentele parameters mogelijk maakt. De geoptimaliseerde, absolute detectielimieten verkregen voor Co en Cu zijn respectievelijk 7-8 ng cm^{-2} en 5-6 ng cm^{-2} voor een meettijd van 20 s en een excitatie energie voor Co van 7.7 ± 0.1 keV en van 9.0 ± 0.1 keV voor Cu. De lage detectielimieten, samen met de snelle detectie en de kleine X-straalafmetingen, maken dat dit een zeer goede techniek voor toepassing.

Een vergelijking van de kobaltoppervlakconcentraties op de elektrochemisch gemodificeerde elektroden, verkregen via elektrochemische en SR-XRF data, heeft aangetoond dat deze van de elektrochemische data significant lager zijn. Dit geeft aan

dat er buiten elektrochemisch actieve ftalocyanines in dit geval ook elektrochemisch inactieve ftalocyanines op het elektrodeoppervlak aanwezig zijn. Bovendien werd vastgesteld dat in het begin van de modificatie het concentratieverschil tussen de twee technieken uiterst klein is en dat het verschil toeneemt met stijgend scannummer. Op het breekpunt is de kobaltoppervlakconcentratie onafhankelijk van de CoTSPc concentratie in oplossing, gedurende de modificatie en na het breekpunt blijft de kobaltoppervlakconcentratie toenemen volgens de SR-XRF data. Uit de UV-Vis data werd vastgesteld dat in de ftalocyanine-oplossingen, gebruikt tijdens de modificatie, zowel monomeren als dimeren aanwezig zijn. Bovendien werd door vergelijking van ftalocyanines van verschillende leveranciers aangetoond dat het monomeer-dimeer evenwicht het modificatie proces sterk beïnvloedt. Een hoge monomeerconcentratie in oplossing heeft een positief effect op de modificatie van het elektrodemateriaal. Gebaseerd op deze resultaten en uit informatie van de literatuur, die aangeeft dat CoTSPc een zescoördinatie prefereert, werd er gepostuleerd dat CoTSPc monomeren elektrochemisch actief zijn terwijl de dimeren elektrochemisch inactief zijn. Bovendien werd er aangetoond dat er in het begin van de modificatieprocedure een snelle groei is van elektrochemisch actieve species (monomeren) op het elektrodeoppervlak in vergelijking met de elektrochemisch inactieve species. Hieruit blijkt dat op een blanco goudelektrode eerst CoTSPc monomeren worden geadsorbeerd. Zodra een dunne elektrochemisch actieve CoTSPc monomeerlaag wordt gevormd, beginnen elektrochemisch inactieve dimeer species te adsorberen. Het actieve elektrodeoppervlak is op dat ogenblik de beperkende factor betreffende de hoeveelheid monomeren geadsorbeerd op het oppervlak en er wordt een gelimiteerde hoeveelheid dimeren geadsorbeerd op deze monomeerlaag. Door de continue potentiaalvariatie na het breekpunt worden de elektroactieve species verder gestabiliseerd en wordt deze monomeerlaag beter gedefinieerd. Hierop wordt een toenemende hoeveelheid dimeren geadsorbeerd waardoor de homogeniteit van de laag afneemt.

Gelijkaardige experimenten voor de modificatie van goudelektroden met CuTSPc tonen aan dat de berekende koperoppervlakconcentratie van de elektrochemische en SR-XRF data hetzelfde zijn. Dit duidt erop dat enkel elektrochemisch actieve ftalocyanines op het goudoppervlak aanwezig zijn. Zoals reeds vermeld werd er voor de elektrodepositie van CuTSPc op goud geen breekpunt

vastgesteld en blijft de koper oppervlakconcentratie stijgen met toenemend scannummer. Er werd bovendien vastgesteld dat de koperoppervlakconcentratie onafhankelijk is van de CuTSPc concentratie in oplossing in het bestudeerde concentratiegebied (1-16 mmol L^{-1}). De UV-Vis data tonen bovendien aan dat in de ftalocyanine-oplossingen voornamelijk dimeren aanwezig zijn. Deze verschillen kunnen verklaard worden door de voorkeur voor vier-coördinatie van CuTSPc. Er werd immers gepostuleerd dat door de vier coördinatie van de CuTSPc moleculen, deze elkaar veel gemakkelijker kunnen benaderen zonder de vorming van gebrugde systemen zoals dit bij CoTSPc het geval is. Dit maakt dat de dimeervorming bij CuTSPc veel gemakkelijker gebeurt dan bij CoTSPc wat de hoge dimeerconcentratie verklaart en het feit dat deze dimeren elektrochemisch actief zijn. Dit betekent dat tijdens de afzetting zowel de monomeren als de dimeren elektrochemisch afgezet worden en bovendien elektrochemisch actief zijn. Dit resulteert in de vorming van een compacte laag die elektron transfer toelaat. Dit verklaart ook de afwezigheid van het breekpunt tijdens de elektrodepositie aangezien er geen interferentie optreedt van een elektrochemisch inactief species wat maakt dat de stapeling van de ftalocyanine aggregaten vanaf de eerste scan mogelijk wordt. In dit verband kon ook de invloed van de positie van de sulfonzure groepen op de ftalocyanine ring op de modificatie verklaard worden. Er werd immers gepostuleerd dat de sulfonzure groepen deelnemen aan de π-π stabilisatie gedurende de laagvorming wat een voordeel is bij 3,4',4'',4'''-CuTSPc aggregaatvorming.

In het laatste deel van dit werk werden de elektrochemisch gemodificeerde elektroden gebruikt voor de oxidatie van 4-Cp in een pH 12 bufferoplossing en vergeleken met zijn oxidatie aan een blanco goudelektrode. Er werd vastgesteld dat de gemodificeerde goudelektroden geen elektrokatalytisch gedrag vertoonden ten opzichte van de oxidatie van 4-Cp. Er werd echter wel vastgesteld dat de laagopbouw van CoTSPc en CuTSPc dunne lagen een grote invloed heeft op de gevoeligheid en de reproduceerbaarheid van de elektrode. Grote hoeveelheden elektrochemisch inactieve species moeten vermeden worden. Daarom worden ftalocyanines die een vier coördinatie verkiezen, verkozen als elektrontransfermediator en moeten zescoördinerende ftalocyanines vermeden worden.

In de toekomst kan de in dit werk beschreven studie verder uitgebreid worden naar andere elektrodematerialen (vb. Pt) en andere ftalocyanines (vb. Fe, Ni, Zn als centraal ion) om de theorie over de laagopbouw na elektrochemische modificatie van de ftalocyanines te verfijnen en te generaliseren. De studie kan ook nog uitgebreid worden met X-straal-absorptiemetingen waarmee de ionisatietoestand en de dichtste nabuur van het onderzochte metaalion kan bepaald worden. Bovendien werd in deze studie enkel de aanzet gegeven naar de detectie van doelmoleculen met elektrochemisch gemodificeerde elektroden. Het aantal verschillende doelmoleculen dat kan getest worden is echter bijna onuitputtelijk.

Wat betreft de bepaling van de heterogeniteit en morfologie van de dunne lagen op elektrodematerialen kan gesteld worden dat niet enkel de elektroden elektrochemisch gemodificeerd met ftalocyanines kunnen bestudeerd worden. Ook bijvoorbeeld covalentgebonden ftalocyanines of andere moleculen zoals onder andere elektrochemisch actieve enzymen die een transitiemetaal bevatten kunnen bestudeerd worden. De eigenschappen en flexibiliteit van deze techniek is inderdaad van die aard dat de heterogeniteit- en morfologiestudie op een groot aantal dunne lagen en elektrodematerialen mogelijk is.

List of publications

1. K. Peeters, K. De Wael, L. Vincze, and A. Adriaens, Comparison of different surface modification techniques for electrodes by means of electrochemistry and micro synchrotron radiation X-ray fluorescence. Dimerization of cobalt(II)tetrasulfonated phthalocyanine and its influence on the electrodeposition on gold surfaces, Analytical Chemistry 77 (2005) 5512-5519.
2. K. Peeters, K. De Wael, A. Adriaens, G. Falkenberg, L. Vincze, Non-destructive characterization of CoTSPc electrochemically deposited on gold electrodes by means of synchrotron X-ray microfluorescence, Electrochemistry Communications 7 (2005) 1157–1162.
3. K. De Wael, K. Peeters, D. Bogaert, H. Buschop, L. Vincze, A. Adriaens, Electrochemical and micro SR-XRF study of a random and 3,4',4'',4''' copper(II) tetrasulphonated phthalocyanine modified gold electrode, Journal of Electroanalytical Chemistry, submitted for publication.
4. K. Peeters, K. De Wael, A. Adriaens, G. Falkenberg, L. Vincze, Quantitative synchrotron micro-XRF study of CoTSPc and CuTSPc thin-films deposited on gold by electrodeposition, Journal of Analytical Atomic Spectrometry, submitted for publication.
5. K. Peeters, K. De Wael, A. Adriaens, G. Falkenberg, L. Vincze, The investigation of X-ray Raman scattering effects on the detection of CuTSPc thin-films deposited on gold electrodes, Spectrochimica Acta Part B: Atomic Spectroscopy, submitted for publication.